Université de Montréal

Autocrine Loop in the Purinergic Control of Airway Surface Liquid Volume: *Monitoring with a novel side-view imaging technique*

par
David Dubois
Département de Médecine, Université de Montréal
Faculté de médecine

Mémoire présenté à la Faculté des études supérieures
en vue de l'obtention du grade de
Maître en sciences (M.Sc.)
en sciences biomédicales
Option générale

Mars, 2010

PAGE D'IDENTIFICATION DU JURY

Université de Montréal
Faculté des études supérieures

Ce mémoire intitulé:

Autocrine Loop in the Purinergic Control of Airway Surface Liquid Volume:
Monitoring with a novel side-view imaging technique

Présenté par:
David Dubois

A été évalué par un jury composé des personnes suivantes :

Président-rapporteur : _____ Ashok Srivastava

Directeur de recherche : _____ Ryszard Grygorczyk

Codirecteur de recherche : _____ Yves Berthiaume

Membre du jury : _____ Larry Lands

Mémoire accepté le : _____

Sommaire

La Fibrose Kystique (FK) est une maladie dégénérative qui entraine une dégénération des poumons dû au problème de clairance mucociliaire (CMC). Le volume de surface liquide (SL) couvrant les cellules pulmonaires est essentiel à la clairance de mucus et au combat contre les infections. Les nucléotides extracellulaires jouent un rôle important dans la CMC des voies aériennes, en modifiant le volume de la SL pulmonaire. Cependant, les mécanismes du relâchement de l'ATP et de leurs déplacements à travers la SL, restent inconnus. Des études ultérieures démontrent que l'exocytose d'ATP mécano-sensible et Ca^{2+}-dépendant, dans les cellules A549, est amplifié par les actions synergétiques autocrine/paracrine des cellules avoisinantes. Nous avions comme but de confirmer la présence de la boucle purinergique dans plusieurs modèles de cellules épithéliales et de développer un système nous permettant d'observer directement la SL. Nous avons démontrés que la boucle purinergique est fonctionnelle dans les modèles de cellules épithéliales examinés, mis appart les cellules Calu-3. L'utilisation de modulateur de la signalisation purinergique nous a permis d'observer que le relâchement d'ATP ainsi que l'augmentation du $[Ca^{2+}]_i$ suivant un stress hypotonique, sont modulés par le biais de cette boucle purinergique et des récepteurs P2Y. De plus, nous avons développé un système de microscopie qui permet d'observer les changements de volume de SL en temps réel. Notre système permet de contrôler la température et l'humidité de l'environnement où se trouvent les cellules, reproduisant l'environnement pulmonaire humain. Nous avons démontré que notre système peut identifier même les petits changements de volume de SL.

Mots-clés: ATP, Boucle autocrine purinergique, Cellules épithéliales pulmonaires, Fibrose Kystique, Microscopie, Nucléotides extracellulaires, Stimulation purinergique, Surface liquide épithéliales, Transport ionique.

Summary

Cystic Fibrosis (CF) patients suffer from respiratory problems associated with pulmonary infections and exacerbations, due to improper mucociliary clearance (MCC). The airway surface liquid (ASL) covering pulmonary epithelial cells plays a pivotal role in MCC and infection control. Extracellular nucleotides control MCC in airway epithelia by modulating ASL volume, ciliary beating and mucin secretion. The mechanism(s) of their release and dispersal within the ASL remain incompletely understood. Studies with A549 cells, a human alveolar type II cell model, have shown that mechanosensitive, Ca^{2+}-dependent ATP secretion is strongly amplified by the synergistic autocrine/paracrine actions of released nucleotides. The aim of this study was to examine whether the autocrine purinergic loop operates in different lung epithelial cell models and to develop an imaging system allowing the direct monitoring of ASL height during purinergic stimulation. We demonstrated that the signaling loop is functional in all epithelial cells tested, with the exception of Calu-3 epithelial cells. With different purinergic signaling modulators, we demonstrated that ATP release and $[Ca^{2+}]_i$ elevations evoked by hypotonic stress were strongly amplified by autocrine/paracrine effects in cells expressing the P2Y receptor family. To monitor ASL volume changes in real time, we developed a novel epi-fluorescence, side-view microscopy system to observe ASL height. During experiments, cell cultures grown on permeable filters were mounted in a custom-designed chamber that allows control of the temperature, humidity and air flow above the cell monolayer, mimicking the pulmonary environment. This system detects even small changes in ASL volume following purinergic stimulation.

Key words: ATP, Cystic Fibrosis, Extracellular nucleotides, Ionic transport, Pulmonary epithelial cells, Purinergic stimulation, Microscopy.

Table of Content

LIST OF TABLES:

Chapter 1: INTRODUCTION

LIST OF FIGURES:

Chapter 1: INTRODUCTION

Chapter 2: MANUSCRIPT

Chapter 3: RESULTS

List of Abbreviations:

16HBE14o^{-}: Carcinomic Human Bronchial epithelial cell line

A549: Carcinomic Human Alveolar epithelial cell line

ABC: ATP binding cassette transporters

ADP: Adenosine Di-phosphate

AMP: Adenosine Mono-phosphate

ASL: Airway surface liquid

ATI: Alveolar type 1 cells

ATII: Alveolar type 2 cells

ATP: Adenosine Tri-phosphate

Ca^{2+}: Calcium Ion

CaCC: Calcium activated chloride channel

Calu-3: Human Adenocarcinoma pulmonary cell line

CAVD: Congenital absence of the vas deferens

CFBE: Human Cystic Fibrosis Bronchial Epithelial cell line

CFTR: Cystic Fibrosis Transmembrane conductance Regulator

Cl^{-}: Chloride Ion

CO_2: Carbon dioxide

DAG: Diacyl Glycerol

DIDS: 4,4'-diisothiocya-nostilbene-2,2'-disulfonic acid

ENaC: Epithelial sodium channel

ER: Endoplasmic Reticulum

FBS: Fetal Bovine Serum

HCO_3^-: Bicarbonate

HS: Hypotonic Shock

IP_3: Inositol 1,4,5-triphosphate

MCC: Mucociliary Clearance

MS: Mechanosensitive

MEM: Minimum essential medium

NBD: Nucleotide binding domain

O_2: Oxygen

PCL: Peri-ciliary Liquid

PIP_2: Phosphatidylinositol Biphosphate

PLC: Phospholipase C

PS: Physiological Solution

RyR: Ryanodine Receptor

Serca: Sarco/Endoplasmic Reticulum Ca^{2+}-ATPase

SEM: Scanning Electron Micrograph

SP: Surfactant proteins

TG: Thapsigargin

TMD: Transmembrane domain

UDP: Uridine Diphosphate

UTP: Uridine Triphosphate

VDAC: Voltage-dependent anion channel

VRAC: Volume-regulated anion channel

WT: Wild-type

Acknowledgements:

Firstly, I would like to thank my research director, Dr. Ryszard Grygorczyk for having me as a student in his laboratory. His help and guidance throughout my master's degree took me a long way from where I started. My scientific knowledge, my capacity to trouble shoot and my ability to write using a proper scientific format and vocabulary were greatly improved on during the time I spent in the laboratory. Finally, I would like to thank Dr. Grygorczyk for his understanding of my medical situation during my master's degree, as he was always very caring and helpful in these situations.

I would also like to thank Dr. Yves Berthiaume, my research co-director, for helpful advice as I progressed through my research project.

Furthermore, I would like to thank Dr. Sabina Tatur for her help in the beginning of my research project. She gave me the basic knowledge and helpful tips that were needed to continue the project on the right path. Our research assistant Helene Chabot was also very helpful in cell culture and trouble shooting with the microscopy side-view imaging technique. Her help and guidance early in my master's project allowed me to advance at a steady speed, all while fully grasping the important concepts of our technique. I would also like to thank the other employees and students in

the lab, Slava Grygorczyk, Siham Cherkaoui, Marius Grygorczyk and Anita Sahu for their encouragement and advice when it was needed.

Finally, I send out many thanks to Dr. Emmanuelle Brochiero for her continuous availability when help was needed during the term of my studies.

CHAPTER 1

INTRODUCTION

1.1. The respiratory system

1.1.1. Structure and function

Human life is dependent on the proper functioning of many organ systems. The respiratory system plays an essential, complex role in every day life. It is split into different regions that execute their necessary function. The upper respiratory tract consists of the nasal passages, the mouth (for air intake), the pharynx and larynx, and the lower respiratory tract that is split into the trachea, the primary bronchi and the lungs [1]. This system is also split into different zones. The conducting zone permits for gas transport from the environment to the upper portion of the lungs, the transitional zone which consists of the space that allows air flow into the lungs and alveoli, and finally the respiratory zone which allows for gas exchange between the alveoli and the blood stream (Fig 1A) [1].

The lung is an essential major organ that is always in contact with the environment. The lungs play several very important roles in human physiology. Primarily, the capillaries of the lung create an environment that allows for gas exchange, a process that is essential for survival, replenishing the organs and muscles of the body with oxygen (O_2), while liberating them from carbon dioxide (CO_2) (Fig 1B) [1]. Secondly, they act as a barrier between the outside environment and the blood, and protect lung tissue from airborne insults (Fig 1A) [1].

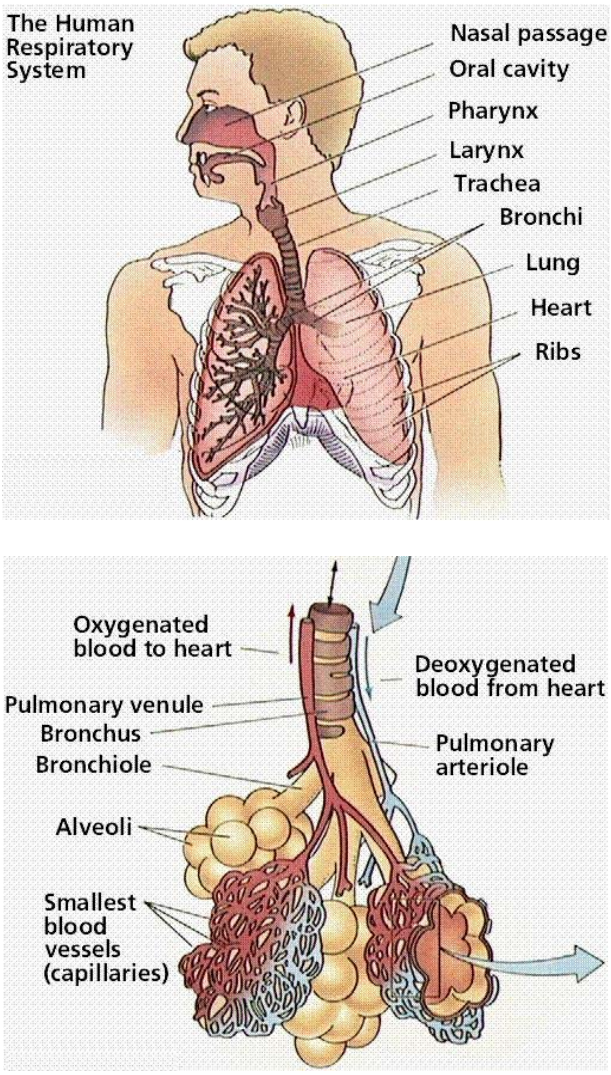

A) B)

Figure 1: **The human respiratory system:** *(A) the entire human respiratory system and (B) the pulmonary oxygenation system* [1].

1.1.2. Cellular composition of the lungs

The respiratory system is comprised of many different cell types acting together to ensure proper gas exchange, as well as the overall functioning of the lungs. Each cell type has its distinct function. The different epithelial cell types present in the lower tract, which includes the trachea, bronchi and

alveoli, are thought to secrete a thin layer of fluid called the airway surface liquid (ASL). This ASL is essential for proper mucociliary clearance (MCC). For the objective of our project, we will be concentrating on these cells due to the possibility that they are capable of secreting ASL.

The trachea is composed mainly of ciliated cells, but also contains goblet cells. The bronchi contain ciliated cells, as well as goblets cells, basal cells and Clara cells are mostly found in the bronchioles [2]. Further into the lung, the alveoli are constituted mainly of alveolar type I (AT I) and alveolar type II (AT II) epithelial cells. Ciliated cells are numerous in both the central and peripheral airways. They attach to the basal lamina and to one another through tight junctions on their apical surface and laterally by desmosomes. They have nearly 200 to 250 cilia per cell and many microvili at the cell surface, acting together to clear most inhaled substances and mucus, increasing MCC. This keeps the lower respiratory tract sterile and prevents mucus build-up in the lungs [2]. The cilia move with a uniform, coordinated beat to direct secreted mucus towards the oropharynx for expectoration. Basal cells are triangular shaped cells with their bases attached to the basal lamina. They are numerous in the proximal airways but decrease in number in the more distal airways (i.e. bronchioles). They function as reserves for epithelial repopulation as cells die / shed off, but they also help attach columnar epithelial cells to the basement membrane [2]. Goblet cells are numerous in the proximal parts of the lungs (i.e. trachea, bronchus, larger

bronchioles). The more distal parts such as the smaller bronchioles rarely contain goblet cells. Their nuclei are normally at the basal end of the cell, whereas the apical side of the cells contains the mucinogen granules [2]. This non-ciliated secretory cell releases mucins and sulfomucins, which trap inhaled substances in order to facilitate their elimination. Mucins are normally secreted in response to stimuli such as injury, infection or allergens [3]. Closely related are the Clara non-ciliated bronchiolar secretory cells that are columnar or cuboidal in shape and are found primarily in the membranous bronchioles [2]. They contain Clara-cell specific proteins that help detoxify harmful substances inhaled into the lungs through the action of cytochrome P450 enzymes and degrade mucus synthesized in the upper airways [3]. Clara cells and alveolar type II (AT II) cells have 2 common properties. They both multiply and differentiate in order to replace damaged ciliated cells of the bronchiolar epithelium. They also both produce surfactant in order to reduce lung surface tension [4], which is comprised of surfactant proteins (SP-A, SP-B, SP-C and SP-D) [5]. AT I cells are thin cells stretched over a large surface area of the alveoli. They are the main cell type forming the structure of the alveolar wall, joined together by tight junctions. They cover about 95% of the surface area of alveoli and contain pinocytic vesicles that transport materials in both directions of the air-blood barrier. Because they don’t replicate, they are susceptible to a large number of toxic insults, leading to cell death. Their major action is to mediate gas exchange in the alveoli. AT II cells are cuboidal in shape and account for

about 5% of the surface area of the alveoli [2]. They have 2 functions. Firstly, they secrete fluid and surfactants which lower the surface tension in the alveoli. Secondly, they differentiate into AT I cells and replace damaged cells [6].

Neuroendocrine cells are flask-like in shape and span from the basement membrane to the airway lumen. They contain many types of peptides which are secreted at both the basal side of the cell and laterally to neighbouring cells. Their appearance in early gestation as well as their increasing growth in numbers hints towards a role in the control of lung development [2]. They are driven to proliferate by autocrine and paracrine neuropeptide growth factor stimulation [7].

The pulmonary cells we're mostly investigating in this project are models of type 2 alveolar cells (A549), bronchial cells (16HBE14o$^-$), serous cells (Calu-3) and Cystic fibrosis cells (CFBE) (Fig 2) [8]. These epithelial cells have the important function of regulating the ASL and controlling MCC, through the formation of a thin film of liquid comprised of a periciliary liquid layer (PCL) and mucus. ASL volume is controlled by intracellular and extracellular signalling, ion transport and cell-cell interactions. Pulmonary epithelial cells secrete ASL onto the surface of the apical (luminal) side of the cells, whereas the basolateral side serves as a contact with the interstitial space. The cells of interest in this project are pulmonary epithelial

cells, such as A549, 16HBE14o-, Calu-3, wild-type human cystic fibrosis bronchial cells (CFBE) and CFTR mutated CFBE cells (that express a mutation, a deletion at the phenylalanine 508 position – ΔF508).

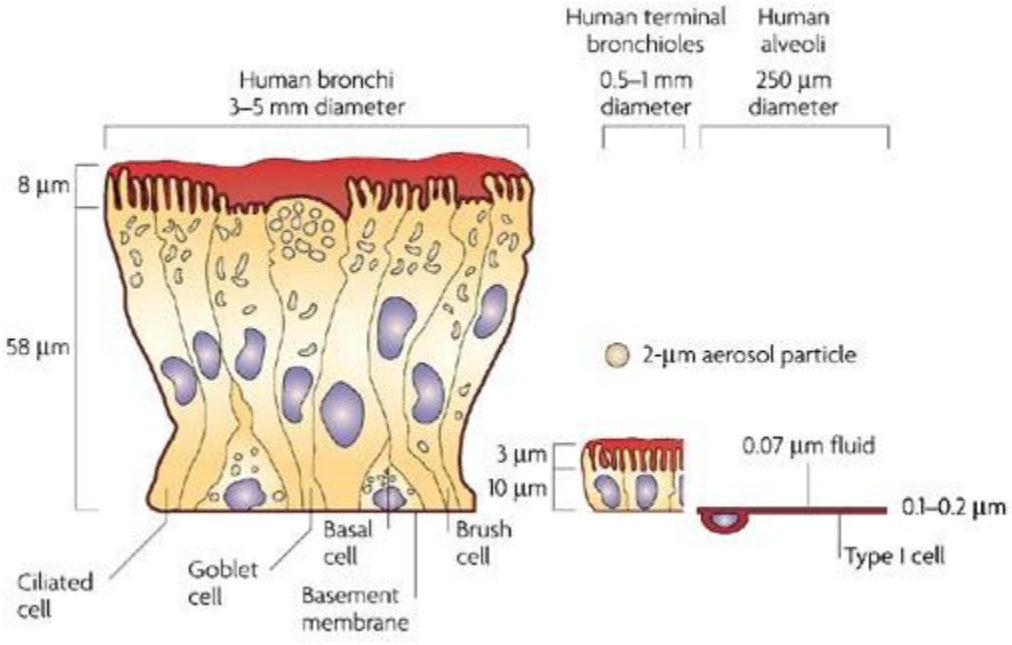

Figure 2: **Human Pulmonary epithelium**: *Bronchial cells* [8]

1.1.3. Ion transport in the normal lung

Electrolyte and fluid transport plays a vital role in the regulation of ASL volume. The proper transport of ions such as bicarbonate (HCO_3^-), chloride (Cl^-), potassium (K^+) and sodium (Na^+) across the cell membrane is necessary for normal pulmonary function.

The net transepithelial fluid secretion (or absorption) involves the active (energy consuming) transport of ions along with water, which follow the osmotic gradient generated by ion movement. In airway epithelia, fluid secretion (from the blood side to the lumen) is driven by the secretion of Cl^- ions that involves the coordinated activity of several transporters located at both the apical and basolateral membranes. Cl^- enters the cell at the basolateral membrane, through the Na^+-K^+-$2Cl^-$ co-transporter. This co-transporter is electrically neutral and driven by the movement of Na^+ down its electrochemical gradient. As a result, Cl^- accumulates in the cell above its electrochemical equilibrium. This transporter also accumulates K^+ ions in the cell, which then exit the cell passively across the basolateral membrane through other K^+ channels. In turn, the basolateral K^+ conductance hyperpolarizes the cell, providing the driving force for the movement of Na^+ and Cl^- ions across the apical membrane. Na^+, which enters the cell coupled to Cl^- or K^+, is recycled via the activity of the Na^+/K^+ ATPase, the Na^+ pump. This energy (ATP)-consuming enzyme maintains a low concentration of intracellular Na^+ resulting in a large Na^+ concentration gradient across the cell membrane. The Na^+ gradient is the primary source of energy for all secondary ion transport systems, including transepithelial Cl^- secretion [9, 10].

Cl^- ions, which are accumulated in the cell above their electrochemical equilibrium, exit passively through an apical membrane Cl^- channels. The

two main types of apical membrane Cl^- channels are the cystic fibrosis transmembrane conductance regulator (CFTR), activated by an intracellular increase of cAMP and protein kinase A(PKA), and a group of Ca^{2+}-activated chloride channels (CaCC), activated by an intracellular calcium ($[Ca^{2+}]_I$) increase. The latter may include bestrophins and TMEM 16 proteins [11].

To maintain proper MCC, the ASL volume (height) must be tightly regulated, allowing for different components of the MCC system (cilia beating, mucus secretion and movement) to work efficiently. In CF related problems the main deficiency involves reduced or absent anion (Cl^-, HCO_3^-) transport, which may also perturb the transport of other ions, such as Na^+. Because the ASL volume depends critically on transepithelial Cl^- and Na^+ transport within the pulmonary epithelium [12-18], these ion transport abnormalities result in an altered volume of ASL (dehydration) and abnormal rheological properties of the mucus, which appears more viscous and sticky in CF patients. In non-CF individuals, the apical secretory anion channels such as the CFTR chloride channel play the largest role in the regulation of ASL volume, although the non-CFTR CaCC also has an important role [19, 20]. On the basolateral side of the cell, Cl^- secretion occurs via the Na^+-K^+-$2Cl^-$ cotransporter (NKCC) (Fig 3) [10, 17]. For CF patients lacking CFTR function, activation of the alternative, non-CFTR chloride channels may help restore the normal ion transport in the lung [10, 20].

Under basal conditions, Na^+ absorption appears to be responsible for fluid absorption. When the epithelium is treated with amiloride and agonists that increase cellular levels of cAMP, fluid secretion ensues. The key to effective trans-epithelial electrolyte transport is the coordinated activity of the apical and basolateral ion channels [9]. CF individuals have a dehydrated ASL due to the lack of functional trans-epithelial ion transport [16, 18]. *In vitro* and *in vivo* studies of trans-epithelial electrolyte transport indicate that there are two main abnormalities in CF airway epithelia. Firstly, CF airway epithelia show reduced or absent cAMP-stimulated Cl^- secretion. In contrast, Ca^{2+} activated Cl^- secretion remains intact in CF airway epithelia. Secondly, CF airway epithelia may have a two to three fold increased Na^+ absorption rate caused by increased apical membrane Na^+ permeability compared to non-CF epithelia. This increase is attributed to Na^+ transport through amiloride-sensitive apical membrane Na^+ channels (ENaC) that are tonically inhibited by CFTR in normal cells but lack this inhibition in CF [20]. It was therefore proposed that both abnormalities, the increased permeability of Na^+ and decreased permeability of Cl^- produces respiratory tract fluid abnormalities in quantity and composition [9]. This hypothesis was contradicted, however, by several other laboratories that showed that CFTR does not cause inhibition of ENaC [21].

Na^+ ions play an essential role in the homeostasis of the ASL, through the function of the absorptive epithelial sodium channel ENaC. In healthy

individuals, ENaC re-absorbs Na^+ ions back into the cell [13]. The schematic in figure 3 depicts an airway epithelial cell with ion transporters essential for ASL regulation (Fig 3) [15]. The apical membrane contains ENaC, cAMP-dependent Cl^- channels (CFTR), as well as Ca^{2+}-activated Cl^- channels (CaCC), while the basolateral side expresses the Na^+/K^+ pump and the Na^+-K^+-$2Cl^-$ co-transporter [17, 22, 23]. The downregulation of ENaC and the upregulation of CFTR and CaCC may favor net anion secretion which in turn will increase fluid secretion and hydration of the airway surface and mucus layer [15, 24].

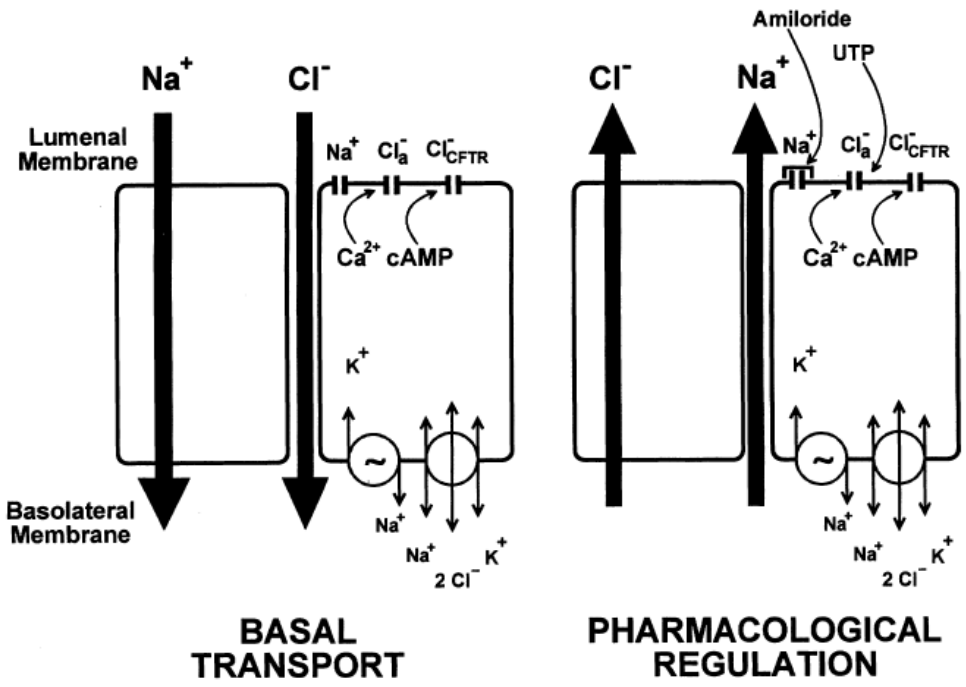

Figure 3: **Basolateral and luminal ionic transport in the pulmonary epithelium** [15]

Human airway epithelia normally generate a transepithelial electrical potential difference (V_t , given in mV) between -10 and -30 mV, with the lumen negatively charged relative to the submucosal surface. During Ussing chamber experiments, where the transepithelial voltage is clamped to 0mV, the resulting current is mainly accounted for by Na^+ absorption from the mucosal to the submucosal surface, as well as the Cl^- secretion from the submucosal to the mucosal surface [9].

1.1.4. Mucociliary clearance

The purpose of the upper respiratory tract is to conduct air and trap large inhaled particles. Trapping of the particles occurs due to the sticky, wet mucus that is found along the surface of the respiratory tract. Once trapped, ciliated cells (cilia) move the particle from the nasopharyngeal area into the posterior pharynx, at which point it can be swallowed [25]. The thin lining of mucus that is found through most of the respiratory tract plays a vital role in mucociliary clearance (MCC) (Fig 4).

MCC is an essential function of the lung and its three components: mucus secretion, fluid secretion and cilia beating, must function properly in order to avoid mucus build-up and plugging, which eventually could lead to the accumulation of bacteria, bacterial infection followed by pulmonary exacerbation. In airways, the three components of MCC are controlled by purinergic signals that physiologically involve the apical release of

nucleotides, activating ion transporters and initiating mucin secretion, ion transport across the epithelial membrane, water secretion and increased ciliary beat frequency. These mechanisms maintain a conductive and sterile environment in the respiratory tract [26].

The basolateral and apical release of nucleotides constitutes a paracrine mechanism by which a mechanical or chemical stress is signaled to several cells and then propagated to other adjacent cells, leading to the auto-stimulation of the cells in the monolayer. The ensuing nucleotide release from pulmonary epithelial cells, followed by the auto-stimulation of neighboring cells, constitutes the autocrine purinergic loop. The efficient MCC needed to keep the airway environment sterile can only occur when ASL height is maintained at a height of about 7μm for optimal cilia beating and movement of the mucus layer [27, 28].

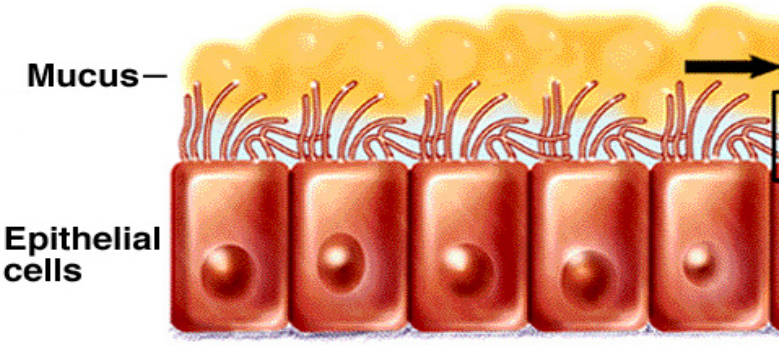

Figure 4: **Mucociliary clearance in pulmonary epithelial cells**

1.1.5. Role of airway surface liquid (ASL) in MCC

The airway epithelium that forms the respiratory tract is covered by a thin ASL layer normally measuring 7 μm to 70 μm in height, *in vivo* [27]. The ASL defends the lung against infectious and noxious agents, and conditions inhaled air which is associated with the so-called 'insensible water loss' from the ASL [29]. MCC critically depends on airway surface liquid (ASL) composition and volume. A deficiency in ASL volume is a key component of many airway diseases such as cystic fibrosis, asthma, COPD and other diseases of the airways, which result in decreased MCC in the airways [30].

Lining the airways are cilia, tiny hair-like structures that move in a specific upward motion that allow for inhaled particles, trapped in the mucus layer, to be moved up and out of the airways [31]. For mucus to be expelled from the airways, an ASL layer with height between 7 and 10μm is required for optimal cilia flexibility and motility [27, 29, 31].

1.2. Cystic Fibrosis

1.2.1. Introduction to CF

Cystic Fibrosis (CF) is a genetic, Mendelian recessive disease, which is caused by a mutation in the CFTR gene and leads to deficient ASL volume and MCC dysfunction.

The CFTR gene, located on the human chromosome 7, on the long arm at position q31.2, contains about 170,000 base pairs. CFTR is a glycoprotein containing 1480 amino acids. The normal CFTR protein is found in the lungs, liver, pancreas, intestines, reproductive tract and the skin.

The CFTR membrane protein has two transmembrane helical domains, each having six spans of alpha helices. They are connected to a nucleotide binding domain (NBD) in the cytoplasm. The first NBD is connected to the second transmembrane domain by a regulatory "R" domain that is unique to CFTR and not found in other members of ABC transporter proteins. The ion channel only opens when its R-domain has been phosphorylated by PKA and ATP is bound at the NBDs [32]. The carboxyl terminal of the protein is anchored to the cytoskeleton [33].

To date, over 1600 mutations in the CFTR gene have been discovered [34]. These mutations result in two main genetic disorders: CF disease and the congenital bilateral absence of the vas deferens (CAVD). The pulmonary aspect of the disease arises due to the blockage of ion and fluid movement across the membrane of epithelial cells, while the basis of CAVD is still unknown. The most common mutation, being the ΔF508 genetic mutation, occurs due to the deletion of three nucleotides, resulting in the deletion of the amino acid phenylalanine at position 508.

The mutated CFTR gene results in many different outcomes, forming 5 classes of defective CFTR proteins: (Class 1) mutations altering the production of the protein and stability of the mRNA, (Class 2) mutations altering the cellular maturation of the protein, (Class 3) mutations disturbing the regulation of Cl^- channel activity, (Class 4) mutations altering the conduction of Cl^- channels and (Class 5) mutations altering the stability of mature CFTR protein [35-36]. Class 1 mutations are caused by nonsense mutations or premature stop codons in the gene. This mutation class results in the formation of unstable mRNA that will hamper proper protein synthesis, or in the case of the produced protein, it remains unstable and is rapidly degraded. The overlying consequence of such mutation, such as G542X, is the loss of apical membrane Cl^- conductance in the affected epithelia [37]. Furthermore, the previously known as class 5 mutations are now fused and classified as class 1 mutations. These mutations are characterized by a lack of CFTR protein synthesis, due to an unstable, mis-spliced mRNA which cannot produce any functional protein. The 621+1 G>T CFTR mutation is example of this class of mutant [37]. Class 2 mutations alter the maturation of the proteins, therefore the proteins are either absent from the plasma membrane or present in a very small quantity. The class 2 mutations represent the majority of CF mutations, as is the case with the ΔF-508 mutation. Class 3 mutations are usually occurring in the ATP binding domain and cause the deregulation of Cl^- channel activity due to reduced probability of channel open state P_o. The G551D mutation is an

example of a CFTR protein with low channel activity due to reduced P_o [37]. Class 4 mutations alter the conductivity of Cl^- channels. The missense mutation caused by this class of mutations produce a correctly positioned protein at the cellular membrane, with cAMP dependent Cl^- channel activity, but the characteristics of the channels are different from those of endogenous CFTR channels. R117H is a class 4 mutation and the ensuing protein is characterized by a diminution of ion flux (single-channel conductance) and modified selectivity [37]. Finally, class 5 mutations alter the properties of the CFTR protein, rendering it unstable and unable to carry out its original function [35].

Any of the previous mutations will initially cause reduced Cl^- / HCO_3^- secretion, eventually leading to mucus accumulation in the lungs of the patient, which is normally proceeded by mucus stasis, chronic infection and respiratory cell death. The most critical aspect of the disease is mucus stasis, which needs to be limited in order to escape more serious problems. This aspect is primarily under the control of the ASL that covers the apical membrane of the pulmonary epithelial cell. In normal lungs, the ASL measures approximately 7μm, whereas it only measures between 2-4 μm in CF airways [20, 31]. Furthermore, whereas mucus of the healthy airways is comprised of 98% water, 1% salt and 1% mucins and macromolecules, mucus of CF airways is dehydrated and comprised of up to 15-20% solids [12].

1.2.2. ASL regulation in CF

In CF, the ASL volume is diminished due to dysfunctional ion transport. This results in the formation of mucus plugs in the airways, leading to non-functional, hardened, bent and packed cilia that lose their original purpose. This process leads to the eased accumulation of mucus in the airways [12, 13, 20, 31].

Contrary to ion transport in healthy individuals, the ion transport in CF patients is characterized by reduced Cl^- and HCO_3^- transport onto the epithelial cell surface, resulting in dehydration of the epithelial cell surface and causing mucus stasis and accumulation of bacteria within the mucus plugs [13, 16, 31].

Although the main function of CFTR is anion (Cl^-, HCO_3^-) transport, it may have other functions which could play a role in disease pathogenesis, including the regulation of a variety of other channels and transporters [12-13, 20, 29, 31]. Anion transport remains nonetheless a primary function of CFTR contributing to proper ASL hydration, as depicted in figure 5 [38].

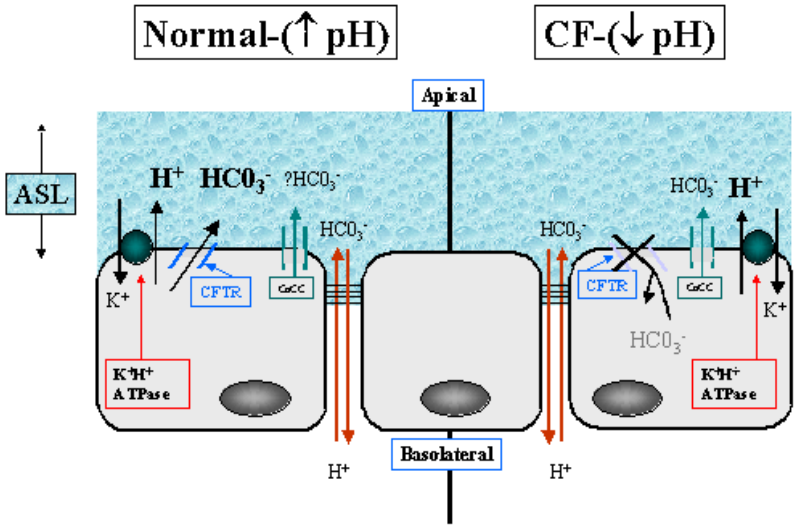

Figure 5: **The ASL pH depends majorly on anion transport in airway epithelial cells** [38]

The Na^+/K^+ ATPase pump activity might also be affected by elevated apical Na^+ absorption in CF epithelia. This transporter moves Na^+ actively out and K^+ into the basolateral membrane of epithelial cells, and it appears to be significant in CF disease pathogenesis. The inhibition of the Na^+/K^+ ATPase in human pulmonary Calu-3 cells leads to reduced transcription of CFTR [22]. Another experiment using ouabain, an inhibitor of the Na^+/K^+ ATPase, caused CFTR dysfunction [22]. The Na^+/K^+ ATPase, as well as the NKCC, have been shown to play essential roles in ionic movement, aiding in the stabilization of the ASL volume [10, 23]. The dysfunction of these transporters can affect the physiology of the lung [10]. The overall movement of ions across the epithelium, including the entrance of HCO_3^- through the Na^+-HCO_3^- co-transporter, generates a driving force for fluid secretion and ASL replenishment [10, 23]. In order to repair this ion flow

problem, it is crucial to restore the expression of functional anion secretive channels at the cellular membrane.

1.2.3. CF Phenotype, infectious status and outcome

The ion transport deficiency in CF cells, caused by a mutation in the CFTR gene, leads to the phenotype of the CF patient. The phenotypical state of the disease is characterized by the hyper-secretion and accumulation of mucus in the lungs and the pancreatic ducts. Many other CFTR mutations lead to the congenital bilateral absence of the vas deferens in about 95% of male CF patients [34].

Congenital absence of the vas deferens (CAVD) is a condition in which the vasa deferentia, male reproductive organs, fail to develop properly. In CAVD, the CFTR protein may still be functional but at reduced efficiency, leading to the production of thick mucus which blocks the developing vas deferens. The lack of development of the vas deferens results in the infertility of the CF patient. However, the patient is able to create sperm, but it is unable to be transported appropriately. Therefore, CF patients must opt for in-vitro fertilization in order to have children [39].

Furthermore, some CF patients are only diagnosed with CF after discovering they are having problems conceiving a child and have CAVD. In these instances, CF patients acquired mutations in CFTR that are less

severe and result in a later diagnosis (at an elder age), which also signifies a less prominent CF phenotype [35, 39].

Due to the CF-related problems, all patients are subject to several hours of daily treatments. Such treatments include daily physiotherapy in order to unblock the airways of sticky mucus, which in long term can result in continuous infections and inflammation if it remains in the lungs. For the same reason, CF patients are obliged to follow a strict medical regimen, including a cocktail of different medications, in order to treat infections and inflammation, or simply in prevention of the accumulation of infectious bacteria in the lungs.

The airways of CF patients can be colonized by a multitude of bacteria, predominantly by pseudomonas aeruginosa, but also by hemophilus influenzae, aspergillus fumigatus, staphylococcus aureus, stenotrophomonas maltophilia, achromobacter xylosoxidans and in rare cases, burkholderia cepacia [40-46]. The accumulation of pseudomonas aeruginosa (most common CF bacteria) in the lungs most often results in chronic infections and pulmonary exacerbations.

Furthermore, the pancreatic insufficiency caused by the disease leads to the improper digestion of foods and a difficulty in absorbing the fat content of ingested food. Pancreatic enzymes are therefore taken by CF patients in

order to retain fat and maintain a proper, healthy weight. Essentially, weight gain is a good indicator of a healthy patient [47].

1.3. The purinergic regulation of ASL

Extracellular nucleotides, such as ATP, UTP and their degradation products, control a diverse range of physiological processes by interacting with a large group of cell-surface P2X and P2Y receptor families (i.e. purinergic receptors). In the lungs, extracellular nucleotides regulate airway surface liquid homeostasis and mucociliary clearance by modulating epithelial ion and fluid transport, as well as ciliary beating [48]. After the release of ATP into the extracellular space, the action of cell surface nucleotidases extend its signaling potential by converting it to ADP, AMP and adenosine, which is a ligand for another family of G protein-coupled receptors (A_1, A_{2A}, A_{2B}, A_3). The A2B receptor is coupled to an increase in cAMP levels and the activation of CFTR in airway epithelia.

1.3.1. Mechanism (s) of ATP release

Nucleotide release is stimulated by cellular mechanical perturbations, such as shear stress, membrane stretch, media change, hypo-osmotic swelling, and hypoxia [48]. The physiology of the lung exposes the pulmonary environment to many mechanical stresses during lung expansion and relaxation, resulting in the constant release of ATP as a stress-responsive molecule [49].

Although ATP release plays a vital role in the homeostasis of the lung, it is also essential to the function of other organs and tissues. The increase in flow shear stress, hypoxia and cell swelling results in ATP release from vascular endothelial cells [50-52]. Furthermore, ATP release in the urinary bladder arises from the stretching of the epithelium and was proposed as a full bladder-sensing mechanism [53-54]. Finally, nucleotides released locally by mechanical stimulation are also implicated in bone remodeling [55].

Recent studies suggest that the release of ATP (and UTP) from pulmonary epithelial cells is exquisitely sensitive to mechanical perturbations, resulting in a host-defense mechanism that involves fluid secretion and an increase in ciliary beat, helping to clear the epithelial surface of particulates [56-59]. Our laboratory has explored the exocytosis of ATP-enriched vesicles as the main source for extracellular ATP, but another hypothesis was also viable [48]. Two main hypotheses, not involving cell lysis, explain the mechanism

of ATP release in epithelial cells: (1) it is secreted from the cytosol via vesicle-associated nucleotide-conducting channels or transporters transiently expressed at the plasma membrane as a consequence of vesicle-plasma membrane fusion or (2) nucleotides can be delivered to the extracellular medium as cargo molecules within exocytotic vesicles.

The first hypothesis formulated by several researchers had reported that CFTR and other ATP binding cassette (ABC) transporters are active transporters; they require energy in the form of ATP to translocate substrates across cell membranes and these proteins harness the energy of ATP binding and/or hydrolysis to drive conformational changes in the transmembrane domain (TMD) and consequently transports molecules [60]. However, experiments using the patch clamp, lipid bilayer and luminometry techniques, univocally demonstrated the absence of detectable CFTR-mediated or CFTR-regulated ATP release [56, 58, 61-65]. On the other hand, some volume-regulated anion channels (VRAC) have been shown to have a certain permeability to cations and large organic anions, suggesting that VRACs are possibly involved in cell swelling-induced ATP release and the autocrine regulation of cell volume [66-72]. Finally, a large conductance (~400 pS) was induced from a voltage-dependent Cl^- channel following cell swelling [73, 74]. This channel was permeable to ATP and resembled the voltage-dependent anion channel (VDAC, porin or maxi Cl^- channel). VDAC mediates the movement of ATP across the outer mitochondrial membrane,

and similar channels have often been found in the plasma membrane of several cells [75, 76], but their physiological role in the plasma membrane remains unclear.

The second hypothesis involves the exocytosis of ATP-containing vesicles. It is well established that ATP is co-stored with several neurotransmitters, this being a source of exocytotic ATP release [77-81]. Chromaffin granules have an ATP concentration that has been reported to reach 100 mM, and other nucleotides (ADP, UTP, CTP) are also present at significant levels [82]. Important amounts of ATP are within the lumen of the endoplasmic reticulum (ER), Golgi apparatus and other organelles. These organelles need ATP to provide the source of energy needed for protein folding and degradation, and as a substrate for numerous reactions. ATP is translocated across the membrane into these compartments via specific transporters that concentrate it in the Golgi/ER lumen 50-100 times above its concentration in the external medium [83, 84]. Exocytosis of these ATP-enriched vesicles was proposed to contribute to constitutive and mechanosensitive ATP release from oocytes [85]. A similar mechanism may operate in other cell types, including lung epithelia as demonstrated by our recent study [86]. The use of quinacrine as a fluorescence marker of intracellular ATP stores has led to the discovery of areas of granular fluorescence, consistent with vesicular ATP storage, detectable in several non-neuronal cell types and in alveolar A549 cells [87-90]. In endothelia,

increased shear stress caused ATP release and a significant reduction of intracellular quinacrine fluorescence [89].

Finally, Boudreault et al. and Tatur et al. have demonstrated that MS ATP release is a Ca^{2+}-dependent process, consistent with regulated Ca^{2+}-dependant exocytosis [91].

1.3.2. Purinergic receptors

A549 and 16HBE14o$^-$ cells express several members of the P2Y purinoceptor family. These receptors are G-protein coupled receptors activated by extracellular nucleotides. Their activation initiates a complex intracellular cascade that is normally followed by a shift in ion transport and osmotic flow across the cellular membrane, leading to a net result of fluid secretion to the extracellular space. Different epithelial cell types express different subtypes of P2Y receptors. Therefore, the overall response to a given stimulus will depend on the variety of P2Y receptors expressed on the surface of a particular cell, in addition to the type of nucleotides that are released by the cell in response to mechanical stimulation and $[Ca^{2+}]_i$ release. Although many P2Y receptors have been discovered, only a few are expressed in the epithelial cells of the lung (Table 1 – Sigma Aldrich).

Both A549 and 16HBE14o$^-$ cell lines express high levels of $P2Y_2$ and $P2Y_6$, but the expression of $P2Y_1$ and $P2Y_4$ is very low, if they are even expressed at all [92]. Interestingly, Calu-3 cells express only a very small number of $P2Y_1$ receptors, and show little ATP and $[Ca^{2+}]_i$ responses following a 50% HS, when compared to other pulmonary epithelial cell types [92]. Earlier studies also confirm the expression of $P2Y_2$, $P2Y_6$, $P2Y_1$ and $P2Y_4$ in A549 cells [48].

Current Name	$P2Y_1$	$P2Y_2$	$P2Y_4$	$P2Y_6$	$P2Y_{11}$	$P2Y_{12b}$	$P2Y_{Ap4A}$
Structural information	372aa (Human)	376aa (Human)	365aa (Human)	328aa (Human)	371aa (Human)	342aa (Human)	-
Selective Agonists	ADPβS 2-MeSADP 2-MeSATP PAPET-ATP	UTPγS ATPγS	UTP	UDP UDPβS	ARC67085MX dATP BzATP	2-MeS-ADP ADP	Ap_4A
Selective Antagonists	A3PSPS PPADS RB-2 MRS 2179 MRS 2279	Suramin	PPADS	RB-2 PPADS Suramin	RB-2 Suramin	ARC670-85MX ARC6993 1MX C1330-7 2-MeS-AMP	Lp_5I
Signal Transduction Mechanism	$G_{q/11}$ Increased IP_3 / DAG	$G_{q/11}$ Increased IP_3 / DAG Possibly G_i	$G_{q/11}$ Increased IP_3 / DAG Possbly G_i	$G_{q/11}$ Increased IP_3 / DAG	$G_{q/11}$ and G_5 Increased IP_3 / DAG and cAMP	G_i cAMP	$G_{q/11}$ Increase IP_3 / DAG

Table 1: **P2Y Subtypes (G protein family)**, Sigma-Aldrich Canada Ltd., Oakville, Ontario, Canada.

1.3.3. Metabolism and conversion of extracellular nucleotides

The constant flow of nucleotides in and out of the cell is a complex mechanism that involves removing, deactivating or recycling extracellular nucleotides. These pathways most often lead to the reuptake of the nucleotides within the cell [93]. Nucleotide hydrolysis involves several families of ecto-enzymes that act in the formation of the respective nucleoside and a free phosphate. The phosphate can be recycled by surrounding cells and re-used for nucleotide re-synthesis. Finally, in the case of adenosine nucleotides, its hydrolysis leads to an adenosine by-product that can initiate additional receptor-mediated functions [93].

1.3.4. Autocrine purinergic loop

The autocrine purinergic loop has been under investigation in our laboratory for several years, mainly in A549 epithelial cells. When a cell is stimulated by a mechanical stress (air bubble) or hypotonic swelling (50% HS), it results in an elevation of $[Ca^{2+}]_i$ due to its release from intracellular stores; this is the initial step of the autocrine purinergic loop [48]. The increase in $[Ca^{2+}]_i$ causes the exocytosis of vesicles containing nucleotides into the extracellular space. The nucleotides, such as ATP, UTP and UDP, then produce their effect interacting with cell surface purinergic receptors of the same cell, as well as on neighbouring cells. The activation of many surface receptors, such as the P2Y family of receptors, will cause the activation of intracellular cascades involving PIP_2, IP_3, PLC and DAG (Fig 6) [48]. This

cascade leads to the release of even more $[Ca^{2+}]_i$, increasing nucleotide exocytosis. This positive feedback loop causes a transient $[Ca^{2+}]_i$ spike (see Fig 6 and Fig 7). At this point, the autocrine purinergic loop attenuates and the response is diminished. The purinergic loop significantly amplifies the release of nucleotides evoked by mechanical stimulation and enables, via activation of P2 receptor signalling pathways, stimulation of anion and fluid secretion that replenishes the ASL.

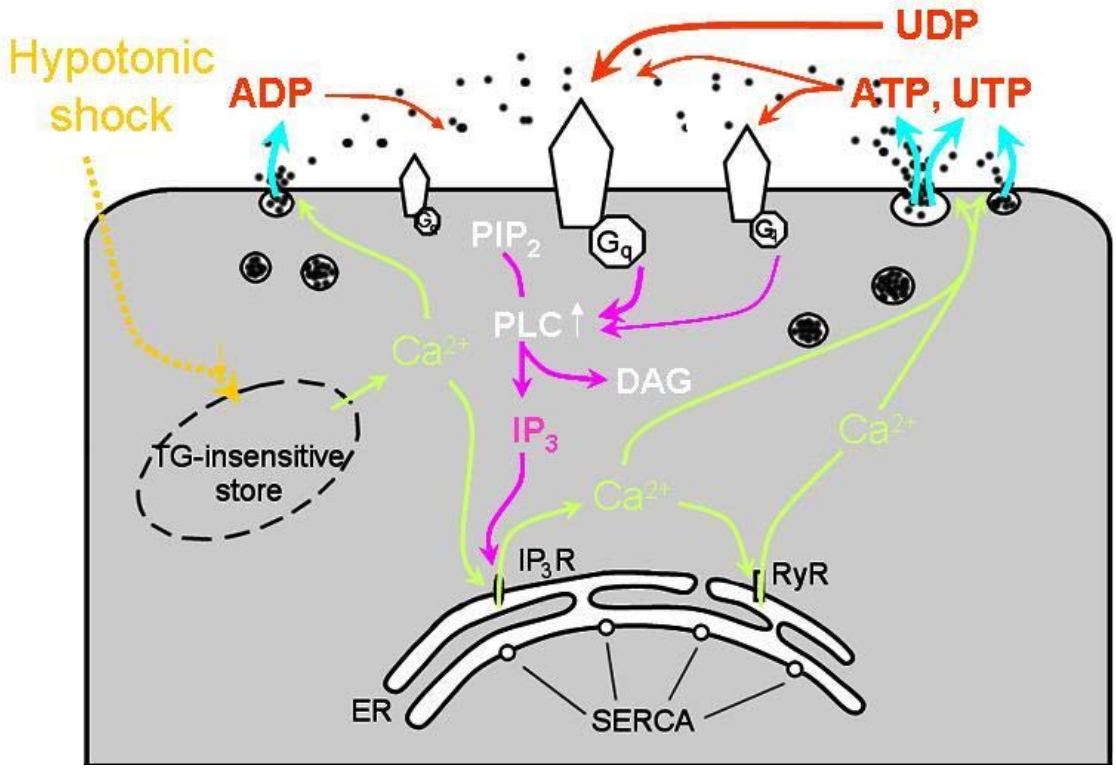

Figure 6: **Autocrine purinergic loop function in A549 alveolar type 2 cells** [48]

Many experiments were performed in order to find a marker of purinergic loop presence/activation. Previous experiments in our laboratory determined that the presence of the autocrine purinergic loop is characterized by 2

components of $[Ca^{2+}]_i$ response to a hypotonic shock [48]. Firstly, we observed that the first component in A549 cells consisted of a rapid $[Ca^{2+}]_i$ spike, which was superimposed on the second component, consisting of the slow, gradual $[Ca^{2+}]_i$ increase over time (Fig 7). The activation of the purinergic loop is initiated by a given cellular stimulus such as a 50% HS, which results in the liberation of $[Ca^{2+}]_i$ from intracellular stores such as the ER, TG sensitive and insensitive stores. Elevated $[Ca^{2+}]_i$ induces the Ca^{2+}-dependent exocytosis of nucleotide-loaded vesicles and their release. Due to autocrine/paracrine actions of release nucleotides on cell surface P2 receptors, a profound $[Ca^{2+}]_i$ spike is observed [48]. This spike became the indicator that the autocrine purinergic loop was active, as it persisted until the $[Ca^{2+}]_i$ stores were severely depleted [48]. In order to determine the functionality of the autocrine purinergic loop in different pulmonary epithelial cells, we used a microscopy calcium monitoring system. The examined cells were the A549, 16HBE14o$^-$, Calu-3 and CFBE cells.

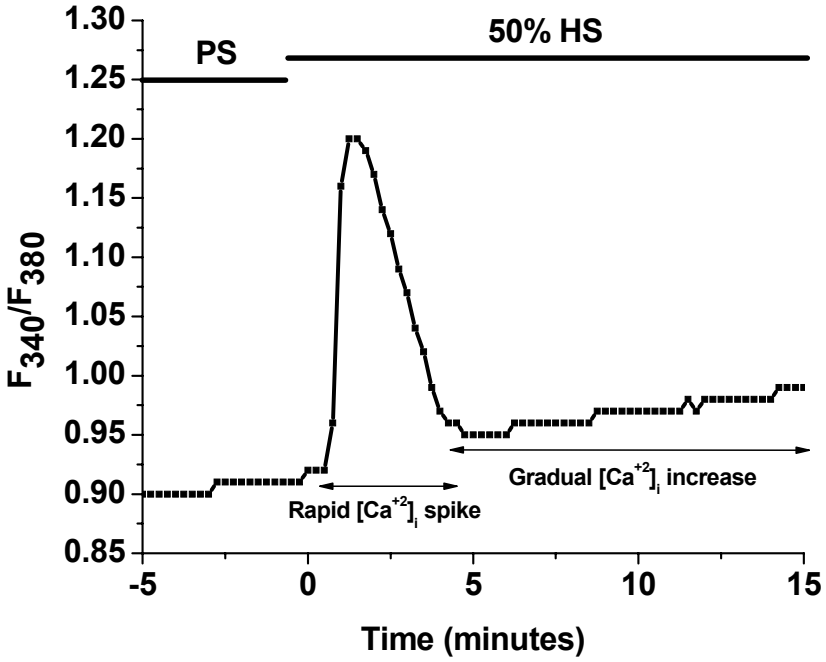

Figure 7: Two components of the $[Ca^{2+}]_i$ response to a 50% HS in A549 cells**: slow gradual elevation and a superimposed rapid spike due to autocrine purinergic loop in A549 cells**.

1.4. Novel Side-view Microscopy technique

1.4.1. Introduction

So far, the ASL height of bronchial and tracheal cell cultures has been studied by laser scanning confocal microscopy (LSCM) [29, 94-95]. The several limitations discussed in the manuscript preclude the possibility of real-time observation of ASL height alterations upon a cell stimulus. Furthermore, laser scanning causes photobleaching and photodamage to the cells due to the exposure to laser light of high average operating power

[96], an outcome which may alter the cell response to a stimulus. Finally, some investigators have also applied perfluocarbons to the apical cell surface in order to prevent ASL evaporation, but this method is a non-physiological condition that may also alter the cell response.

Side-view imaging of the ASL, which directly records both the ASL height and volume, could obviate many problems that hamper other quantitative techniques. Several approaches for side-view imaging with a routine microscope have already been developed [97-102]. These techniques were applied to single cell observation with phase contrast illumination, and the cells were cultured on solid substrata under liquid-covered conditions. None of these techniques was, therefore, suitable for ASL height observation.

We developed a novel approach for side-view ASL observation based on conventional epifluorescence microscopy. The cells were cultured on a filter membrane of a modified Millicell® insert, under air-liquid interface (ALI) conditions, and mounted in a chamber which allowed direct side-view imaging of the ASL profile. The ASL height could be measured with accuracy equal to LSCM with the advantage of faster image acquisition (~ 100 ms). The short illumination and acquisition time make real-time monitoring of ASL height alterations possible, limiting at the same time the phototoxic effects on the cell culture. Furthermore, a technique in which the filter membrane with cell monolayer is tilted at a smaller angle (≤45°),

allowed us to monitor and calculate not only the ASL height at a given point, but also to scan across the cell monolayer and obtain an average volume and pattern of ASL distribution (refer to Fig 6 – p.67).

Finally, although the initial setup of our system was functional, it offered limited room for manipulations and tilting of the filter. In order to solve this problem, we developed a new, optimized side-view chamber that offers increased stability and the possibility of tilting the filter at different angles. Furthermore, we decreased the volume of the chamber, making it easier to attain our target temperature and humidity, with little to no fluctuations. These changes increased the effectiveness of the technique, without changing the overall characteristics of the chamber. See Annex 1 for images of the initial side-view chamber versus the new, optimized chamber (Annex 1).

1.4.2. Image analysis and Calculation of the ASL volume

It was initially thought that the ASL height would be the best experimentally measurable characteristic of ASL from which its volume could be directly calculated. However, early experiments demonstrated that the ASL isn't uniformly spread over the entire cell monolayer. For this reason, the ASL height at one point could have been different than at another point (Fig 8).

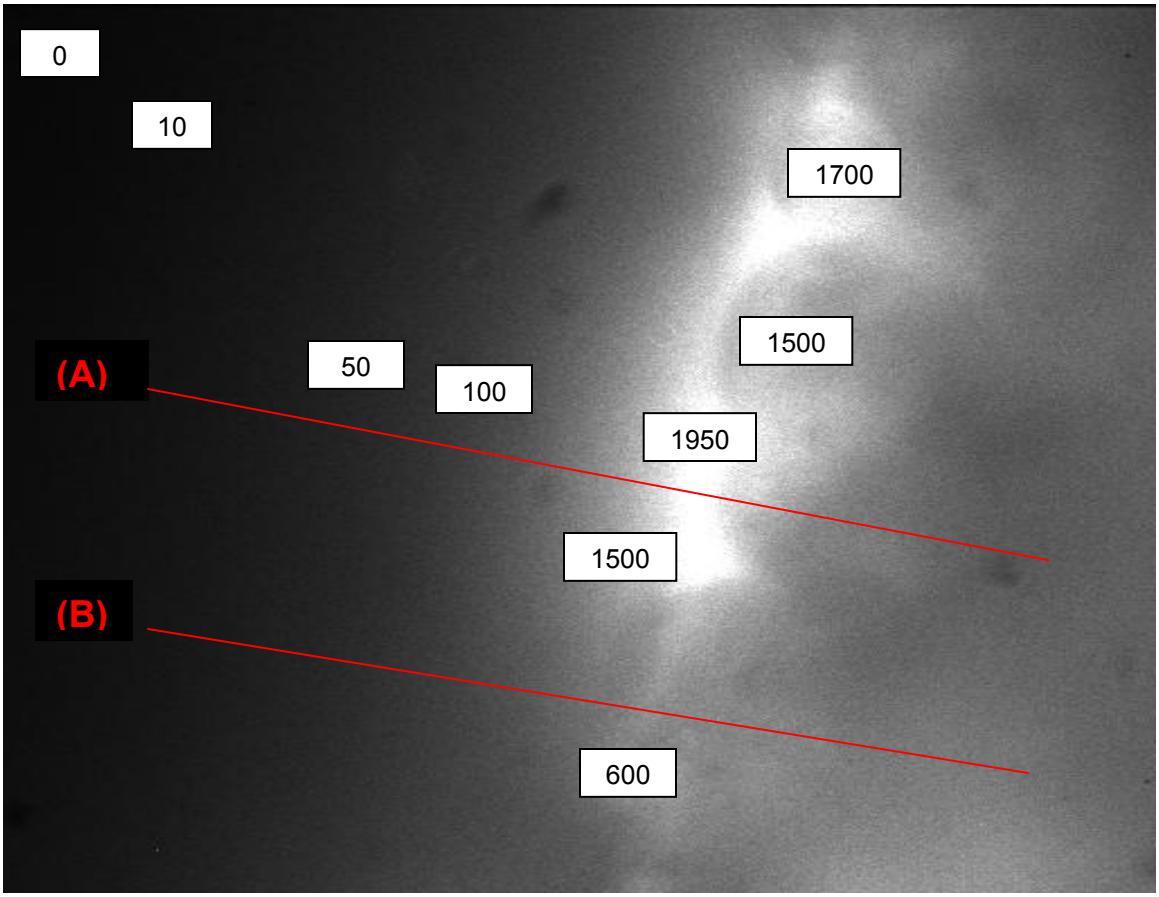

Figure 8: **Image of a Calu-3 cells monolayer viewed at 90º using the side-view microscope.**

The image illustrates that the ASL is unequally spread over the cell monolayer.(A) Linescan passing through a thick layer of ASL and (B) linescan passing through a dehydrated area of the cell monolayer. Numbers on the figure are the pixel intensities in that specific area. On the right of the image is the cell monolayer, covered by the ASL (white area of the image), while the left side of the image is the air layer. The cell monolayer and air layer are separated in this image by the ASL.

Figure 8 depicts that at any given slice of ASL analysed, we obtain a different ASL height, therefore making the height calculations complicated and imprecise. Furthermore, some areas of the epithelium are mostly

dehydrated, while other areas are well hydrated. With this information, we decided to evaluate the ASL as liquid volume per unit of the cell monolayer surface area.

The first step of the image analysis consisted of eliminating the background fluorescence that surrounds the ASL. This was accomplished by determining the intensity of pixels that are outside the ASL and determining the minimal intensity (threshold) of the pixels within the ASL image. To do so, a line-scan across the image of the ASL patch and its surrounding was made, and pixel intensity along that line was plotted (Fig 8). The intensity of pixels located clearly outside the ASL was determined as background fluorescence (ex: intensity of 1500 and below), while pixels above this threshold, for example very bright pixels that had intensities anywhere from 1500 to 1900, were considered as part of the ASL (Fig 8). Secondly, we calculated the surface area of the pixels that were included in the ASL. With the images taken at different times during the experiment, we tabulated the surface area of ASL at each time point.

In order to determine the best way to obtain an initial threshold intensity value, an image of a 4μm microbead was taken and analysed with our set-up. The analysis demonstrated that a 4μm microbead caused a certain amount of background fluorescence, giving the impression that the microbead was larger in diameter, due to the background fluorescence. In order to find the proper cut off point, a linescan analysis was performed

using the Metavue program, which produced a graph of the intensity profile across the entire field. It was determined that the 4μm length (diameter of microbead) corresponds to half of the maximum value of the peak height. Thus, the half maximum principle was used to find the pixel intensity threshold that delimits the ASL area and to select the pixels of interest. At this point, the ASL area selected and the integrated intensity of the ASL was tabulated using Metavue. According to the initial integrated intensity value, which stays fairly constant during the experiment (unless we are drying the filter or ASL is moving out of our field of view) we can analyse the set of images in an experiment. This technique allows the detection of even minute ASL volume changes.

1.5. Hypothesis and objectives

The aim of this study was to develop an imaging system allowing the direct monitoring of ASL height during purinergic stimulation. In order to test our technique, we will examine the functionality of the autocrine purinergic loop in different pulmonary epithelial cell models and whether the modification of the loop can alter ASL volume.

1.5.1. Side-view imaging technique

The objectives of this project were to (1) further develop a system that allows the direct monitoring of ASL, in real-time, under conditions that mimic

the pulmonary micro-environment and, (2) to develop an analysis method that will allow the quantification of the ASL volume.

1.5.2. Autocrine purinergic loop

The completion of the side-view imaging technique will allow us to pursue a project related to the autocrine purinergic loop. Our lab has previously demonstrated that the purinergic loop operates in A549 cells [86], therefore we want to investigate whether this loop operates in other pulmonary epithelial cell types. The objectives of this study were (1) to examine whether the autocrine purinergic loop operates in different airway epithelial cell models and (2) to verify, with our technique developed in the first section of this project, whether or not the presence of the autocrine purinergic loop will contribute to the modification of the ASL volume.

We hypothesize that the autocrine purinergic loop occurs in all pulmonary epithelial cells, with an overall response depending on the type and level of expression of cell surface purinergic receptors, as well as the cell's ability to secrete nucleotides upon the stimulus.

CHAPTER 2:

Manuscript 1

Method for evaluating Surface Liquid volume of *in vitro* Airway Epithelial Cell Cultures with Epifluorescence Microscopy

David Dubois, Sabina Tatur, Hélène Chabot and Ryszard Grygorczyk

Submission to the *American Journal of Physiology*, Methods section, 2010

Method for evaluating Surface Liquid volume of *in vitro* Airway Epithelial Cell Cultures with Epifluorescence Microscopy

David Dubois, Sabina Tatur, Hélène Chabot and Ryszard Grygorczyk

Research Centre, Centre Hospitalier de l'Université de Montréal (CHUM) – Hôtel-Dieu, and Department of Médicine, Université de Montréal, Montréal, Québec, Canada

Running title: ASL Imaging with Epifluorescence Microscopy

Abstract

Lung epithelial cells are covered by a thin, typically <10 µM layer of airway surface liquid (ASL), whose height is of vital importance for proper functioning of airway clearance mechanisms. ASL regulation studies utilizing *in vitro* epithelial cell models are hampered by a lack of appropriate and affordable techniques for monitoring ASL height with sufficient precision in real-time and are limited to complex laser scanning confocal microscopy (LSCM). In this study, we describe an alternative approach; a side-view imaging technique, which permits real-time recording of ASL height variations on airway epithelial cultures, using conventional epifluorescence microscopy. The system requires a custom-designed side-view chamber mounted on the microscope stage, equipped with a temperature/humidity control system to maintain cells at air/liquid interface (ALI), with controlled temperature, humidity and air flow, closely mimicking the lung micro-environment. A cell monolayer grown under ALI conditions, on the filter membrane of a Millicell® insert, is mounted in a chamber and its surface is tilted at 45º or 90º to the microscope objective. In this orientation, fluorescently labelled ASL can be directly observed by epifluorescence microscopy to evaluate its height and volume. Our technique is comparable to LSCM, but our system has several extra advantages: real-time imaging with an acquisition time of about 100ms, a micro-environment that closely mimics the lung environment, and the real-time treatment of cells with pharmacological tools of choice, all while monitoring ASL volume changes. By treating 16HBE14o$^-$ and Calu-3 cells with different ASL modulating pharmacological tools, we have demonstrated the feasibility of precise ASL volume monitoring using our side-view technique.

Keywords: optical system, side-view microscopy, epifluorescence microscopy, airway surface liquid height, humidity chamber, airway epithelial cells

INTRODUCTION

The airway epithelium which lines the entire respiratory tract is covered by a thin ASL layer measuring *in vivo* 7 µm to 70 µm in height [1]. The ASL defends the lung against infectious and noxious agents, and conditions inhaled air which is associated with the so-called 'insensible water loss' from the ASL [2]. The ASL volume is a key parameter in normal airway physiology and its deficiency is thought to contribute to the pathophysiology of cystic fibrosis, asthma, and other diseases of the airways [3]. Up to date, the ASL height of bronchial and trachea cell cultures has been studied by laser scanning confocal microscopy (LSCM) [2, 4, 5]. However, this expensive and complex technique has downsides, such as low temporal resolution and photobleaching. Accordingly, the acquisition of an image or a sequence of images can take several seconds up to 1 min depending on the chosen image resolution. These limitations preclude the possibility of real-time observation of ASL height alterations upon a cell stimulus. Furthermore, laser scanning causes photobleaching and photodamage to the cells because of the exposure to laser light of high average operating power [6], an outcome which may alter the cell response to a stimulus.

Side-view imaging of the ASL, which would directly record the profile of the ASL, could obviate these problems. Several approaches for side-view imaging with a routine microscope have already been developed [7-12]. All of

these techniques were applied to single cell observation with phase contrast illumination, and the cells were cultured on solid substrata under liquid-covered conditions. None of these techniques was, therefore, suitable for ASL height observation.

We developed a novel approach for side-view ASL observation based on conventional epifluorescence microscopy. The cells were cultured on a filter membrane of a modified Millicell® insert, under air-liquid interface (ALI) conditions, and mounted in a chamber which allowed direct side-view imaging of the ASL profile. The ASL height could be measured with accuracy equal to LSCM with the advantage of faster image acquisition (~ 100 ms). The short illumination and acquisition time make real-time monitoring of ASL height alterations possible, limiting at the same time the phototoxic effects on the cell culture. Furthermore, a technique in which the filter is tilted at a smaller angle (≤45°), allows us to monitor and calculate not only the ASL height at a given point, but also the ASL volume of the cell monolayer.

MATERIALS AND METHODS

Filter Preparation and Cell Culture

In this study we used the 12 mm Millicell® inserts with a 0.6 cm^2 membrane area (PIHA01250; Millipore Corp., Billerica, MA, USA) with cells grown on the outer surface of the filter membrane. For 90˚ ASL observations, i.e. with surface of cell culture perpendicular to microscope stage (parallel to the optical axis of the objective) the inserts were modified as shown in Fig. 1A, to remove the rim of the polystyrene cylinder, which would otherwise obscure direct side-viewing of cells and the ASL. The modification was accomplished manually with a scalpel, working under sterile conditions. For 45˚ observations, the above modifications were unnecessary and unmodified filters were used. The outer surface of the filter membrane was coated with type I collagen (120 µl/insert, Vitrogen-100; Collagen Corp., Palo Alto, CA, USA) and left to dry overnight at 37°C and neutralised by washing with PBS before seeding the cells.

The Millicell® inserts were placed into autoclaved biocompatible Tygon® tubing pieces (# 54007; United States Plastic Corp., Lima, OH, USA) with outer membrane surface facing upwards. The Tygon tubing enabled the deposition of culture media, seeding and culturing cells on the outer side of the filter membrane. Initial experiments were performed with the human bronchial epithelial cell line 16HBE14o$^-$, a generous gift from Dr. D. Gruenert, The cells were seeded at a density of 2.5 * 10^5 cells*cm^{-2} in DMEM: F-12 (Gibco, # 12400-024) supplemented with 2% Ultraser G (Life Technologies, Paisley, UK), 1.2 g*l^{-1}

$NaHCO_3$, 100 $U*ml^{-1}$ penicillin, 100 $\mu g*ml^{-1}$ streptomycin, and 2 mM L-glutamine. After 2 days of culture (37°C, 5% CO_2) the excess medium was removed from the apical side and cells were afterwards cultured under air-liquid interface (ALI) conditions [13]. The medium on the basal side of the filter was replaced every 48 hours. The cells were used for experiments between day 7 and day 12 after seeding. Calu-3 cells were obtained from the American Type Culture Collection (ATCC #HTB-55, Manassas, VA, USA) and were grown in MEM medium already containing glutamine (Gibco # 61100-061, Burlington, Canada), and supplemented with 1.2 $g*l^{-1}$ $NaHCO_3$, 100 $U*ml^{-1}$ penicillin, 100 $\mu g*ml^{-1}$ streptomycin, 10 mM non-essential amino-acids, 100 mM sodium pyruvate and with 15% FBS gold (PAA laboratories Inc., Ontario, Canada). The medium was replaced every 48 hours and the cells were used for experiments at about 3 weeks post-seeding. All constituents of the culture medium were from Gibco-BRL, Burlington, ON, Canada, unless otherwise specified.

ASL and cell fluorescent labelling

To label the ASL, 50 µl of an Alexa Fluor 488 (or 594) conjugated Dextran (10 kD; Invitrogen-Molecular Probes, Kingston, ON, Canada) was deposited on top of the cell monolayer for approximately 1 min. The excess liquid was then aspirated and cells were placed in the incubator (37°C, 5% CO_2) for 1h to recover their original ASL volume. For confocal microscopy measurements, 2 $mg*ml^{-1}$ Alexa Fluor Dextran in PBS was used, whereas for epifluorescence microscopy measurements the solution was further diluted to 2 $\mu g*ml^{-1}$ in PBS, in

order to reduce background fluorescence coming from beyond the focus plane. In some experiments the cell membrane was stained either with 5-hexadecanoylaminofluorescein (HAF, 10 $\mu g*ml^{-1}$) or dapoxyl sulfonic acid (DSA, 10 µM), by covering the cell culture with 30 µl PBS containing HAF or DSA, for 5 minutes. The cells were then rinsed with PBS. During all control experiments, the cells were perfused from the basal side with physiological saline solution (PS) which contained (in mM): 140 NaCl, 5 KCl, 1 $MgCl_2$, 1 $CaCl_2$, 10 glucose and 10 HEPES, pH 7.4 adjusted with NaOH. All PS components were obtained from Sigma-Aldrich Canada, Ltd., Oakville, ON. HAF and DSA were purchased from Invitrogen-Molecular Probes, Kingston, ON, Canada.

The following excitation filters and emission filter blocks (Chroma Technology Corp., Rockingham, VT, USA) were used: a 495 nm excitation filter with a GFP filter block was used for Alexa 488 and HAF, a 340 nm excitation filter with a Fura-2 filter block was used for DSA, and a Texas Red filter block was used for Alexa 594.

The side-viewing imaging setup

For side-view imaging the the Millicell® filter insert with cells grown on the outer surface of the filter membrane was attached to a custom built holder inside a minincubator chamber resting on the stage of a Nikon TE300 inverted microscope (Nikon Canada Inc., Montreal, QC), equipped with an epi-fluorescence illumination system and ELWD CFI objective (Nikon, 40x/0.60, WD 3.7-2.7, CR 0-2). The holder, Fig. 1B, was made of non-fluorescent black delrin

and comprised a knob with six inlet and one outlet channel. The inlet channels were coupled to an in-line heater (Warner Instrument Corp., Hamden, CT, USA) and a peristaltic pump (Gilson Miniplus 3, Worthington, OH, USA), which continuously provided the cells with warm PS (37°C, 0.5 ml*min^{-1}) on the basal side. The knob was designed to rotate the filter insert with cells around its axis and was secured by a fixation screw. This feature was useful for inspecting the entire circumference of the cell monolayer. The mini-incubator was made of non-fluorescent black delrin (Fig. 2A), and connected to a temperature and humidity control system (Fig. 2B). The temperature and humidity sensors were placed close to the cell monolayer on both sides of the filter holder inside the mini-incubator, to precisely control its microenvironment. The system allowed the controlled maintenance of the mini-incubator at an air temperature of 37°C, with air flow rate typically of 6-8 l/min, and 80-95% humidity to minimize insensible water loss from the cell surface. Warm, humidified air entered the incubator from the bottom and was leaving through an opening at the top. This opening also allowed for brightfield illumination of the cell culture during initial positioning of the filter insert, and locating region of interest.

The temperature and humidity control system Air-Therm^{TM} ATX Humidifier (ATX-H) (World Precision Instruments, Inc., Sarasota, FL, USA), consisted of an air heater connected to an ultrasonic humidifier (Fig.2B). The air continuously circulated in a closed circuit and was coupled to the microscope stage mini-incubator via a coupling valve and tubing branching off the main circuit. The warm, humid air was fed into the incubator from underneath the

microscope stage and along the surface of the cell culture mimicking the *in vivo* conditions in the airways. This arrangement also prevented the objective from being in the direct path of the humid air flow, thus, keeping the objective fog free. Furthermore, the objective was preheated to 40°C, using a custom built objective heater, avoiding fog formation. The whole set-up was flushed with dry warm (37°C) air for about 1 hour before turning on the humidifier. This procedure prevented water condensation on any part of the system. Since inhaled air, *in vivo*, is gradually humidified up to 100% relative humidity by the upper airways [14], the humidity in the mini-incubator needed to reach similar levels. In our system, the relative humidity at the cell culture surface varied between 85% and 90% at a steady temperature of 37 ±1 °C. High humidity minimized evaporative water loss from the ASL, allowing the monitoring of ASL volume without covering it with a protective layer of e.g. perfluorocarbon, a typical approach used by other investigators [4, 5, 15].

Calibration and evaluation of ASL fluorescence intensity profile

To calibrate the system for ASL height determination, from the fluorescence intensity profile, an image of yellow-green fluorescent microbeads (505/515) of 4 µm diameter (# F8859 Invitrogen-Molecular Probes, Kingston, ON, Canada) was taken and their fluorescence intensity profiles were plotted. The width at the half peak of the fluorescence intensity curve was close to the 4 µm value corresponding to the bead diameter. Accordingly, a line was made perpendicularly crossing the ASL, and this line was used to determine the ASL

height. The width, at half the peak of the ASL fluorescence profile curve, was the actual ASL height.

Image Acquisition and Analysis

During experiment the microscope was focused on the lower edge of the vertically-oriented filter with the cell culture and the brightfield or fluorescent side-view images of the cell monolayer and ASL layer were acquired with a monochromatic T57 Micromax CCD camera (Princeton Instruments, Trenton, NJ, USA) under control of MetaVue software (version 7.0, Molecular Devices Corp., Sunnyvale, CA, USA). The camera chip had 512 × 512 imaging pixels with an individual pixel size of 13 µm. The acquired images were initially processed using MetaVue software (Molecular Devices Corp., Sunnyvale, CA, USA). Background flattening was applied to reduce stray light coming from fluorescence beyond the plane in focus. This procedure subtracted the large gradient of background fluorescence and revealed additional details without loosing image data. A line scan across the image and passing through the ASL produced a fluorescence intensity profile from which the ASL height was determined.

Considering that ASL isn't spread homogeneously over the entire cell monolayer (see Results), the ASL height at any arbitrary point is not a good measure of ASL volume. Therefore, the volume of fluorescently-labelled liquid per surface area (in µl/cm^2) was evaluated. To do so, we measured the area of

the ASL cross-section, as observed in 45º side-view images, and were able to calculate the ASL volume of the cell monolayer.

The images were analyzed using Matlab software (The Mathworks Inc., Natick, MA, USA). The program counted pixels above a certain threshold of brightness, which was set to half the difference between the background and the pixels within the ASL of maximal fluorescence intensity.

Confocal Microscopy

For comparison of our side-view imaging technique some experiments were also performed with a confocal laser-scanning microscope. Images of fluorescently labelled ASL were recorded using a TE300 inverted microscope (Nikon Canada Inc., Mississauga, ON) equipped with a confocal laser-scanning system (BioRad MRC 1024, Hercules, CA, USA) and a monochrome CoolSnap-Fx CCD camera (Photometrics, Tucson, AZ, USA). The camera chip had 1300 × 1030 imaging pixels with an individual pixel size of 6.7 μm. The ASL height was determined by scanning the x-y-plane and x-z-plane [1, 3]. Each scanning plane was separated by 1.2 μm. The images were analysed using the Confocal Assistant software version 4.02 (© Todd Clark Brelje). While x-z scanning directly displayed side-view images of the ASL, the x-y-scanning planes had to be merged and processed to generate a side-view image of the ASL.

RESULTS AND DISCUSSION

Monitoring ASL by 90˚ side-view approach

To verify the evenness and smoothness of the Millicell® insert after its modification, we took side-view images of the Millicell® insert with and without cell culture. Fig. 3A shows brightfield images of the modified insert without cell culture (left side) and with a cell monolayer (right side). Whereas the Millicell profile without cell culture was even and flat, the profiles with a cell monolayer appeared undulated. All profiles in brightfield illumination clearly displayed an airy pattern as a result of light diffraction at the air-cell frontier line. Fig. 3B shows a side-view image of fluorescently labelled ASL, the fluorescence intensity profiles at three different locations are displayed on the right side of the image. The fluorescence intensity profiles of three different locations are displayed on the right side of the image. The width of the fluorescence peak corresponds to the ASL height and, at the half peak level it measures between 4 and 6 µm. On the cell side the fluorescence is slightly elevated compared to the side facing the air compartment, likely due to uneven monolayer surface and scattering of fluorescence light by cells.

To validate the results obtained with epifluorescence side-view microscopy, the ASL height of 16HBE14o$^-$ cell cultures was evaluated with confocal microscopy. Fig. 4A was recorded by rapid x-z-scanning and is displayed unprocessed. In comparison with Fig. 3B, we notice that both images depict similar characteristics and that the ASL height determined from both

pictures is aso comparable measuring 5 ± 1µm. Fig. 4B was also generated by confocal microscope, but from x-y-scans. The resolution along z axis is determined by the distance of the scanning planes, which was chosen to be 1.2 µm, in order to keep the acquisition time reasonably short. Although the resolution is evidently lower than in Fig. 4A (confocal) and Fig. 3B (side-view epifluorescence), the ASL height can still be estimated to be around 5 µm. From Fig. 3 and Fig. 4, it is clear that our side-view imaging technique compares favourably with the confocal microscopy technique, having similar resolution and the ability to evaluate ASL height and volume.

To verify that our technique allows real-time detection of SL volume changes, Calu-3 cell cultures were used and were subjected to interventions expected to modify the SL volume. The SL volume was quantified from SL cross-sectional areas, using Matlab (see Methods). Figure 5A depicts flurescently-labelled SL images observed during hypotonic shock that was applied by basolateral perfusion of a 50% HS. The time-course shown in Fig. 5B, demonstrates that SL volume increased within 6 min > 60% (from 0.4 to 0.65 µL/cm^2) in response to 50% hypotonic shock. Returning to PS resulted in the restoration of the SL volume near its basal level within 5 minutes. When we stopped perfusion allowing the SL to dry its volume rapidly decreased significantly below the basal level within 10-12 min. The time course experiment clearly demonstrated that real-time imaging and quantification of the ASL is possible using this technique. Although the 90˚ side-view imaging technique

permitted real-time monitoring of SL volume an important set-back was that only the cells at the edges of the filter could be monitored. The distance is limited by the objective working distance, which for the 40x was 0.8 mm. The SL height at the filter edge might differ from that deeper in the monolayer. This limitation could be overcome, however, by imaging the cell monolayer after tilting the filter insert at a 45º angle.

45º Imaging

To monitor the cells throughout the entire monolayer of cells (i.e. filter scanning), a 45º imaging technique was developed. To do so, a square piece of solid fibreglass was custom cut, in order to form a triangle with an angle of 45º. This extra piece was used as a base for our filter holder, which fit onto the microscope stage and kept the filter at a 45º angle for the entire experiment. Using this technique, it was possible to scan the entire cell monolayer in order to find areas/cells of interest. Furthermore, 45º imaging is performed without having to modify the filter insert, which was an extremely time consuming and difficult procedure. Examples of the three different views, including 90° side-view imaging, top-view imaging and 45° imaging are shown in Fig. 6. When analyzing an image at a 45º angle, the angle difference should be taken into account when measuring the ASL height (Fig. 7). The following equation must be applied when calculating ASL height at a certain point: ASL height (h) = w / $\sqrt{2}$. When monitoring ASL volume changes, this angle doesn't need to be accounted for in

the calculations because we are calculating the ASL volume of an image as a whole.

Using this new procedure, Calu-3 cells were treated with a 50% HS, similar to the experiment showed in the previous section, causing an increase in ASL volume. These changes were perfectly observable at 45º. The acquisition of many pictures (Fig. 8A), at different time points, allowed us to complete a 50% HS time course (Fig. 8B). In this experiment, we observed a similar increase in ASL volume, peaking at 20 minutes post HS, with a 2 fold increase in ASL volume. Returning the cells in PS led to the restoration of the ASL near its basal volume, within 5 minutes of the start of PS infusion. Furthermore, treatment of Calu-3 cells with thapsigargin (Tg), an inhibitor of a SERCA (sarco/endoplasmic reticulum Ca2+ ATPase) known to cause an intracellular calcium spike, was expected to result in a transient increase in ASL volume [16, 17]. To further demonstrate that our technique could allow the visualization of these changes, images were taken at different time points (Fig. 9A), and then a time course of ASL volume changes was completed (Fig. 9B). The experiment started with simple PS perfusion to the Calu-3 cells. The first two images, taken at t = 0 and t = 5 minutes, demonstrate that without a potent stimulus of the autocrine system, the ASL volume didn't change significantly. After 8 minutes of PS perfusion and no observable change in ASL volume, we treated the cells with 1µM Tg solution. After 10 minutes (3 min of Tg perfusion), we notice a transient increase in ASL volume. After the peak in ASL volume, the ASL volume decreased despite the

cells still being perfused with Tg solution. The results from these experiments demonstrate the facility and accuracy of our technique for the real-time monitoring of ASL volume.

CONCLUSION

A precise adjustment of surrounding temperature and humidity was essential for accurate and reproducible measurements of the ASL height on living cell cultures. The temperature and humidity system allowed the control of the temperature inside the stage mini-incubator to ± 0.5°C and the air humidity to a precision of ± 3%. The perfusion system on the side-view chamber supplied the cells with warm (37°C) solution to nourish and bathe them from the basal side. Both a humidity level of 85-90% and a continuous perfusion of the basal side of the cell monolayer were necessary to prevent the cell monolayer from drying out. During short-term experiments (up to 30 min), the cells were perfused with PS. For specific cell stimulation, selected drugs were added to PS and perfused basolaterally onto the cell monolayer.

The temperature and humidity control system, together with the stage set-up for side-view imaging, allows real-time imaging of ASL height/volume and its variations during cell stimulation with epifluorescence microscopy. This technique provides similar images to confocal microscopy, with the advantage of requiring a considerably lower acquisition time, as well as real-time monitoring of the ASL following stimulation with pharmacological tools. Images recorded by epifluorescence microscopy and confocal x-z-scanning have a comparably high resolution ($r = 0.65$ and 0.5 µm, respectively), whereas the resolution of the calculated images from x-y-scanning confocal microscopy is noticeably lower ($r = 1.2$ µm) and limited by the distance of the scanning planes. However, x-y-

scanning confocal microscopy had the advantage of not being limited to the edge of the filter membrane of the Millicell® insert and generates ASL images throughout the filter area. For this reason, the 45º angle monitoring technique was developed, which allows the scanning and image acquisition throughout the entire filter area, providing all the advantages of confocal microscopy, without its disadvantages. Although the recent advancements in this system have allowed for more versatility with the side-viewing technique, image analysis remains the main area of improvement. Finally, this technique could also be useful for real-time imaging with other cell lines, and in many other fields of research.

ACKNOWLEDGEMENTS

This study was supported in part by the Canadian Institutes of Health Research and the Canadian Cystic Fibrosis Foundation (CCFF). D.D. and S.T. were the recipients of CCFF studentships. The authors acknowledge Jean Soucy (Atelier d'usinage du Groupe technologique de l'Université de Montréal) for manufacturing the set-up components, and Denis Flipo (Département des sciences biologiques at the Université de Québec à Montréal) for assistance with the acquisition of the confocal microscopy images.

Figure legends:

Figure 1: Modification of Millicell® inserts for cell culture growth and incorporation into the filter holder.

A. Manual modification of the Millicell® insert: the rim of the polystyrene cylinder was cut away with a scalpel, under sterile conditions, for obstruction-free cell side-view observation.

B. Three-dimensional view of the custom made side-view chamber, accommodating the Millicell® insert with a cell culture grown on the outer side of the filter membrane. The chamber consists of a chamber frame which fits on a microscope stage and a filter holder with inlet and outlet tubes to supply the basal side of the cell monolayer with physiological solution.

Figure 2: Set-up components and system arrangement.

A. Cross-section of the complete microscope stage assembly. The stage assembly consists of a stage ring with an air-inlet tube, an incubator and the side-view chamber. The microscope condenser illuminates the cell profile through the top opening of the incubator for brightfield images. Recorded brightfield and fluorescent images of the cell profile are shown at the bottom right. The cells in the right image were stained with HAF, fluorescent cell dye.

B. Temperature and humidity control system connected to the microscope stage assembly. The air circulates in a closed circuit and is coupled to the stage incubator via a coupling valve through the air-inlet tube of the stage ring. A small opening behind the coupling valve regulates the air pressure within the circuit. Two sensors, one for humidity and one for temperature, are placed in the micro-incubator from the top, near the cells, in order to regulate the entire system.

Figure 3: Side-view images recorded by epifluorescence microscopy.

A. Two brightfield images of the modified Millicell® insert without cell culture (left) and with cell culture (right). The picture on the right was cultured using 16HBE14o$^-$ cells, cultured for 12 days under ALI conditions. Images were taken with an ELWD 40X objective.

B. Fluorescence image of the ASL of 16HBE14o$^-$ cells, labelled with Alexa Fluor 488 Dextran recorded with a conventional epifluorescence microscope (illumination time: 100 ms). The fluorescence intensity profiles at three different

locations are displayed separately on the right side and superimposed below the image, taken with the ELWD 40X objective.

Figure 4: Side-view images of 16HBE14o- cells, by confocal microscopy. The ASL was stained with Alexa Fluor 488 Dextran.

A. X-Z fluorescence image of the ASL, reconstructed from y-z sections recorded by scanning confocal microscopy.

B. X-Z fluorescence image of the ASL of recorded by x-y-scanning confocal microscopy.

Figure 5: 50% HS time course with Calu-3 cells, using 90º side-view imaging.

A. Images of Calu-3 cells were taken with the 90º side-view imaging technique. Calu-3 cells were cultured on the filter for 3 weeks before the experiment. Images were acquired using the ELWD 40X objective, and the ASL was stained with Alexa fluor 488 dextran.

B. Time course graph of Calu-3 ASL volume during the 50% HS.

Figure 6: Comparison of side-view imaging techniques and angles.

The Calu-3 cells were grown into a tight monolayer, for 3 weeks, and then treated with Alexa Fluor 488 Dextran to monitor the ASL distribution over the monolayer.

A. 90º, side-view image of the cell and ASL.

B. 180º, top-view image of the cell monolayer, demonstrating the ASL distribution is not homogenous, and that it accumulates in crests, between bigger cells, with thinner ASL volumes on the top of the cells.

C. 45º, side-view imaging of the cell and ASL demonstrates that only a thin strip in the middle of the image is in focus. The upper and lower parts of this image are therefore not in focus, therefore proper focus must be obtained to calculate the precise ASL volume.

Figure 7: ASL height in 45° side-view images

When calculating the ASL height at a 45º angle, only a single strip at the middle of the field of view is in focus. For this reason, we must account for the fact that above or below the in focus field of view, the image is out of focus. Furthermore, we need to account for the 45º angle because the ASL is viewed to the side, and not directly at 90º.

Figure 8: 50% HS time course with Calu-3 cells, with 45° imaging.

A. Images of Calu-3 cells were taken with the 45º side-view imaging technique. Calu-3 cells conditions and microscopy/ASL staining were identical to those in Fig 5.

B. Time course graph of Calu-3 ASL volume during the 50% HS.

Figure 9: Thapsigargin time course with Calu-3 cells.

A. Images of Calu-3 cells were taken with the 45º side-view imaging technique. Calu-3 cells were cultured on the filter for 3 weeks before usage. Images were acquired using the ELWD 40X objective, and the ASL was stained with Alexa fluor 488 dextran.

B. Time course graph of Calu-3 ASL volume during the Tg treatment.

A

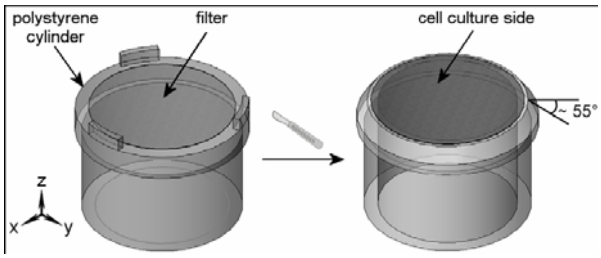
polystyrene cylinder
filter
cell culture side
~ 55°
z
x
y

B

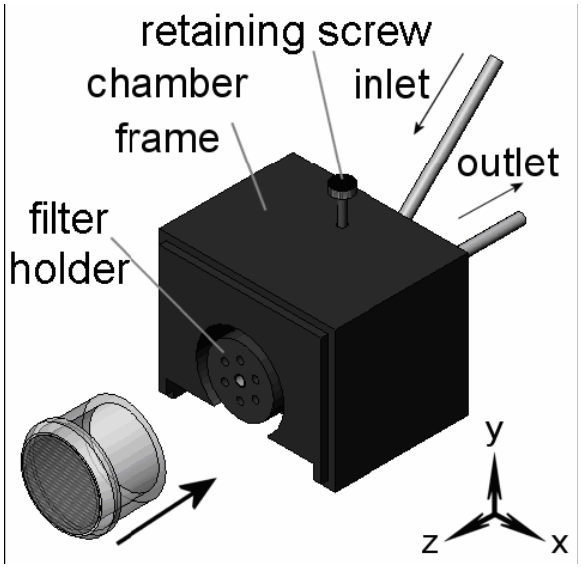
retaining screw
chamber
inlet
frame
outlet
filter holder
y
z
x

Figure 1

A

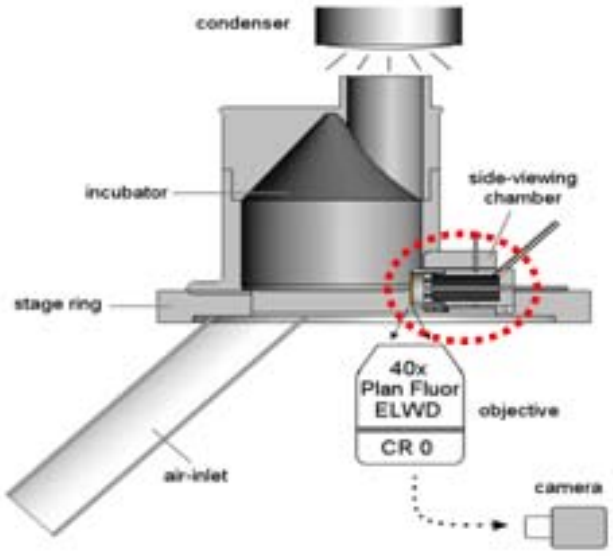
condenser
incubator
side-viewing chamber
stage ring
40x Plan Fluor ELWD
objective
CR 0
air-inlet
camera

B

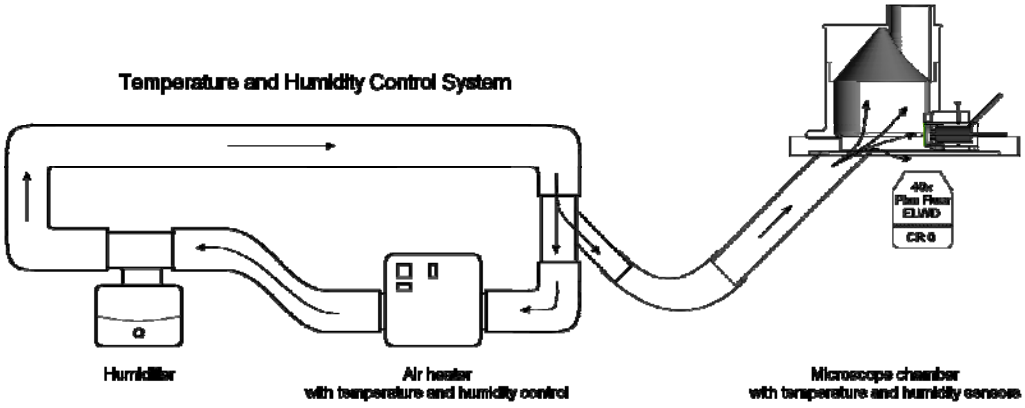
Temperature and Humidity Control System
Humidifier
Air heater with temperature and humidity control
Microscope chamber with temperature and humidity sensors

Figure 2.

A

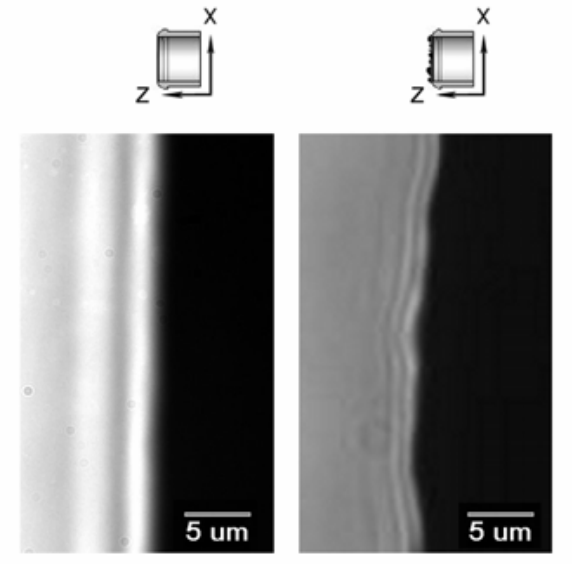
X
Z
X
Z
5 um
5 um

B

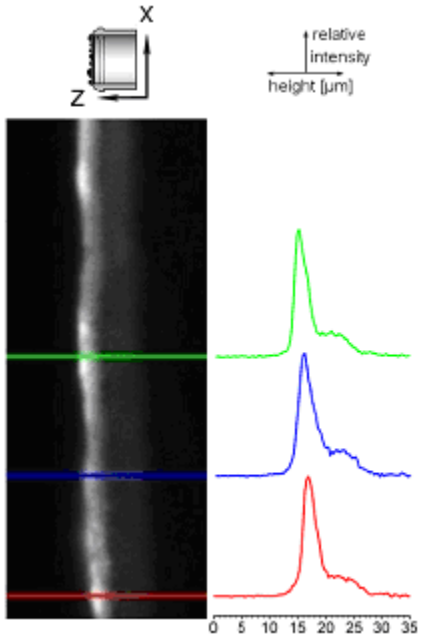
X
Z
relative
intensity
height [µm]
0 5 10 15 20 25 30 35

Figure 3

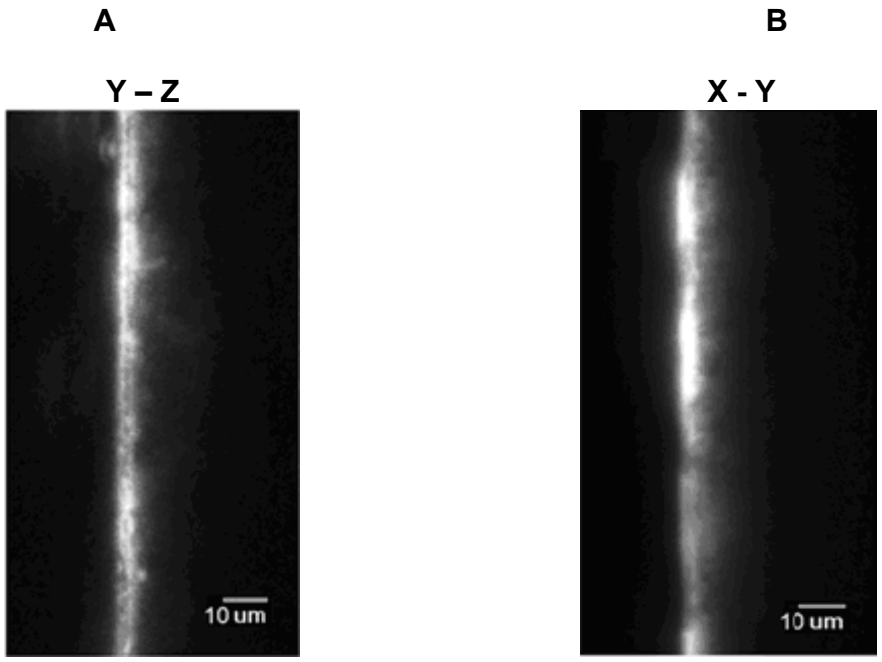

Figure 4

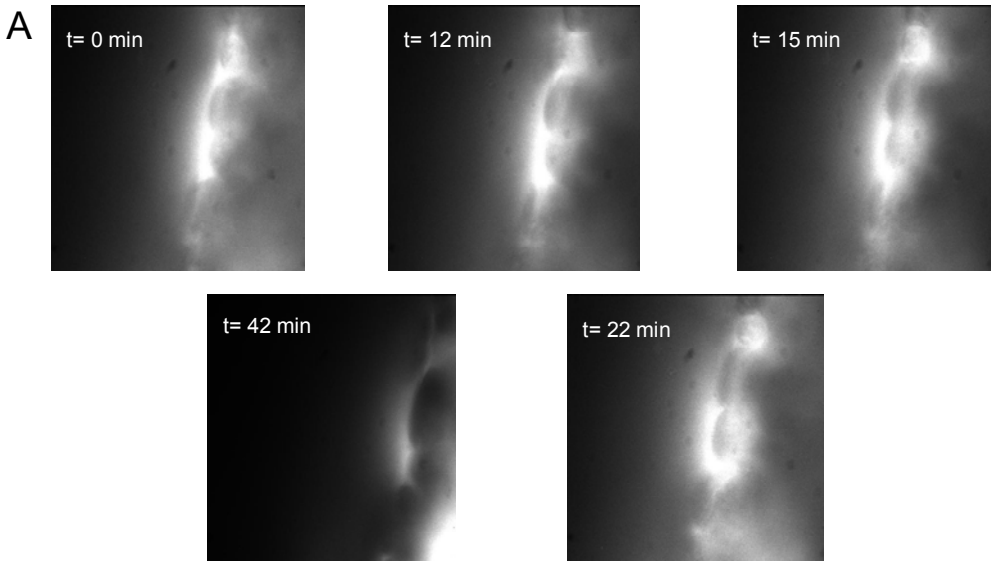
A
t= 0 min
t= 12 min
t= 15 min
t= 42 min
t= 22 min

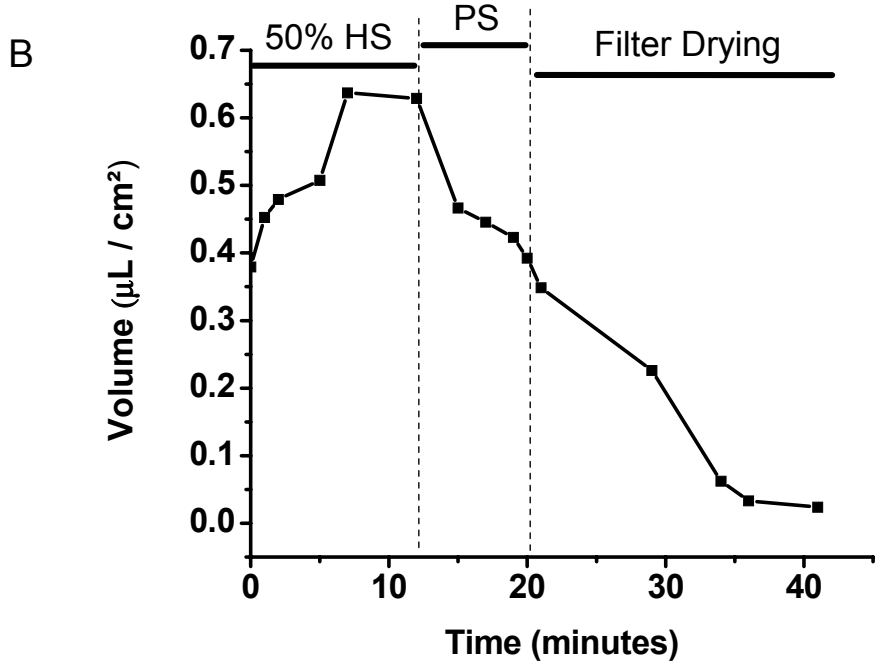
B
50% HS
PS
Filter Drying
Volume (µL / cm²)
0.0
0.1
0.2
0.3
0.4
0.5
0.6
0.7
0
10
20
30
40
Time (minutes)

Figure 5

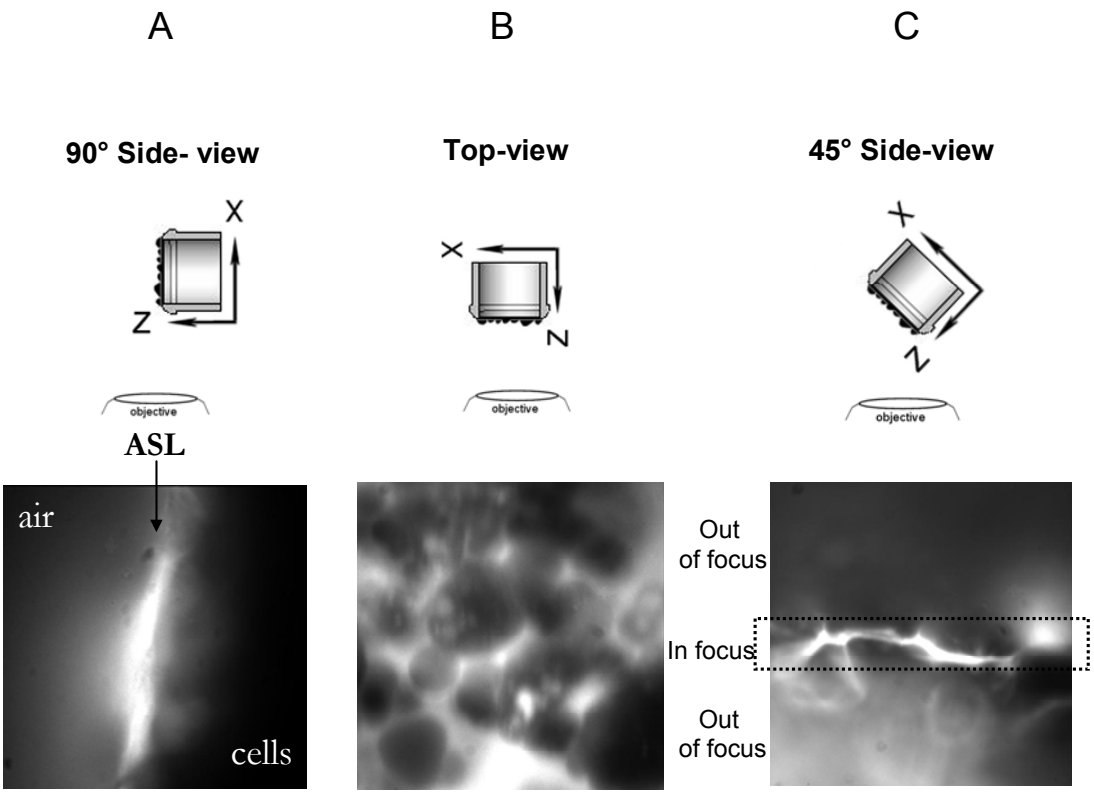
A
B
C
90° Side- view
Top-view
45° Side-view
X
Z
X
Z
X
Z
objective
objective
objective
ASL
air
cells
Out
of focus
In focus
Out
of focus

Figure 6

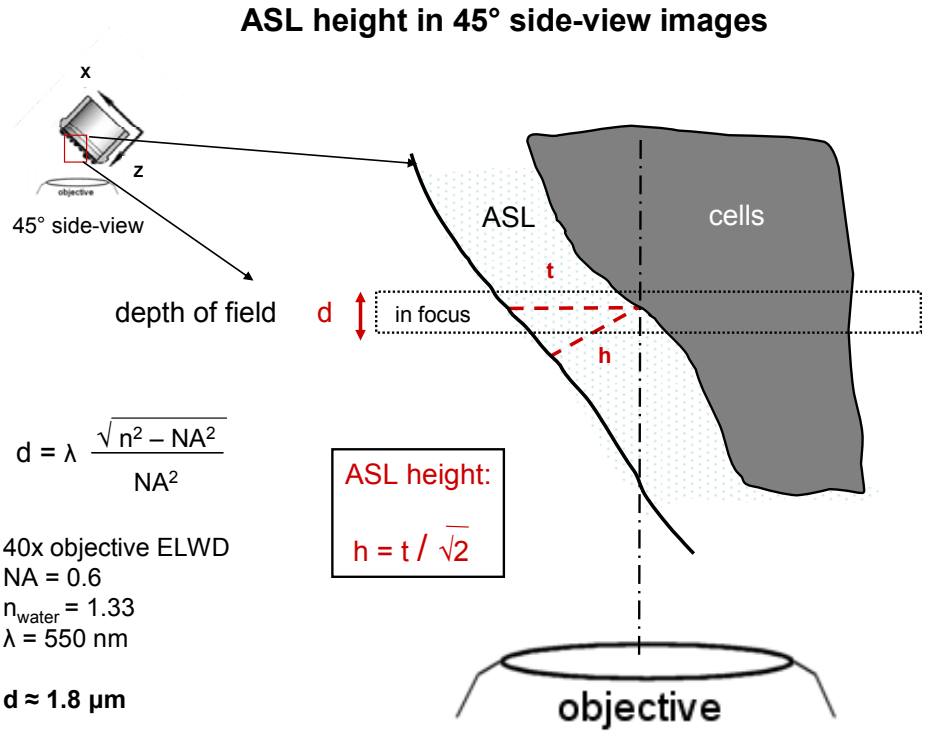
ASL height in 45° side-view images
x
z
objective
45° side-view
depth of field
d
in focus
ASL
cells
t
h
objective
$d = \lambda \frac{\sqrt{n^2 - NA^2}}{NA^2}$
40x objective ELWD
NA = 0.6
n_{water} = 1.33
λ = 550 nm
d ≈ 1.8 µm
ASL height:
$h = t / \sqrt{2}$

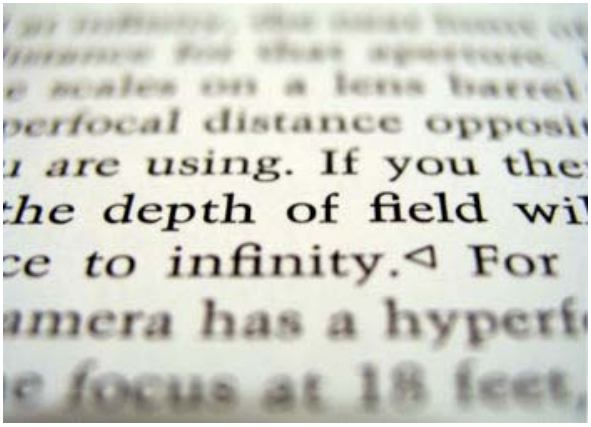
scales on a lens barrel
perfocal distance opposi
are using. If you the
the depth of field wi
ce to infinity. For
amera has a hyperf
focus at 18 feet,

Figure 7

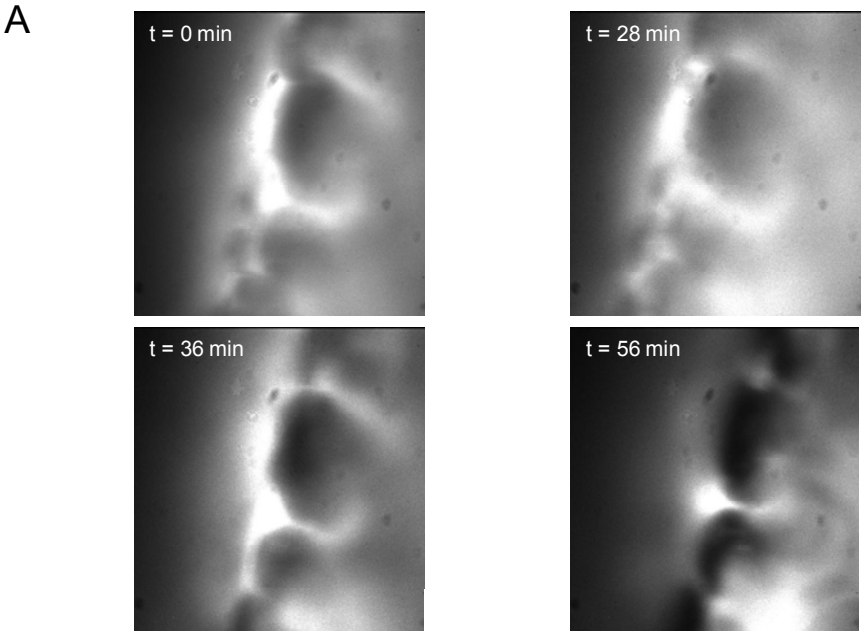
A
t = 0 min
t = 28 min
t = 36 min
t = 56 min

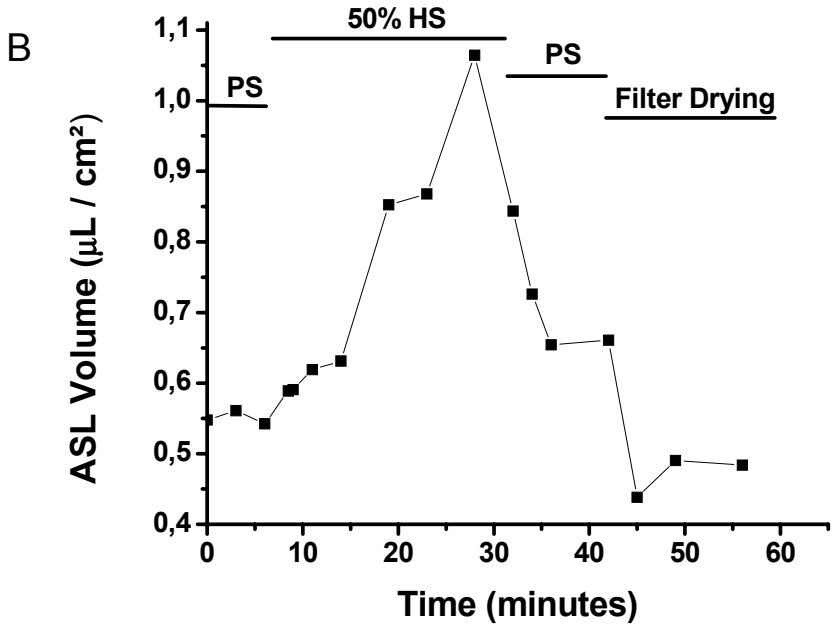
B
50% HS
PS
PS
Filter Drying
ASL Volume (µL / cm²)
1,1
1,0
0,9
0,8
0,7
0,6
0,5
0,4
0
10
20
30
40
50
60
Time (minutes)

Figure 8

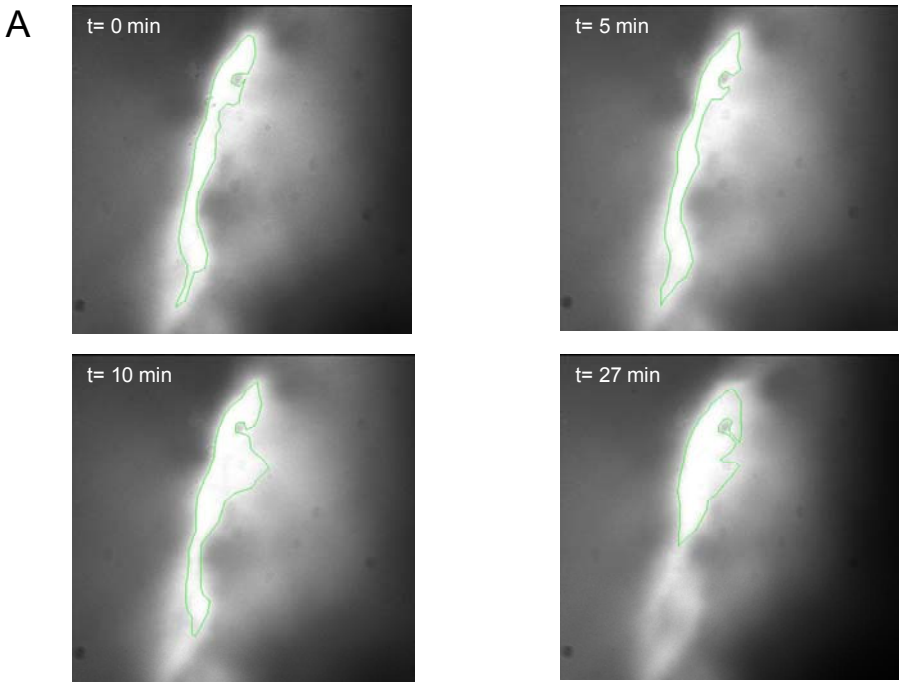
A
t= 0 min
t= 5 min
t= 10 min
t= 27 min

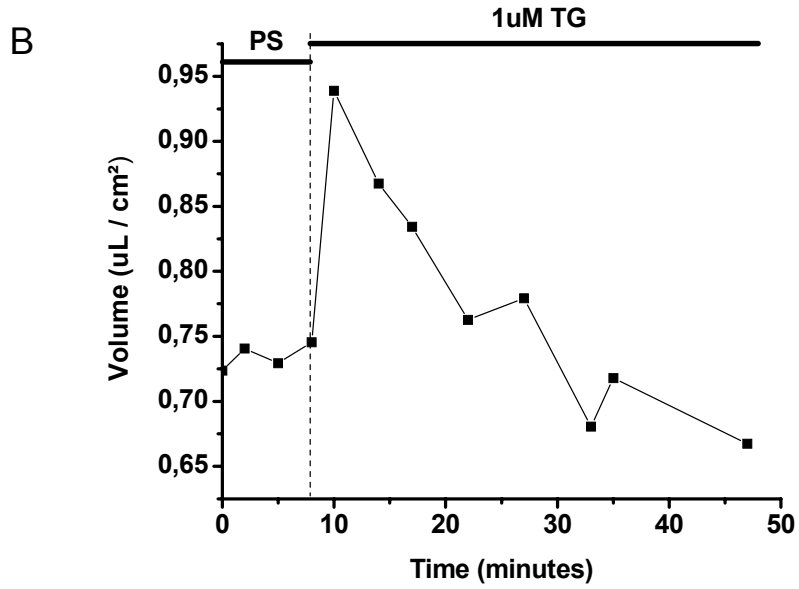
B
PS
1uM TG
Volume (uL / cm²)
0,95
0,90
0,85
0,80
0,75
0,70
0,65
0
10
20
30
40
50
Time (minutes)

Figure 9

REFERENCES

[1] Tarran, R. (2004) Regulation of airway surface liquid volume and mucus transport by active ion transport. *Proc. Am Thorac. Soc* **1** [1], 42-46.

[2] Boucher, R.C. (1999) Molecular insights into the physiology of the 'thin film' of airway surface liquid. *J. Physiol* **516** [Pt 3], 631-638.

[3] Verkman, A.S., Song, Y. & Thiagarajah, J.R. (2003) Role of airway surface liquid and submucosal glands in cystic fibrosis lung disease. *AJP - Cell Physiology* **284** [1], C2-15.

[4] Jayaraman, S., Song, Y., Vetrivel, L., Shankar, L. & Verkman, A.S. (2001) Noninvasive in vivo fluorescence measurement of airway-surface liquid depth, salt concentration, and pH. *J Clin Invest* **107** [3], 317-324.

[5] Roomans, G.M., Kozlova, I., Nilsson, H., Vanthanouvong, V., Button, B. & Tarran, R. (2004) Measurements of airway surface liquid height and mucus transport by fluorescence microscopy, and of ion composition by X-ray microanalysis. *J. Cyst. Fibros.* **3 Suppl 2**, 135-139.

[6] Piston, D.W. (1999) Imaging living cells and tissues by two-photon excitation microscopy. *Trends Cell Biol.* **9** [2], 66-69.

[7] Boocock, C.A., Brown, A.F. & Dunn, G.A. (1985) A simple chamber for observing microscopic specimens in both top and side views. *J Microsc.* **137** [Pt 1], 29-34.

[8] Boudreault, F. & Grygorczyk, R. (2004) Evaluation of rapid volume changes of substrate-adherent cells by conventional microscopy 3D imaging. *J. Microsc.* **215** [Pt 3], 302-312.

[9] Cao, J., Usami, S. & Dong, C. (1997) Development of a side-view chamber for studying cell-surface adhesion under flow conditions. *Ann. Biomed. Eng* **25** [3], 573-580.

[10] Ingram, V.M. (1969) A side view of moving fibroblasts. *Nature* **222** [5194], 641-644.

[11] Sanders, E.J. & Prasad, S. (1979) Observation of cultured embryonic epithelial cells in side view. *Journal of Cell Science* **38**, 305-314.

[12] Tsai, J.W., Yi, Y.S. & Lin, C.H. (2004) Cell Observing Method and the System Thereof. [00594011]. Patent of the Republic of China.

[13] Forbes, B., Shah, A., Martin, G.P. & Lansley, A.B. (2003) The human bronchial epithelial cell line 16HBE14o- as a model system of the airways for studying drug transport. *International Journal of Pharmaceutics* **257** [1-2], 161-167.

[14] Zuchner, K. (2006) Humidification: Measurement and Requirements. *Respiratory Care Clinics of North America* **12** [2], 149-163.

[15] Song, Y., Thiagarajah, J. & Verkman, A.S. (2003) Sodium and Chloride Concentrations, pH, and Depth of Airway Surface Liquid in Distal Airways. *J Gen Physiol.* **122** [5], 511-519.

[16] Kreda, S.M., Okada, S.F., Van Heusden, C.A., O'Neal, W, Gabriel, S., Abdullah, S., Davis, C.W., Boucher, R.C. & Lazarowski, E.R. (2007) Coordinated release of nucleotides and mucin from human airway epithelial Calu-3 cells. *J Physiol* **584** [1], 245-259.

[17] Tatur, S., Groulx, N., Orlov, S.N. & Grygorczyk, R. (2007) Ca2+-dependent ATP release from A549 cells involves synergistic autocrine stimulation by coreleased uridine nucleotides. *J. Physiol.* **584,** 419-435.

CHAPTER 3

RESULTS – not included in the manuscript

The development of a side-view imaging method, described in chapter 2, was the initial step of a wider project to determine the involvement of the purinergic loop in ASL volume control. The microscopy method developed in this study is essential to verify whether changes to the ASL volume occur following stimulation of the purinergic loop in different types of epithelial cells. Furthermore, the purinergic loop and ASL volume experiments, described in this chapter allowed us to optimize our side-view imaging system as well as our analysis method. Tatur et al. have already demonstrated the functionality of the purinergic loop in A549 cells, as well as the possibility of blocking the purinergic loop with pharmacologic modulators such as suramin and apyrase [86]. Figure 9, taken from Tatur et al. [86], depicts the purinergic loop amplification in A549 cells, which occurs due to increases in $[Ca^{2+}]_i$ followed by ATP release into the extracellular space [86]. To further pursue this issue, we set out to investigate if other pulmonary epithelial cell types, such as 16HBE14o$^-$, Calu-3 and CFBE cells, exhibit similar purinergic loop dynamics, while using our novel microscopy system to monitor the ASL changes in real-time. Figures 10 to 19 are experiments completed during the term of this project, firstly to examine the activation of the purinergic loop and conjunctly to determine whether or not this has an effect on ASL volume by utilising the side-view imaging technique. Finally, the technique developed in this project, as well as the findings on the purinergic loop will in hope eventually lead to the discovery

of pharmacological tools that will restore the ASL volume on the surface of CF epithelial cells.

In order to test for the presence of the autocrine purinergic loop in different epithelial cell models, both calcium imaging, as well as ATP efflux assay analysis methods were used. Cells used for these experiments were cultured in the same conditions as presented in the “Materials and Methods” section of chapter 2. These experiments allowed us to determine whether the autocrine purinergic loop functionality was similar in different epithelial cell types.

ATP efflux during hypotonic challenge was measured with high temporal resolution using a custom designed, low-volume (325 μl), flow-through chamber [86, 98]. A 24mm×60mm coverslip covered with a confluent cell monolayer was mounted in the chamber and perfused with a warm (37ºC, in-line SF-28 heater, Warner Instrument Co., Hamden, CT, USA) solution at 1.3 ml per minute. After an equilibration period in PS (5-15 min), a 50% hypotonic shock was applied by HS perfusion (t =0), and the perfusate was collected at 30 s intervals during the initial burst of ATP secretion (0-5 min) and every 1 min thereafter. ATP in the samples was quantified by a luciferase–luciferin-based assay, using ATP Assay Mix and ATP Assay Mix Dilution Buffer supplied by Sigma-Aldrich Canada, Ltd. ATP release rates were expressed in pmol per minute. Total ATP release was calculated by summing all ATP values collected, starting from the application of the 50%

HS, until the release rate returned to baseline, typically after about 15-20 minutes [86].

For $[Ca^{2+}]_i$ measurements, a cell monolayer at about 80-90% confluency was loaded for 30 to 60 minutes (at 37ºC) with 7 *μ*m Fura-2-AM in physiological solution containing 0.02% Pluronic F127 and 2.5mm probenecid, followed by a 30-45 minute de-esterification period in PS containing probenecid. For fluorescent imaging, a coverslip with Fura-2-loaded cells was mounted in an imaging/perfusion chamber (RC-20, volume 48 *μ*l) attached to a heated platform (P-5, Warner Instrument Co.) on the stage of an inverted microscope (Nikon TE300). The imaging chamber was perfused continuously with a warm solution (37ºC) via an in-line heater (SF-28, Warner Instrument Co.) at 0.5 ml per minute. The cells were illuminated for 100 ms with alternate light wavelengths of 340 and 380 nm, using a high-pressure mercury lamp (100W) via interference filters (Chroma Technology, Brattleboro, VT) mounted on a filter wheel (Sutter Lambda 10-C, Sutter Instrument Co., Novato, CA) and a dichroic mirror (510/540 nm, Chroma TechnologyCorp., Brattleboro, VT, USA). Fluorescence images were recorded at 5 to 15 second intervals, depending on the substance being perfused (shorter time intervals when stimulated with a 50% HS), with the digital camera images stored for later analysis. Fura-2 measurements are presented as the fluorescence *F*340/*F*380 ratio [86]. Test compounds such as apyrase and suramin were added to the perfusate during the experiments, and the 50% HS was added only after 2-3 minutes of pre-

treatment with these inhibitors. Finally, Tatur et al. demonstrated that the test compounds used in our experiments didn't interfere with Fura-2 fluorescence [86].

3.1. Testing for the presence of the Autocrine Purinergic loop in different airway epithelial cell models

In addition to the microscopy results previously described in the manuscript, calcium imaging and ATP release experiments were completed in order to test for the presence of the autocrine purinergic loop.

Tatur et al. have demonstrated that A549 cells respond to a 50% HS through the elevation of $[Ca^{2+}]_i$ released from intracellular stores [48, 86]. The $[Ca^{2+}]_i$ rise triggered the vesicular exocytosis of nucleotides into the extracellular space. It was shown that several nucleotides were co-released together with ATP from A549 cells, including ADP, UTP and UDP [86]. The released nucleotides activate P2Y purinoceptors on the surface of the cell and neighbouring cells, triggering an intracellular cascade that results in more and more $[Ca^{2+}]_i$ release, depicted as the rapid $[Ca^{2+}]_i$ spike in Figure 9A [86]. A demonstration of the auto-amplification via the purinergic loop, and its inhibition using suramin, a wide-spectrum P2 receptor antagonist, is shown in Fig 9A [48, 86]. It was also shown that the rapid $[Ca^{2+}]_i$ spike occurs simultaneously with the release of ATP from the cell (Fig 9B). The inhibition of the purinergic receptors also diminished the amount of nucleotide release (Fig 9B). In the following study we used the same

methods to test for the presence of the autocrine purinergic loop in other pulmonary epithelial cell lines; 16HBE14o$^-$, Calu-3 and CFBE cells.

(A)

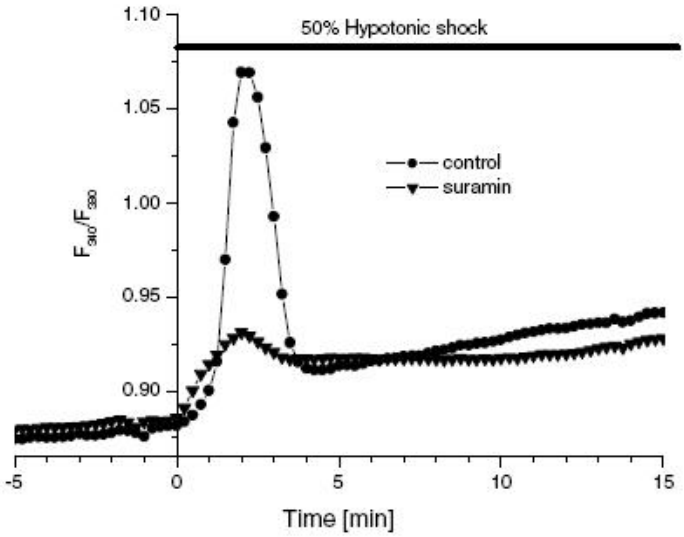

(B)

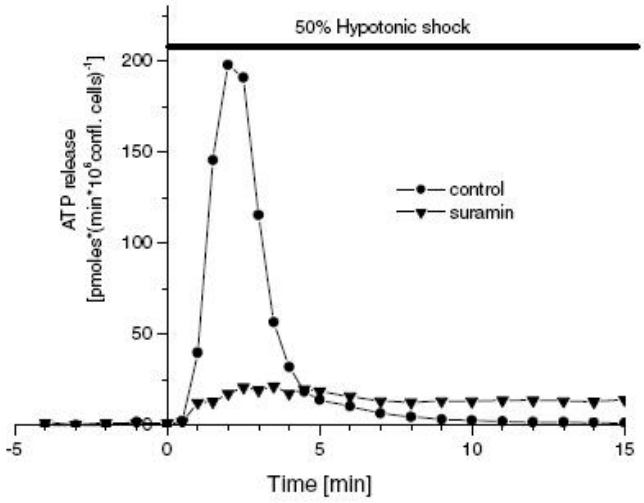

Figure 9: **Time course of the hypotonic shock-induced $[Ca^{2+}]_i$ and ATP release responses in A549 cells following a 50% HS [86].**

(A) The presence of the autocrine purinergic loop is characterized by a quick $[Ca^{2+}]_i$ *increase in A549 epithelial cells, (B) followed by the exocytosis of nucleotides in the same time frame.*

We first tested the 16HBE14o$^-$ cell line and showed that they responded similarly to the A549 cells when stimulated with a 50% HS. Results displayed in figure 10A and C, obtained in our laboratory by Tatur et al. [86], are comparable to our experiments with 16HBE14o$^-$ cells (fig 10B and D), with the exception that the $[Ca^{2+}]_i$ spike lasted about three times longer in 16HBE14o$^-$ cells [86]. The magnitude of the $[Ca^{2+}]_i$ response, on the other hand, was similar in both cell types. We also demonstrated that the autocrine purinergic loop was inhibited by apyrase and suramin. Apyrase hydrolyzes nucleotides in the extracellular space, preventing them from binding and activating the purinergic receptors, therefore inhibiting the $[Ca^{2+}]_i$ spike that is characteristic of loop activation. Similar inhibition was observed with suramin, a non-selective P2Y receptor antagonist which prevents P2Y activation. In A549 cells, 2U/ml apyrase, or 100μM suramin were needed in order to inhibit the $[Ca^{2+}]_i$ spike (Fig 10 A & C). The inhibition of this response in 16HBE14o$^-$ cells required 10 times higher concentrations, reaching levels of 20U/ml apyrase or 1mM suramin (Fig 10 B & D). Following preliminary side-view experiments using 16HBE14o$^-$ cells, we determined that the ASL volume was minimal in most of our cell cultures and decided that Calu-3 cells, which secrete more fluid than 16HBE14o$^-$ cells, were a better choice for experiments to optimize our side-view imaging system as well as our image analysis method. Although Calu-3 cells have weak purinergic properties, their abundance of ASL / mucus secretion was essential for the optimization of our microscopy system.

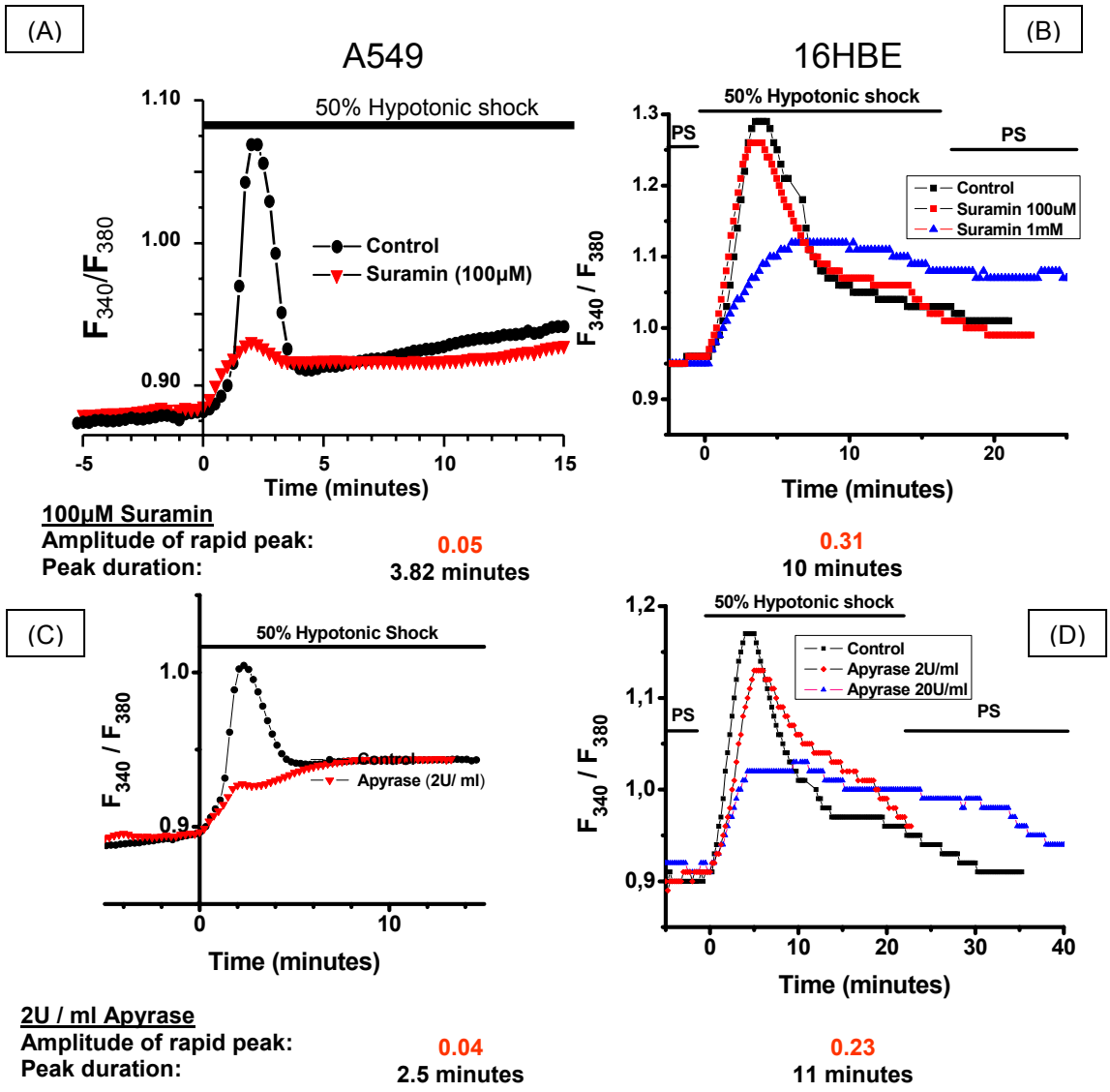

Figure 10: **Monitoring the** $[Ca^{2+}]_i$ **response to a 50% HS following treatment with suramin and apyrase.**

Comparison of the time course of $[Ca^{2+}]_i$ *changes in A549 completed by Tatur et al. (A & C) [86] and 16HBE14o- (B & D) following a 50% HS completed during this project.*

Although the Calu-3 cells responded to a 50% HS, the response was minimal and consistent with the absence of autocrine amplification due to absence or minimal amount of purinergic receptors on the cells (Fig 11)

[19]. However, thapsigargin (Tg), an inhibitor of the sarco/endoplasmic reticulum Ca^{2+} ATPase (SERCA), caused an increase in $[Ca^{2+}]_i$, resulting from the inhibition of Ca^{2+} uptake into the stores (Fig 11), and led to significant ATP release from Calu-3 cells, in a time frame identical to the $[Ca^{2+}]_i$ spike (Fig 12). Thus, Calu-3 cells are capable of Ca^{2+}-dependent ATP release. Therefore, absence of autocrine amplification in response to hypotonic shock is likely due to the very low expression level of cell surface P2Y receptors. In order to test this theory, we treated the epithelial surface of the monolayer with exogenous extracellular ATP. We showed that adding 100uM of extracellular ATP didn't cause significant $[Ca^{2+}]_i$ release. At a high concentration of 2mM ATP, a $[Ca^{2+}]_i$ response is observed over a long time span, demonstrating again that the purinergic loop isn't activated due to the minimal amount or lack of P2Y surface receptors (Fig 13).

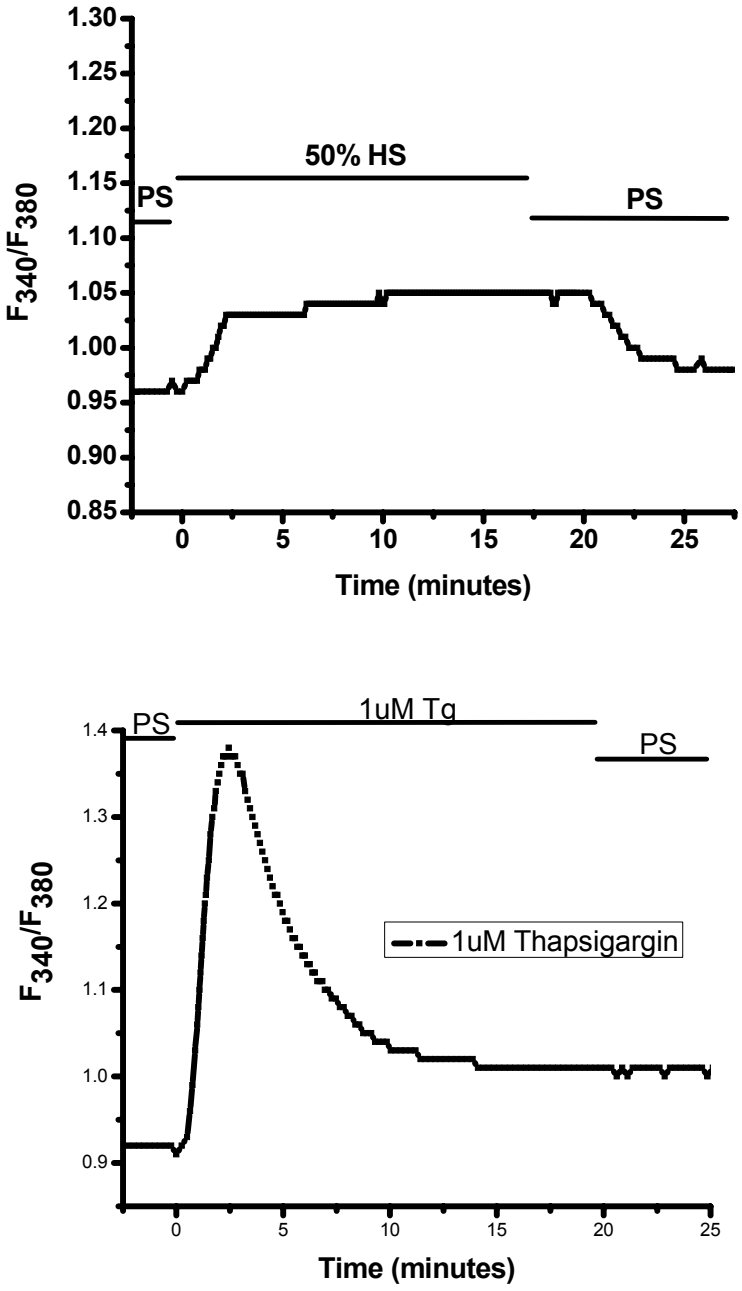

Figure 11: **Monitoring the** $[Ca^{2+}]_i$ **response following a 50% HS or Thapsigargin in Calu-3 cells.**

(A) A minimal response is observed to a 50% HS but (B) a large response is observed with the treatment of 1uM Thapsigargin in the absence of hypotonic shock

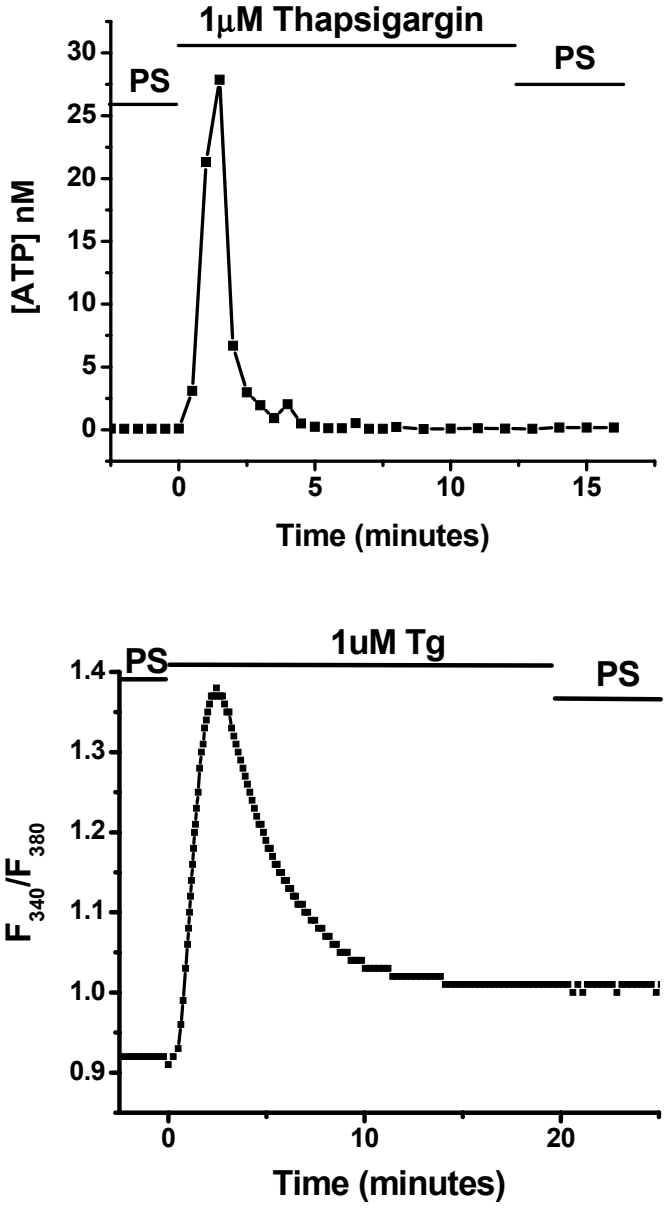

Figure 12: $[Ca^{2+}]_i$ **response and ATP release response following TG treatment.**

Thapsigargin potently stimulates $[Ca^{2+}]_i$ *and ATP release in Calu-3 cells*

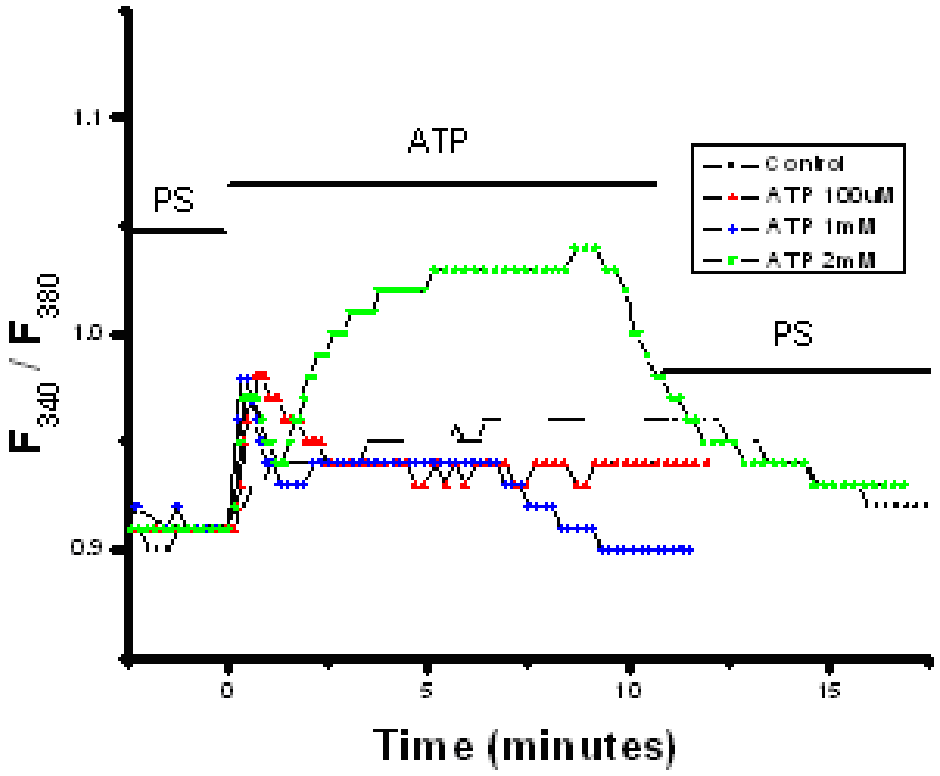

Figure 13: **Role of extracellular ATP on the release of** $[Ca^{2+}]_i$ **in Calu-3 cells**

The treatment of Calu-3 cells with extracellular ATP induces only a small $[Ca^{2+}]_i$ response

Initially, we hypothesized that the presence of ecto-ATPases on the membrane surface of Calu-3 cells could explain the lack of response to a 50% HS. In order to test the hypothesis, we used an ecto-ATPase inhibitor, ARL 67156 (Sigma-Aldrich). We demonstrated that in Calu-3 cells, ecto-ATPase inhibitors do not change the $[Ca^{2+}]_i$ response following a 50% HS, and that the presence of ecto-ATPases does not change the functionality of the autocrine purinergic loop (Fig 14). Together, these results suggest the possibility that P2Y receptors are absent or in small number in Calu-3 cells.

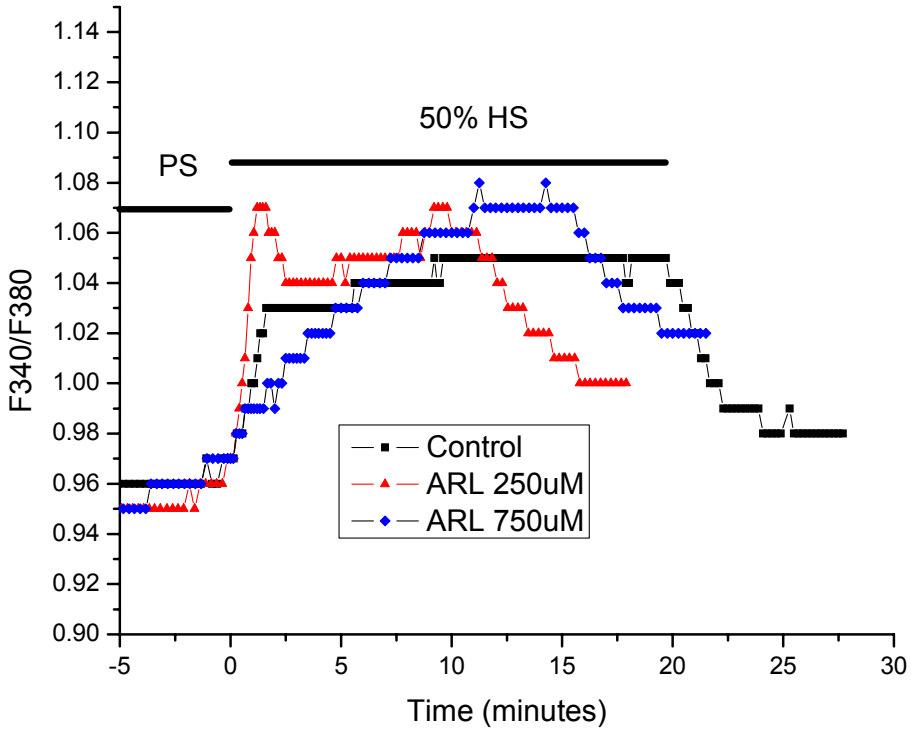

Figure 14: **The effect of ARL67156 on the release of** $[Ca^{2+}]_i$**, during a 50% HS in Calu-3 cells**

The ecto-ATPase inhibitor ARL67156 has little effect on the $[Ca^{2+}]_i$ *response in Calu-3 cells*

The purinergic loop also operates in CF cells. In experiments using both wild-type and ΔF508 mutated CFBE cells, a 50% HS caused an $[Ca^{2+}]_i$ spike similar to what was observed in A549 and 16HBE14o$^-$ cells, although smaller in magnitude. The inhibition of the loop in CFBE cells, using apyrase, was comparable to 16HBE14o$^-$ cells, as its inhibition required between 20 and 30U/ml of apyrase (Fig 15 A, B). Most interestingly with the CFBE cells was their response to suramin. In other epithelial cell types

tested, the inhibition of purinergic receptors with the use of suramin led to the inhibiton of the purinergic loop and $[Ca^{2+}]_i$ spike (Fig 10). Surprisingly, the treatment of CFBE cells with suramin elicits a $[Ca^{2+}]_i$ spike all by itself, even in the absence of a 50% HS (Fig 15 C, D). 100uM suramin in normal PS elicited an $[Ca^{2+}]_i$ response comparable to the response obtained with a 50% HS alone. Furthermore, a 50% HS with 100μM suramin induced an $[Ca^{2+}]_i$ response that was about 3-fold the response obtained with suramin alone (Fig 15 C, D).

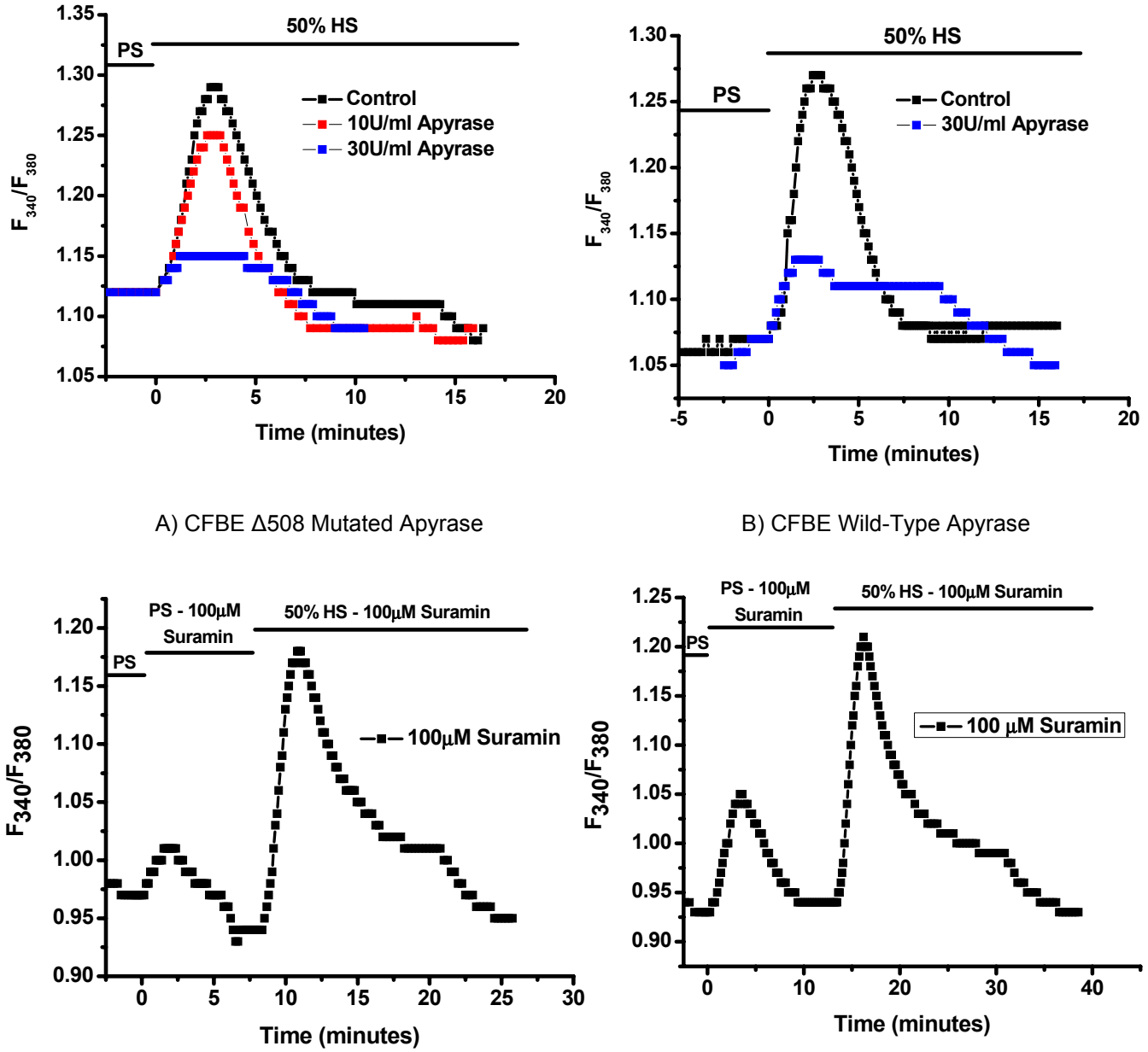

Figure 15: **Time course of the 50% HS-induced** $[Ca^{2+}]_i$ **response in CFBE cells**

(A and B) High dose apyrase (30U/ml) inhibits the autocrine purinergic loop in both CFBE cell types during a 50% HS, (C and D) Suramin (100μM) elicits an $[Ca^{2+}]_i$ *response without a 50% HS. The* $[Ca^{2+}]_i$ *response following a 50% HS is not dimished when given in conjunction with 100 μM suramin compared to a 50% HS alone.*

Finally, ATP release experiments using CFBE cells also demonstrated that in the case of a stimulus causing the release of an $[Ca^{2+}]_i$ spike, ATP release also occurs in the same time frame (Fig 16), as previously observed in the other pulmonary epithelial cell types.

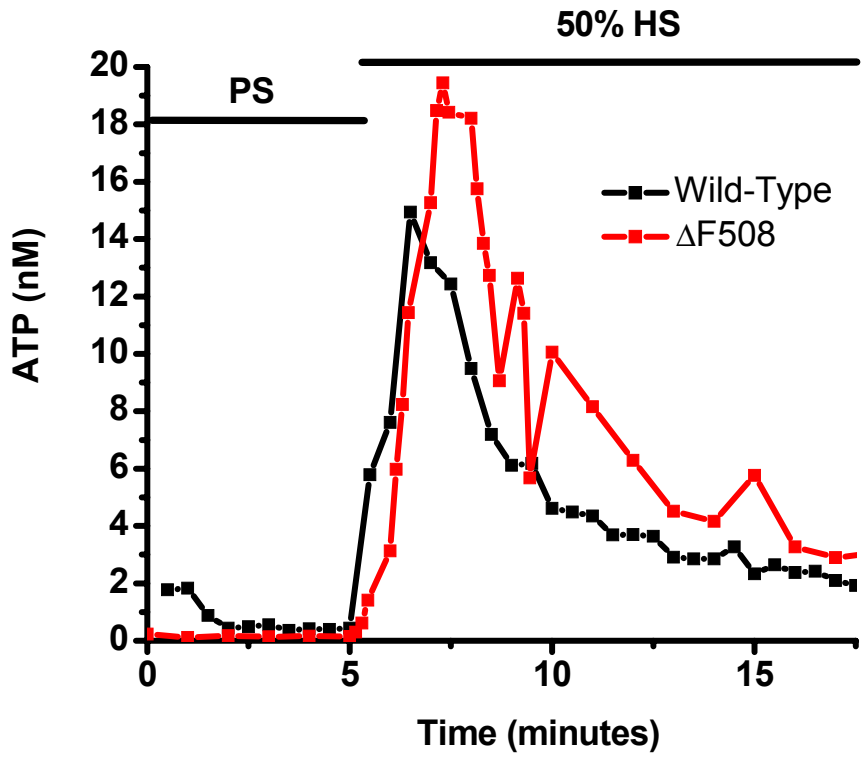

Figure 16: **Time course of ATP release induced by 50% HS from confluent CFBE cell monolayers**

ATP released from CFBE cells in response to a 50% HS follow the same dynamics and time frame as the $[Ca^{2+}]_i$ response.

Furthermore, in order to prove that our $[Ca^{2+}]_i$ spike was due to the liberation of Ca^{2+} from internal stores and not by an influx from the external Ca^{2+} containing physiological solution, we used Ca^{+2}-free PS, and tested

the effect of a Ca^{2+}-free 50% HS and Tg, on the activation of the purinergic loop. Both stimulators of intracellular Ca^{+2} confirmed that its release comes uniquely from intracellular stores, and does not directly involve the Ca^{2+} present in our extracellular solution (Fig 17).

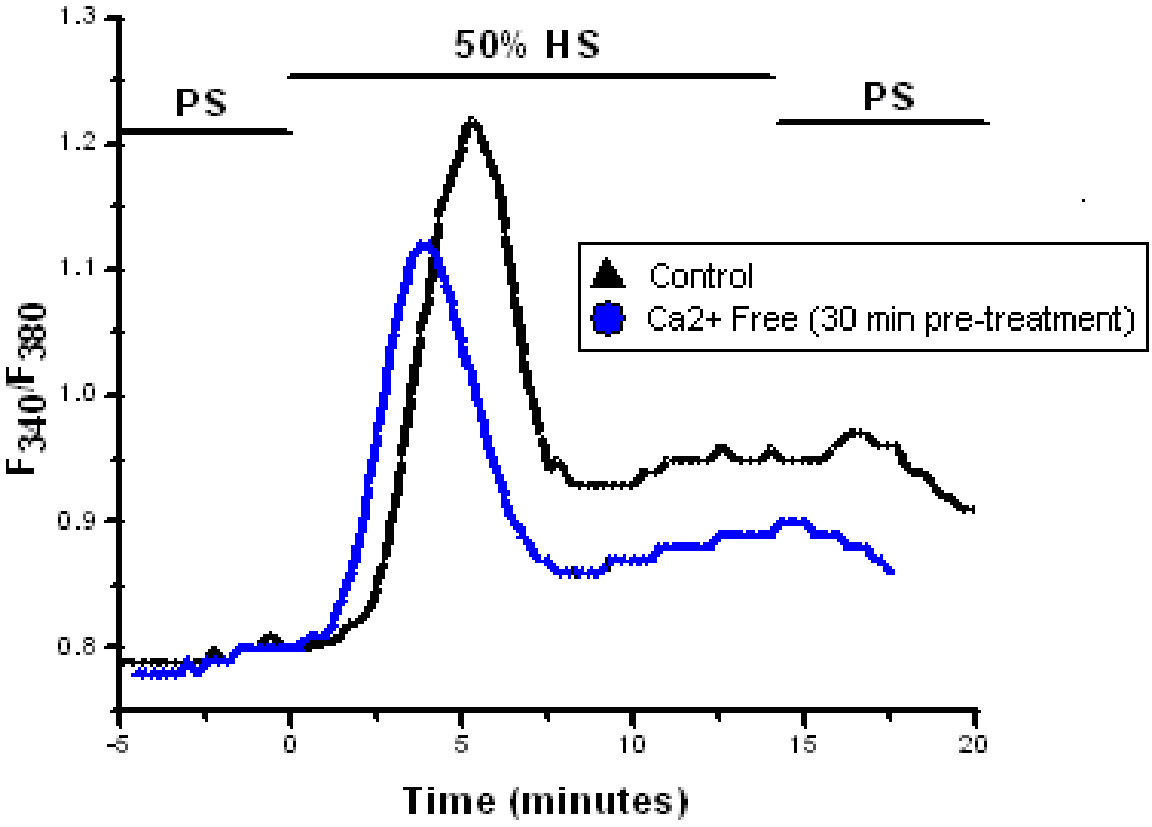

Figure 17: **Effect of extracellular Ca^{2+} removal on the hypotonic shock-induced $[Ca^{2+}]_i$ response**

The response following treatment with calcium-free HS in 16HBE14o- is similar to the control.

3.2. ASL Monitoring and volumes changes during Purinergic Stimulation

Although the many functions of the purinergic loop are still unknown, it seems that they could play a vital role in the control of the ASL volume. As previously stated, Calu-3 cells were most widely used due to their ability to secrete more ASL than other epithelial cells. Nonetheless, we are still aware that the purinergic loop in these cells is very weak. We demonstrated that the activation of the loop by a 50% HS or Tg, led to an increase in ASL volume, seen in Fig 18 and Fig 19 (Fig 5 and 9 from chapter 2, respectively). The ASL volume time course, in all cell types tested, indicated that the ASL volume increase (Fig 18) occurred in the same time frame as both the $[Ca^{2+}]_i$ and ATP release responses (Fig 12), suggesting that the three processes of the purinergic loop are connected (i.e. $[Ca^{2+}]_i$ release, ATP release and ASL volume increase). In CFBE cells, the ASL volume increase wasn't as pronounced, but it occurred in conjunction with the $[Ca^{2+}]_i$ and ATP responses. Previous experiments point towards the possibility that one of the functions of the purinergic loop is to increase the ASL volume, through the increase in $[Ca^{2+}]_i$ and ATP release, and demonstrates the feasibility of increasing the ASL volume of epithelial cells, including the most important CFBE cells. However, more work is needed in order to confirm these statements.

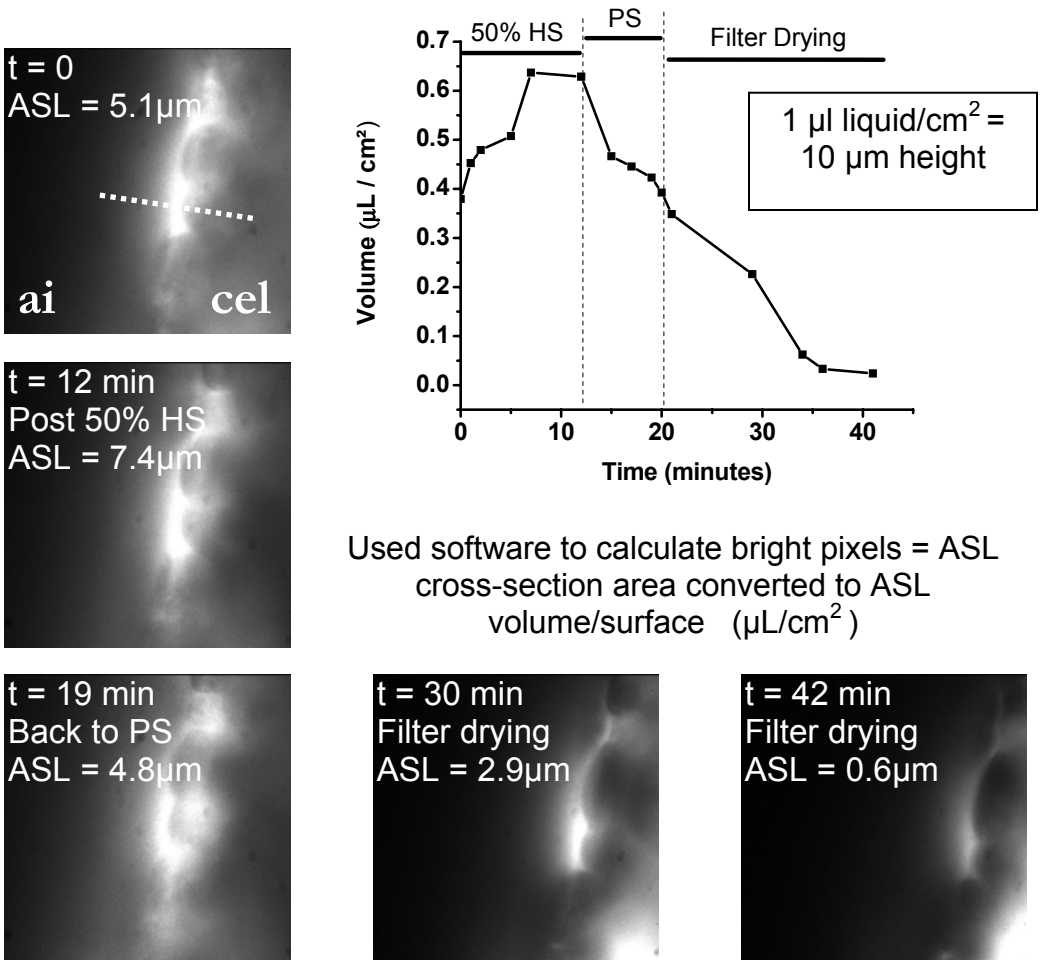

Figure 18: **Time course of ASL volume changes during a 50% HS in Calu-3 cells. (Figure 5 in chapter 2 (manuscript)**

A 50% HS induces ASL changes in both ASL height and volume in Calu-3 cells when monitored with side-view microscopy, at a 90°

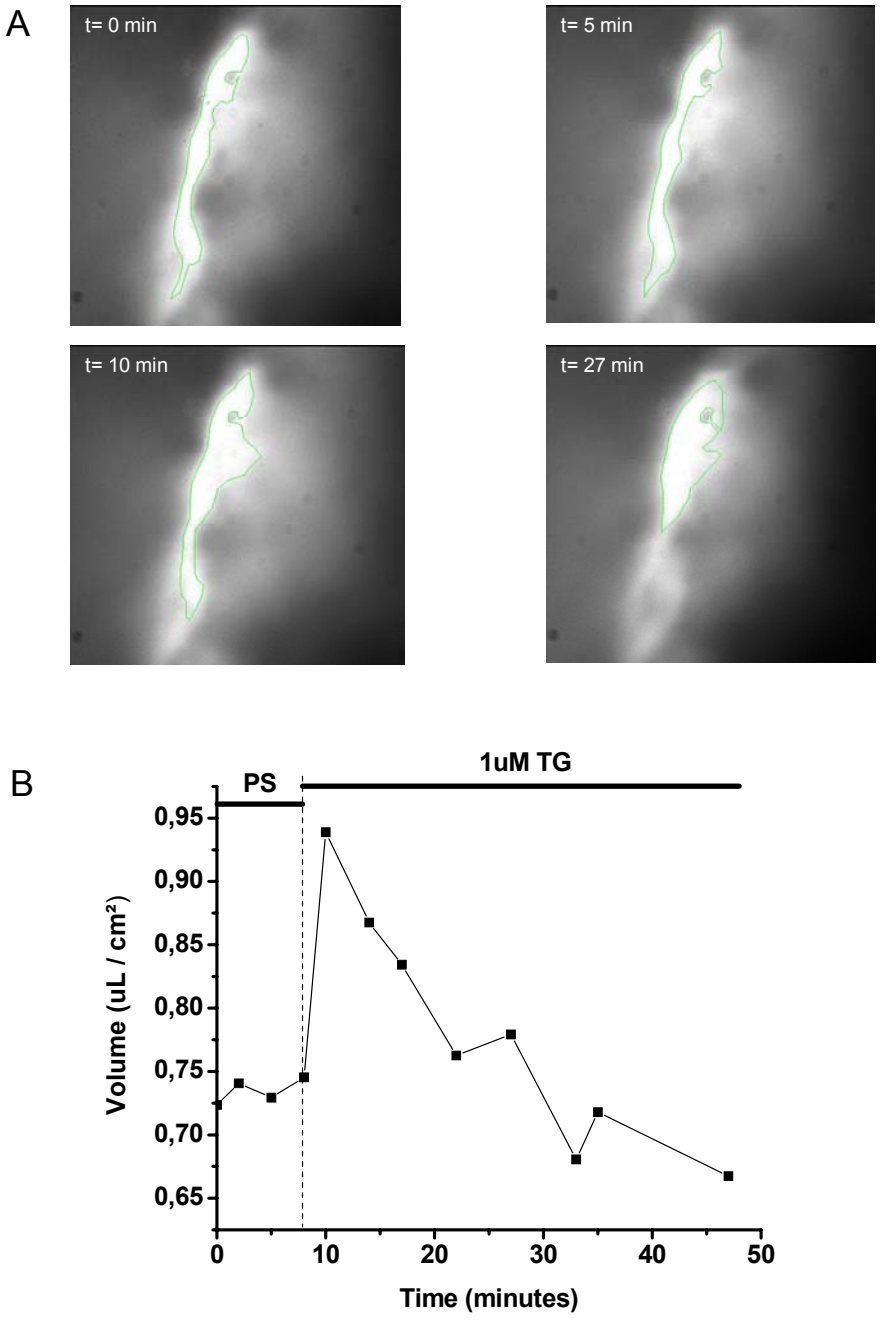

Figure 19: Thapsigargin time course with Calu-3 cells. **(Figure 9 in chapter 2 (manuscript)**

A. *Images of Calu-3 cells were taken with the 45º side-view imaging technique. Calu-3 cells were cultured on the filter for 3 weeks before usage. Images were acquired using the ELWD 40X objective, and the ASL was stained with Alexa fluor 488 dextran.*

B. *Time course graph of Calu-3 ASL volume during the Tg treatment.*

CHAPTER 4

DISCUSSION

As described in chapters 2 and 3, the side-view imaging technique has been developed in order to detect minimal changes in ASL volumes during given experiments. However, other techniques have already been developed for the same purpose. Each technique has its advantages and limitations, which will be discussed in sections 4.5 and 4.6.

The purinergic loop experiments we've completed have demonstrated the possibility of a link between the purinergic autocrine loop and ASL volume. Nevertheless, several other hypotheses have been proposed in order to explain the activation, de-activation and inhibition of the purinergic loop, as well as ASL volume changes.

These subjects will be discussed in detail in the sections to follow.

4.1. Autocrine Purinergic loop function in different pulmonary epithelia

Our experiments have demonstrated that different pulmonary epithelial cell types show differential autocrine purinergic loop functionality and respond differently to the same stimulus. We will further discuss the possibilities behind this phenomenon.

The first possibility explaining the variation in autocrine loop responses could involve different levels of P2Y receptor expression. It is widely known that different cell lines express diverse array of P2Y purinergic receptor

subtype levels, leading to different responses to a given stimulus. For example, the A549 and 16HBE14o$^-$ cells, which respond similarly to a 50% HS, express high levels of the $P2Y_2$ and $P2Y_6$ receptor subtypes, whereas Calu-3 cells express only very little receptor activity, mostly $P2Y_1$ [19].

The 50% HS is a clear inducer of $[Ca^{2+}]_i$ elevation in the A549 and 16HBE14o$^-$ cells, leading to ATP release, but in Calu-3 cells, the response is apparent but greatly diminished. In the latter cells, Tg treatment induced a large calcium spike and nucleotide release from the cell. The main, and most important similarity of all cell types including Calu-3 cells, is that any increase in $[Ca^{2+}]_i$ elicited the release of nucleotides into the extracellular space, likely via a Ca^{2+}-dependent exocytosis. This was followed by the activation of P2Y cell surface receptors, on the same cell or neighbouring cells (autocrine / paracrine effect) when they were present, by the nucleotides. The activation of the cell surface receptors then leads to an intracellular cascade that results in the release of more $[Ca^{2+}]_i$. This way, the autocrine loop can function until the $[Ca^{2+}]_i$ system is saturated and $[Ca^{2+}]_i$ stores are depleted.

Another possibility for the lack of purinergic response could have been due to ecto-ATPase activity on the extracellular membrane of the epithelia, but we rapidly disproved this theory. It is known that Calu-3 cells express more ecto-ATPase activity than do A549 and 16HBE14o$^-$ cells [19, 48], but this

didn't change the function or potency of extracellular nucleotides. Treating Calu-3 cells with an inhibitor of ecto-ATPases (ARL 67156 – Sigma Aldrich), confirmed that the inhibition of the ecto-ATPases didn't change the potency of the autocrine purinergic loop. Therefore, the ecto-ATPase activity is not the reason for the absence of the autocrine effects in Calu-3 cells.

The combination of all factors previously described demonstrates that the autocrine loop is functional, following a 50% HS control, in all epithelial cell types we have tested, although weaker in Calu-3 cells. The efficiency of the loop depends on many cell specific factors, such as the expression of specific P2Y receptor subtypes and their number, the amount of $[Ca^{2+}]_i$ release, as well as the amount of ATP and other nucleotides released into the extracellular space.

4.2. Inhibition of the Autocrine purinergic loop

We have shown that it is possible to inhibit the purinergic loop, by blocking its complex pathway at several pivotal points. The removal of any extracellular tri- and di-phospho nucleotides that may activate a cell surface P2Y receptor was shown to block the rapid Ca^{2+} response. For example, the hydrolysis of extracellular nucleotides using apyrase demonstrated that without the activation of cell surface P2Y receptors, the autocrine loop cannot be activated. Furthermore, the inhibition of these receptors by suramin also resulted in the inhibition of the loop. The same results were

obtained using apyrase with CFBE cells. Contrary to the results obtained with the A549, 16HBE14o$^-$ and Calu-3 cell lines, the CFBE cell lines responded differently to suramin. In the absence of a hypotonic shock, a Ca^{2+} spike was observed in response to suramin application. This unexpected result might arise from another action of suramin [103]. Emmick et al. have demonstrated that suramin has a dual effect on calcium fluxes and causes the liberation of calcium from the muscle sarcoplasmic reticulum, but it can also act as an effective anti-cancer agent [103]. Furthermore, suramin exhibited agonistic effects like those of the adenine nucleotide, β,γ-methyleneadenosine 5'-triphosphate [103]. Instead of inhibiting the $[Ca^{2+}]_i$ spike, it evoked an $[Ca^{2+}]_i$ response arising from Ca^{2+} release from the skeletal muscle sarcoplasmic reticulum. Therefore, it is highly possible that suramin-induced $[Ca^{2+}]_i$ in CFBE cells may arise due to its action at another site than the cell surface P2Y receptors.

4.3. Mechanism of ASL volume control and the role of the Autocrine purinergic loop

Extracellular nucleotides, by acting on cell surface P2Y purinoceptors, activate the purinergic loop and modulate the activity of apical ion channels such as the CaCC, CFTR-Cl^- or, ENaC channels, which control ASL hydration. The activation of anion channels and the inhibition of the absorptive ENaC channel leads to the net increase of fluid secretion, resulting in an ASL volume increase [94]. In healthy individuals, this system

functions flawlessly. Ion channels such as ENaC, CFTR chloride channels and CaCC are essential in the control of the ASL volume [10, 17, 19-20], but bicarbonate ions (HCO_3^-) and oxygen (O_2) are also extremely important to the regulation of ASL [10, 23, 104]. Ion transport is compromised in CF airways, mostly due to the lack of proper functional CFTR chloride channels [30]. Several theories have been proposed to explain the correlation between defective CFTR and CF airway disease (Fig 20).

HCO_3^- ion and oxidative stress play a vital function in the CF pathogenesis and bacterial colonization. The “low oxygenation” hypothesis explains that ASL oxygen content is lower in CF, due to increased oxygen consumption by CF epithelial cells, possibly slowing oxygen diffusion into the ASL, resulting in enhanced *P. aeruginosa* growth and biofilm formation, leading to impaired MCC [30, 105]. Another molecule of importance is HCO_3^-, which plays an important role in pH homeostasis of the ASL [94, 104]. The “low pH” hypothesis proposes that a defective CFTR leads to reduced secretion of basic HCO_3^- ions, resulting in a slightly more acidic ASL [10, 23, 30, 104]. The “high salt” hypothesis postulates that defective CFTR Cl^- transport in CF prevents chloride absorption by the airways, leading to a change in ASL [NaCl] from <60mM (non-CF), to >100mM in the CF airway, inhibiting the activity of endogenous antimicrobials such as defensins [30]. The “low ASL volume” hypothesis suggests that the hyperactivity of ENaC and consequent sodium hyperabsorption in CF results in a viscous dehydrated

ASL layer that impairs mucociliary function and facilitates bacterial adherence and colonization [30]. Finally, the “defective gland function” hypothesis claims that reduced fluid secretion by the airway submucosal glands is the primary defect in CF, and it possibly alters secretion of mucous glycoproteins (Fig 20) [30].

The previous hypotheses were tested and results showed that the high-salt hypothesis was false. Furthermore, ENaC hyper-absorption is a hypothesis for which researchers have different opinions, as it seems to be slowly abandoned due to the fact some researchers have produced results that contradict this hypothesis [21]. As for the other hypotheses, the low pH theory is still under investigation but is thought to play an important role in the re-hydration of the ASL [38]. ASL dehydration may occur due to many different reasons and therefore, multiple functions might be compromised simultaneously, causing the CF airway phenotype [30].

Finally, a depleted ASL, due to decreased gland fluid secretion, leads to mucus accumulation and stasis. In this state, the lung environment is favorable to bacterial growth and infection, decreasing bacterial clearance. This results in the accumulation of pulmonary infections, exacerbations and an eventual death by respiratory failure [94].

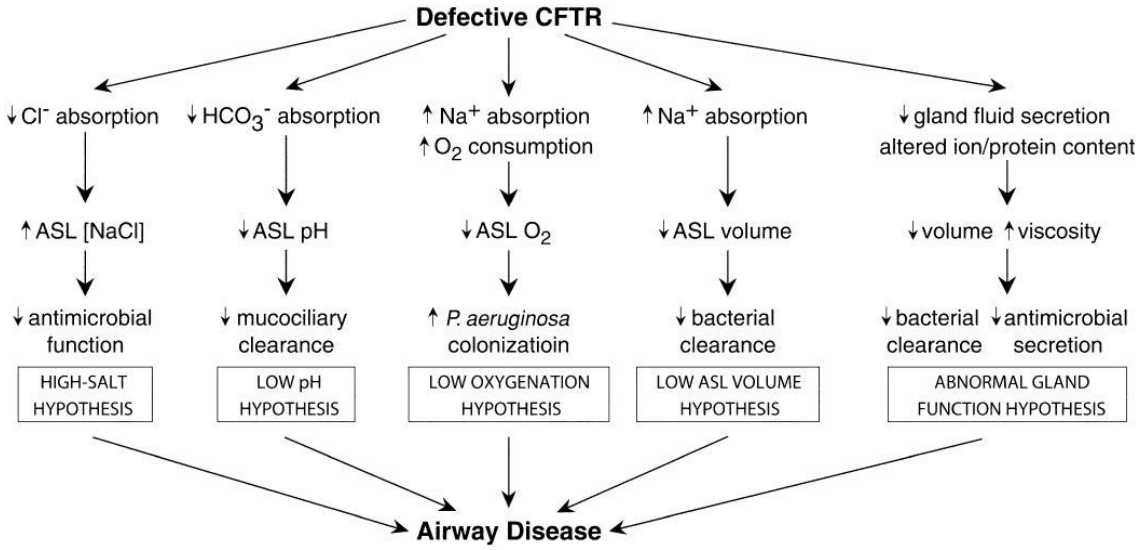

Figure 20: **Hypotheses linking a defective CFTR to the CF phenotype** [30]

Strategies to repair the MCC problem have been investigated by many researchers [20, 29-31]. Although a solution is yet to be found, an initial functional technique that is thought to prevent ASL dehydration was to inhibit sodium absorption. The second logical method to restore ASL is to stimulate chloride secretion. Additionally, it has been demonstrated that P_2Y_2 receptor agonists can restore ASL volume and enhance MCC [13-16, 48].

Some laboratories have put their efforts in the studies of another chloride channel, the CaCC, in order to compensate for the lack of functionality of the CFTR chloride channel [19, 27]. Several researchers have demonstrated that it is possible to restore chloride secretion to a basal level, compensating in part for the CFTR deficiency observed in CF airways. Tarran et al. have shown that in the presence of DIDS, an antagonist of the

CaCC, CF PCL height was significantly reduced from about 8μm to 4μm, suggesting that CaCC was the only functional pathway of Cl^- secretion in CF airways, under phasic motion [27]. Although there are many angles one can take to fix these multiple problems, the activation of the autocrine purinergic loop, which we have shown to increase the ASL volume, could help fix most problems previously described. The continuous activation of the loop would re-hydrate the epithelial surface, aid in MCC and make the liberation of mucus and bacterial growth more feasible.

4.4. ASL pH and MCC clearance

According to many authors [23, 38, 104], another essential variable affecting the efficacy of MCC is the pH of the ASL. The ASL pH depends most prominently on the concentration of HCO_3^- ions present within the ASL. Bicarbonate is an alkaline as well as a vital component of the pH buffering system. It has been demonstrated that the ASL of CF patients is generally more acidic when compared with healthy individuals. The ASL acidification results from reduced bicarbonate secretion via CFTR, leading to a high HCO_3^- concentration within the cell and a low concentration within the ASL. This increased acidity of the ASL might have deleterious consequences on the rheologic properties of mucins in the ASL, their release and hydration status, resulting in the deficiency of the MCC system [10, 38, 104] (Fig 21). The ASL pH also appears to reflect a balance between active transcellular ion transport and passive paracellular ion movement. The basal acidification

(and HCO_3^- depletion) rate was more rapid in CF cultures, reflecting at least in part the apical membrane H^+,K^+-ATPase activity [104]. According to studies by Coakley et al., the simplest explanation for basal differences in ASL pH between CF and normal cell cultures is the lack of HCO_3^- secretion by CF airway epithelia. Restoring the capability of anion secretion channels such as CFTR or other Cl^- channels could repair the ionic balance, resulting in the secretion of bicarbonate back into the ASL, lowering the pH, thus increasing the ASL volume and repairing the defective MCC system [38, 104-105] (Fig 21).

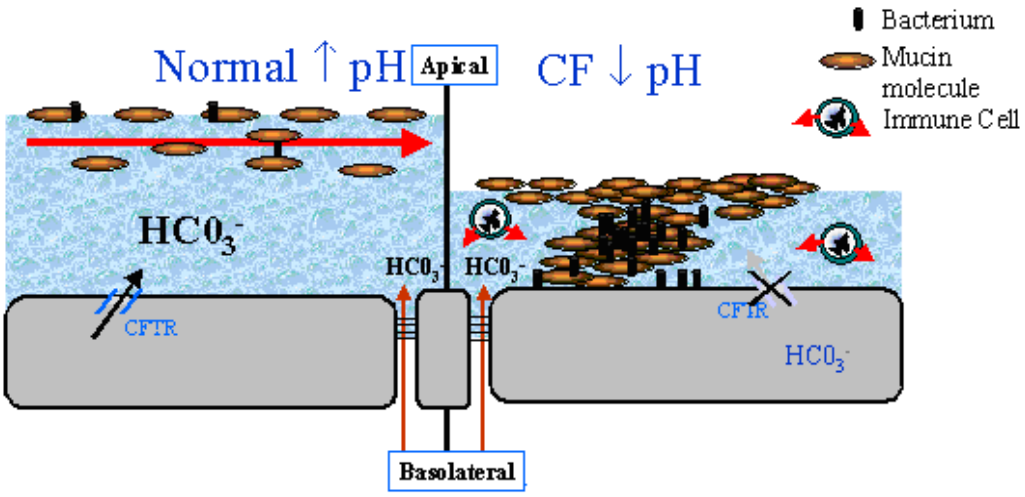

Figure 21: **Dysregulation of ASL pH and its potential consequences in the CF lung** [38]

4.5. Advantages and limitations of our side-view microscopy technique versus other techniques

Several methods have been used and developed in order to monitor the ASL. Confocal microscopy is presently the most common method used for ASL monitoring. By taking stacks of confocal images along the z-axis, a 3D image of the ASL could be reconstructed on the computer. Using this technique, we can monitor the changes in ASL height or volume. To avoid cells drying during image acquisition, some researchers used a layer of perfluocarbons (PFCs) deposited on top of the cell monolayer, to prevent ASL evaporation [27]. Such manipulations, however, could change the homeostatic characteristics of a system and could alter the cellular reaction to a given stimulus.

The confocal microscopy method also has limited temporal resolution and leads to photobleaching. Accordingly, the acquisition of an image or a sequence of images can take from several seconds up to 1 minute depending on the chosen image resolution [48]. This limits the possibility of real-time observation of rapid ASL height alterations upon a cell stimulus, which is possible using side-view imaging. Furthermore, laser scanning causes photobleaching and photo damage to the cells because of the exposure to laser light of high average operating power, an outcome which may alter the cell response to a stimulus.

An alternate method for ASL monitoring and epithelial fluid secretion has been described by Irokawa et al., but does not involve microscopy [106]. The method developed is called the virtual gland and has the capability of measuring the fluid secretion of an epithelial Calu-3 cell by calculating the transepithelial potential difference in an open circuit and collecting the secreted fluid into a compartment containing oil and then quantifying it. Although the method seems interesting, it has several limitations, which are not present in our setup: in the case of the virtual gland, the transepithelial resistance is never measured, consequently the cells might respond differently if there is an absence of a tight monolayer. Moreover, the apical side of the cells is inaccessible in their setup, the cells aren't exposed to conditions that resemble the lung environment and finally, the fluid collection occurs as a transfer into an oil layer, where some quantification mistakes could occur when the fluid components would be mixed [106].

ASL monitoring has also been accomplished by scanning electron micrograph (SEM), following X-Ray microanalysis, in order to determine the ionic composition and size of the ASL [107]. Although this technique permitted the viewing of the ASL, the quantification of the ASL volume was not completed, albeit possible. Furthermore, the cells that are analyzed must be frozen (in this case, frozen trachea parts), in order to keep the ASL intact and prevent evaporation. Finally, they treated and incubated the cells in liquid propane and liquid nitrogen before starting the experiments, and coated the cells with a thin carbon layer during the experiment. This

technique functions adequately for their purposes, but the cells are frozen, thus, this is not a real-time, live cell imaging technique.

None of the previous monitoring methods allow for the precision and pulmonary-like conditions that our system offers. The use of side-view microscopy has also eliminated most of the problems encountered with other methods. We use live cells that are grown on filter inserts and provide them with an environment that is humidified to about 90% and a constant temperature of 37º C. Furthermore, our system allows perfusion of any liquid on the serosal side, allowing us to perfuse the cells with physiological solution or any other pharmacological tool we choose, this solution also being pre-warmed to 37ºC. Finally, we are able to take images and treat cells in real-time, which allow us to take movies or images at any time point, monitoring ASL volume changes that are observable with the naked eye. These much needed improvements to the confocal microscopy method label our technique as highly useful for future experiments. On the other hand, our technique also has disadvantages of its own. The vibration problems that arose with our first chamber prototype led to changes in the focus, making ASL monitoring more problematic. This problem was corrected by building the new, optimized chamber (Annex 1). However, the image analysis method remains non-automated and time consuming, and a solution is still to be discovered.

4.6. Side-view microscopy at 45 º versus 90º

With our side-view imaging technique, imaging was initially performed at a 90º angle, in order to monitor the ASL at a straight angle. This technique worked very well, but had a few disadvantages. First of all, the millicell inserts needed to be modified in order to remove the obstruction caused by the curling of the edges of the filter. This procedure was time consuming and the filters were often broken while hand cutting the edges, leading to a loss of time and material. Secondly, the 90º angle permitted to monitor and view only the cells close to the edges of the filter, due to the limited working distance of the microscope objective. For this reason, we modified our technique in order to view the cells at a 45º angle, which allowed us to eliminate the two problems mentioned previously. Tilting the filter at 45º angle allowed us to use the millicell insert without modifying it, saving a lot of time. Also, filter tilting allows the scanning of the filter, making it possible to view all areas on the filter, including cells at the very middle of the filter.

CHAPTER 5

CONCLUSION

.

The present study, completed in accordance with my masters' degree, has brought about new insights on the purinergic control of ASL volume. Furthermore, during the study, a new highly improved method for monitoring ASL volume changes was developed. Results of our study demonstrated that the ASL is a dynamic layer of liquid that coats the pulmonary epithelium. It is distributed non-homogenously over the epithelial cells resulting in a highly variable ASL depth in different parts of the cell monolayer. We also demonstrated that different pulmonary epithelial cells respond to physical stimuli (hypotonic shock) through the elevation of intracellular Ca^{2+} and Ca^{2+}-dependent ATP release. These responses are greatly amplified by the autocrine purinergic loop, which operates in the pulmonary epithelial cell types tested, but to a lesser extent in Calu-3 cells. Our study suggests that pharmacological tools that modulate various steps of the purinergic signaling could be used to develop treatments in order to increase ASL volume and improve MCC, a process that is essential for the survival of CF patients.

A novel side-view imaging system that we developed allows for precise monitoring of the ASL volume in real-time and under conditions that mimic the pulmonary microenvironment (37ºC, ~90% humidity). Although the currently used image analysis protocol allows for correct ASL volume evaluation, it is a time-consuming process and further improvements are required to automate and speed-up the analysis.

Finally, the technique developed in this project, as well as the findings on the purinergic loop are stepping stones that should eventually lead to the discovery of pharmacological tools that will restore the ASL volume on the surface of CF epithelial cells.

References

[1] Purves W, Sadava D, Orians G, Heller C (2004) The human respiratory system. *Life: The Science of Biology,* 7th edition.

[2] Fraser, R.S. (2005) Histology and gross anatomy of the respiratory tract. *Chapter 1, BC Decker Inc.*

[3] Park K, Korfhagen T.R., Bruno M.D., Kitzmiller J.A., Wan H, Wert S.E., Khurana Hershey G.K., Chen G, Whitsett J.A. (2007) SPDEF regulates goblet cell hyperplasia in the airway epithelium. *The Journal of Clinical Investigation Vol 117*: 978-988.

[4] Wikenheiser K.A., Vorbroker D.K., Rice W.R., Clark J.C., Bachurski, C.J., Oiet H.K., Whitsett J.A. (1993) Production of immortalized distal respiratory epithelial cell lines from surfactant protein C/simian virus 40 large tumor antigen transgenic mice. *Proc. Natl. Acad. Sci. USA Vol. 90*: 11029-11033.

[5] Orgeig S., Daniels C.B. (2003) Pulmonary Surfactant: The Key to the Evolution of Air Breathing. *News Physiol Sci* 18: 151-157.

[6] Miller B.E., Hook G.E. (1990) Hypertrophy and hyperplasia of alveolar type II cells in response to silica and other pulmonary toxicants. *Environ Health Perspect 85*: 15-23.

[7] Kazanjian A, Wallis D, Au N, Nigam R, Venken K, Cagle P.T., Dickey B.F., Bellen H.J., Gilks C.B., Grimes H.L. (2004) Growth Factor Independence-1 Is Expressed in Primary Human Neuroendocrine Lung Carcinomas and Mediates the Differentiation of Murine Pulmonary Neuroendocrine Cells. *Cancer Research 64*: 6874-6882.

[8] Patton J.S., Byron P.R. (2007) Inhaling medicines: delivering drugs to the body through the lungs. *Nature Reviews Drug Discovery 6*: 67-74.

[9] Schultz S.G., Andreoli T.E., Brown A.M., Fambrough D.M., Hoffman J.F., Welsh M.J. (1996) Molecular biology of membrane transport disorders. *Issue 13481:* 606-608.

[10] Itani O.A., Lamb F.S., Melvin J.E., Welsh M.J. (2007) Basolateral chloride current in human airway epithelia. *Am J Physiol Lung Cell Mol Physiol 293*: L991-L999.

[11] Kunzelmann K, Kongsuphol P, Aldehni F, Tian Y, Ousingsawat J, Warth R, Schreiber R (2009) Bestrophin and TMEM16-Ca^{2+} activated Cl^- channels with different functions. *Cell Calcium 46*: 233-241.

[12] Boucher R.C. (2007) Evidence for airway surface dehydration as the initiating event in CF airway disease. *Journal of Internal Medicine 261*: 5-16.

[13] Davies J (2004) Ion transport in lung disease. *Pediatric Pulmonology, Supplement 26*: 147-148.

[14] Knowles M.R., Boucher R.C. (2002) Mucus clearance as a primary innate defense mechanism for mammalian airways. *J.Clin. Invest 109*: 571-577.

[15] Knowles M.R., Olivier K.N., Hohneker K.W., Robinson J, Bennett W.D., Boucher R.C. (1995) Pharmacologic Treatment of Abnormal Ion Transport in the Airway Epithelium in Cystic Fibrosis. *Chest 107:* 71S-76S.

[16] Lazarowski E.R., Tarran R, Grubb B.R., Van Heusden C.A., Okada S, Boucher R.C. (2004) Nucleotide Release Provides a Mechanism for Airway Surface Liquid Homeostasis. *Journal of Biological Chemistry 279* : 36855-36864.

[17] Sartori C, Matthay M.A. (2002) Alveolar epithelial fluid transport in acute lung injury: new insights. *Eur. Respir J 20*: 1299-1313.

[18] Widdicombe J.H., Bastacky S.J., Wu D.X-Y., Lee C.Y. (1997) Regulation of depth and composition of airway surface liquid. *Eur Respir J 10*: 2892–2897.

[19] Kreda S.M., Okada S.F., van Heusden C.A., O'Neal W, Gabriel S, Abdullah L, Davis C.W., Boucher R.C., Lazarowski E.R. (2007) Coordinated release of nucleotides and mucin from human airway epithelial Calu-3 cells. *J. Physiol 584*: 245-259.

[20] Tarran R, Button B, Picher M, Paradiso A.M., Ribeiro C.M., Lazarowski E.R., Zhang L, Collins P.L., Pickles R.J., Fredberg J.J., Boucher R.C. (2005) Normal and Cystic Fibrosis Airway Surface Liquid Homeostasis : The effects of phasic shear stress and viral infections. *The journal of Biological Chemistry 280*: 35751-35759.

[21] Nagel G, Barbry P, Chabot H, Brochiero E, Hartung K, Grygorczyk R (2004) CFTR fails to inhibit the epithelial sodium channel ENaC, when expressed in *Xenopus laevis* oocytes. J Physiol. 564: 671-682.

[22] Eisenhut M (2006) Changes in Ion Transport in Inflammatory Disease. *Journal of Inflammation* 3:5.

[23] Szkotak A.J., Paul Man S.F., Duszyk M (2003) The Role of the Basolateral Outwardly Rectifying Chloride Channel in Human Airway Epithelial Anion Secretion. Am*. J. Respir. Cell Mol. Biol. 29:* 710-720.

[24] J. V. Galietta L, Folli C, Caci E, Pedemonte N, Taddei A, Ravazzolo R, Zegarra-Moran O (2004) Effect of Inflammatory Stimuli on Airway Ion Transport. *The Proceedings of the American Thoracic Society 1*: 62-65.

[25] Crapo J.D., Harmsen A.G., Sherman M.P., Musson R.A. (2000) Pulmonary immunobiology and inflammation in pulmonary diseases. *Am J Respir Crit Care Med* 162 : 1983-1986.

[26] Ito Y, Son M, Sato S, Ishikawa T, Kondo M, Nakayama S, Shimokata K, Kume H (2003) ATP Release Triggered by Activation of the Ca^{2+}-Activated K^+ Channel in Human Airway Calu-3 cells. *Am. J. Respir. Cell Mol. Biol. 30*: 388-395.

[27] Tarran R, Button B (2004) Measurements of Airway Surface Liquid Height (Volume) by Confocal Microscopy. *European Working Group on CFTR Expression*.

[28] Dubois D, Tatur S, Chabot H, Grygorczyk R (2008) Autocrine loop in purinergic control of airway surface liquid volume: monitoring with a novel side-view imaging technique. *Pediatric Pulmonology Supplement 31*: 230.

[29] Boucher R.C. (1999) Molecular insights into the physiology of the 'thin film' of airway surface liquid. *The Journal of Physiology, 516 :* 631-638.

[30] Verkman A.S., Song Y, Thiagarajah J.R. (2003) Role of airway surface liquid and submucosal glands in cystic fibrosis lung disease. *Am J Physiol Cell Physiol 284*: C2–C15.

[31] Boucher R.C. (2007) Airway Surface Dehydration in Cystic Fibrosis: Pathogenesis and Therapy. *Annu. Rev. Med 58*: 157-170.

[32] Sheppard D.N., Welsh M.J. (1999) Structure and Function of the CFTR Chloride Channel*. Physiol Rev 79:* S23-45.

[33] Short D.B., Trotter K.W., Reczek D, Kreda S.M., Bretscher A, Boucher R.C., Stutts M.J., Milgram S.L. (1998) An apical PDZ protein anchors the cystic fibrosis transmembrane conductance regulator to the cytoskeleton. *J Biol Chem. 273* :19797-801.

[34] Cystic Fibrosis Mutation Database (retrieved 2009) *Last updated March 2007.*
URL: http://www.genet.sickkids.on.ca/cftr/app.

[35] Fanen P, Hasnain A (2001) Cystic Fibrosis and CFTR Gene. Atlas Genet Cytogenet Oncol Haematol.
URL: http://AtlasGeneticsOncology.org/Educ/CistFibID30032ES.html.

[36] Welsh M.J., Smith A.E. (1993) Molecular mechanisms of CFTR chloride channel dysfunction in cystic fibrosis. *Cell 73:* 1251-1254.

[37] Dempsey E, Barton D.E., Ryan F (2004) Detection of Five Common *CFTR* Mutations by Rapid-Cycle Real-Time Amplification Refractory Mutation System PCR. *Clinical Chemistry 50*: 773-775.

[38] Coakley R.D., Boucher R.C. (2001) Regulation and functional significance of airway surface liquid pH. *JOP 2*, *Suppl 4*: 294–300.

[39] Grangeia A, Sá R, Carvalho F (2007). Molecular characterization of the cystic fibrosis transmembrane conductance regulator gene in congenital absence of the vas deferens". *Genet. Med. 9*: 163-72.

[40] Austen KF, Frank MM, Atkinson JP, Cantor H (2001) Samter's immunologic diseases. 1318 pages.

[41] Gibson RL, Burns JL, Ramsey BW. (2003) Pathophysiology and management of pulmonary infections in cystic fibrosis. *Am J Respir Crit Care Med. 168*: 918-951.

[42] Hoiby N (1988) Hemophilus influenzae, Staphylococcus aureus, Pseudomonas cepacia, and Pseudomonas aeruginosa in Patients with Cystic Fibrosis. *Chest 94*: 97S-102S.

[43] Lambiase A, Raia V, Del Pezzo M, Sepe A, Carnovale V, Rossano F. (2006) Microbiology of airway disease in a cohort of patients with cystic fibrosis. *BMC Infect Dis. 11*: 6-14.

[44] Steinkamp G, Wiedemann B, Rietschel E, Krahl A, Gielen J, Bärmeier H, Ratjen F (2005) Prospective evaluation of emerging bacteria in cystic fibrosis. *J. Cyst. Fibrosis 4:* 41-48.

[45] Terpstra WJ, Groeneveld K, Eijk PP, Geelen LJ, Schoone GJ, Schegget JT, Van Nierop JC, Griffioen RW, Van Alphen L (1988) Comparison of Two Nonculture Techniques for Detection of Hemophilus influenzae in Sputum. *Chest 94*: 126S-128S.

[46] Waters V, Gómez M, Soong G, Amin S, Ernst R, Prince A (2007) Immunostimulatory properties of the emerging pathogen Stenotrophomonas maltophilia. *Infect Immun 75*: 1698.

[47] Schöni M.H., Casaulta-Aebischer C (2000) Nutrition and lung function in cystic fibrosis patients: review. *Clinical Nutrition 19*: 79-85.

[48] Tatur S, Silvia K, Lazarowski E, Grygorczyk R (2007) Calcium-dependant release of adenosine and uridine nucleotides from A549 cells. *Purinergic Signalling 4(2)*: 139-146.

[49] Douillet C.D., Robinson W.P., III, Zarzaur B.L. et al. (2005) Mechanical ventilation alters airway nucleotides and purinoceptors in lung and extrapulmonary organs. *Am J Respir Cell Mol Biol.* 32: 52-58.

[50] Bodin P, Bailey D, Burnstock G. (1991) Increased flow-induced ATP release from isolated vascular endothelial cells but not smooth muscle cells. *Br J Pharmacol.* 103: 1203-1205.

[51] Bodin P, Burnstock G. (1995) Synergistic effect of acute hypoxia on flow-induced release of ATP from cultured endothelial cells. *Experientia* 51: 256-259.

[52] Schwiebert L.M., Rice W.C., Kudlow B.A., Taylor A.L., Schwiebert E.M. (2002) Extracellular ATP signaling and P2X nucleotide receptors in monolayers of primary human vascular endothelial cells. *Am J Physiol Cell Physiol.* 282: C289-C301.

[53] Ferguson D.R., Kennedy I, Burton T.J. (1997) ATP is released from rabbit urinary bladder epithelial cells by hydrostatic pressure changes--a possible sensory mechanism? *J Physiol (Lond).* 505: 503-511.

[54] Knight G.E., Bodin P, De Groat W.C., Burnstock G. (2002) ATP is released from guinea pig ureter epithelium on distension. *Am J Physiol Renal Physiol.* 282*:* F281-F288.

[55] Naemsch L.N., Dixon S.J., Sims S.M. (2001) Activity-dependent development of P2X7 current and Ca2+ entry in rabbit osteoclasts. *J Biol Chem.*276: 39107-39114.

[56] Grygorczyk R, Hanrahan J.W. (1997) CFTR-independent ATP release from epithelial cells triggered by mechanical stimuli. *Am J Physiol.* 272: C1058-C1066.

[57] Tarran R, Button B, Boucher R.C. (2006) Regulation of normal and cystic fibrosis airway surface liquid volume by phasic shear stress. *Annu Rev Physiol.*68: 543-561.

[58] Grygorczyk R, Hanrahan J.W. (1997) Cystic fibrosis transmembrane conductance regulator and adenosine triphosphate [response]. *Science* 275: 1325-1326.

[59] Donaldson S.H., Lazarowski E.R., Picher M et al. (2000) Basal nucleotide levels, release, and metabolism in normal and cystic fibrosis airways. *Mol Med.*6: 969-982.

[60] Hollenstein K, Dawson R.J., Locher K.P. (2007) Structure and mechanism of ABC transporter proteins. *Curr. Opin. Struct. Biol.* 17: 412-418.

[61] Grygorczyk R, Tabcharani J.A., Hanrahan J.W. (1996) CFTR channels expressed in CHO cells do not have detectable ATP conductance. *J Membr Biol.* 151: 139-148.

[62] Hazama A, Shimizu T, Ando-Akatsuka Y et al. (1999) Swelling-induced, CFTR-independent ATP release from a human epithelial cell line: lack of correlation with volume-sensitive Cl(-) channels. *J Gen Physiol.* 114: 525-533.

[63] Li C, Ramjeesingh M, Bear C.E. (1996) Purified cystic fibrosis transmembrane conductance regulator (CFTR) does not function as an ATP channel. *J Biol Chem.* 271: 11623-11626.

[64] Reddy M.M., Quinton P.M., Haws C et al. (1996) Failure of the cystic fibrosis transmembrane conductance regulator to conduct ATP. *Science.* 271: 1876-1879.

[65] Watt W.C., Lazarowski E.R., Boucher R.C. (1998) Cystic fibrosis transmembrane regulator-independent release of ATP. Its implications for the regulation of P2Y2 receptors in airway epithelia. *J Biol Chem.* 273: 14053-14058.

[66] Nilius B, Eggermont J, Voets T et al. (1997) Properties of volume-regulated anion channels in mammalian cells. *Prog Biophys Mol Biol. 68*: 69-119.

[67] Strange K, Emma F, Jackson P.S. (1996) Cellular and molecular physiology of volume-sensitive anion channels. *Am J Physiol.* 270: C711-C730.

[68] Hisadome K, Koyama T, Kimura C et al. (2002) Volume-regulated Anion Channels Serve as an Auto/Paracrine Nucleotide Release Pathway in Aortic Endothelial Cells. *J Gen Physiol.* 119: 511-520.

[69] Feranchak A.P., Roman R.M., Schwiebert E.M., Fitz J.G. (1998) Phosphatidylinositol 3-kinase contributes to cell volume regulation through effects on ATP release. *J Biol Chem.* 273: 14906-14911.

[70] Wang Y, Roman R, Lidofsky S.D., Fitz J.G. (1996) Autocrine signaling through ATP release represents a novel mechanism for cell volume regulation. *Proc Natl Acad Sci U S A.* 93: 12020-12025.

[71] Mitchell C.H. (2001) Release of ATP by a human retinal pigment epithelial cell line: potential for autocrine stimulation through subretinal space. *J Physiol.* 534: 193-202.

[72] Musante L, Zegarra-Moran O, Montaldo P.G., Ponzoni M, Galietta L.J. (1999) Autocrine regulation of volume-sensitive anion channels in airway epithelial cells by adenosine. *J Biol Chem.* 274: 11701-11707.

[73] Dutta A.K., Okada Y, Sabirov R.Z. (2002) Regulation of an ATP-conductive large-conductance anion channel and swelling-induced ATP release by arachidonic acid. *J Physiol*. 542: 803-816.

[74] Schlichter L.C., Grygorczyk R, Pahapill P.A, Grygorczyk C. (1990) A large, multiple-conductance chloride channel in normal human T lymphocytes*. Pflugers Arch.* 416: 413-421.

[75] Rostovtseva T, Colombini M. (1997) VDAC channels mediate and gate the flow of ATP: implications for the regulation of mitochondrial function. *Biophys J*. 72: 1954-1962.

[76] Bathori G, Parolini I, Szabo I et al. (2000) Extramitochondrial porin: facts and hypotheses. *J Bioenerg Biomembr* 32: 79-89.

[77] Gordon G.R., Baimoukhametova D.V., Hewitt S.A. et al. (2005) Norepinephrine triggers release of glial ATP to increase postsynaptic efficacy. *Nat Neurosci*. 8: 1078-1086.

[78] Burnstock G. (1995) Noradrenaline and ATP: cotransmitters and neuromodulators. *J Physiol Pharmacol*. 46: 365-384.

[79] Sperlagh B, Vizi E.S. (1996) Neuronal synthesis, storage and release of ATP. *Seminars Neurosci.* 8: 175-186.

[80] Fields R.D., Stevens B. (2000) ATP: an extracellular signaling molecule between neurons and glia. *Trends Neurosci.* 23: 625-633.

[81] Satchell D. (2000) Purinergic nerves and purinoceptors: early perspectives. *J Auton Nerv Syst.* 81: 212-217.

[82] Carty S.E., Johnson R.G., Scarpa A. (1981) Serotonin transport in isolated platelet granules. Coupling to the electrochemical proton gradient. *J Biol Chem.* 256: 11244-11250.

[83] Hirschberg C.B., Robbins P.W., Abeijon C. (1998) Transporters of nucleotide sugars, ATP, and nucleotide sulfate in the endoplasmic reticulum and Golgi apparatus. *Annu Rev Biochem.* 67: 49-69.

[84] Puglielli L, Mandon E.C., Hirschberg C.B. (1999) Identification, purification, and characterization of the rat liver golgi membrane ATP transporter. *J Biol Chem*. 274: 12665-12669.

[85] Maroto R, Hamill O.P. (2001) Brefeldin A block of integrin-dependent mechanosensitive ATP release from Xenopus oocyte reveals a novel mechanism of mechanotransduction. *J Biol Chem*. 276: 23867-23872.

[86] Tatur S, Groulx N, Orlov S.N., Grygorczyk R. (2007) Ca2+-dependent ATP release from A549 cells involves synergistic autocrine stimulation by co-released uridine nucleotides. *J Physiol.*

[87] Novak I. (2003) ATP as a signaling molecule: the exocrine focus. *News Physiol Sci.* 18: 12-17.

[88] Mitchell C.H., Carre D.A., McGlinn A.M., Stone R.A., Civan M.M. (1998) A release mechanism for stored ATP in ocular ciliary epithelial cells. *Proc Natl Acad Sci U S A.* 95: 7174-7178.

[89] Bodin P, Burnstock G. (2001) Evidence that release of adenosine triphosphate from endothelial cells during increased shear stress is vesicular. *J Cardiovasc Pharmacol.* 38: 900-908.

[90] Sorensen C.E., Novak I. (2001) Visualization of ATP release in pancreatic acini in response to cholinergic stimulus. Use of fluorescent probes and confocal microscopy*. J Biol Chem*. 276: 32925-32932.

[91] Boudreault F, Grygorczyk R (2002) Cell swelling-induced ATP release and gadolinium-sensitive channels. *Am J Physiol Cell Physiol* 282: C219-C226.

[92] Communi D, Paindavoine P, Place G.A., Parmentier M, Boeynaems J-M (1999) Expression of P2Y receptors in cell lines derived from the human lung. *British Journal of Pharmacology 127*: 562-568.

[93] Zimmermann H (2000) Extracellular metabolism of ATP and other nucleotides. *Naunyn Schmiedebergs Arch Pharmacol* 362: 299–309.

[94] Jayaraman S, Song Y, Vetrivel L, Shankar L, Verkman A.S. (2001) Noninvasive in vivo fluorescence measurement of airway-surface liquid depth, salt concentration, and pH. *J.Clin. Invest. 107*: 317-324.

[95] Kozlova I, Nilsson H, Phillipson M, Riederer B, Seidler U, Colledge W.H., Roomans G.M. (2005) X-ray microanalysis of airway surface liquid in the mouse. *Am J Physiol Lung Cell Mol Physiol 288*: L874–L878.

[96] Piston, D.W. (1999) Imaging living cells and tissues by two-photon excitation microscopy. *Trends Cell Biol.* 9 [2], 66-69.

[97] Boocock, C.A., Brown, A.F. & Dunn, G.A. (1985) A simple chamber for observing microscopic specimens in both top and side views. *J Microsc.* 137 [Pt 1], 29-34.

[98] Boudreault, F. & Grygorczyk, R. (2004) Evaluation of rapid volume changes of substrate-adherent cells by conventional microscopy 3D imaging. *J. Microsc.* 215 [Pt 3], 302-312.

[99] Cao, J., Usami, S. & Dong, C. (1997) Development of a side-view chamber for studying cell-surface adhesion under flow conditions. *Ann. Biomed. Eng* 25 [3], 573-580.

[100] Ingram, V.M. (1969) A side view of moving fibroblasts. *Nature* 222 [5194], 641-644.

[101] Sanders, E.J. & Prasad, S. (1979) Observation of cultured embryonic epithelial cells in side view. *Journal of Cell Science* 38, 305-314.

[102] Tsai, J.W., Yi, Y.S. & Lin, C.H. (2004) Cell Observing Method and the System Thereof. [00594011]. Patent of the Republic of China.

[103] Emmick J.T., Kwon S, Bidasee K.R., Besch K.T., Besch Jr. H.R. (1994) Dual effect of suramin on calcium fluxes across sarcoplasmic reticulum vesicle membranes. *The Journal of Pharmacology and Experimental Therapeutics 269*: 717-724.

[104] Coakley R.D., Grubb B.R., Paradiso A.M., Gatzy J.T., Johnson L.G., Kreda S.M., O'Neal W.K., Boucher R.C. (2003) Abnormal surface liquid pH regulation by cultured cystic fibrosis bronchial epithelium. *PNAS 100*: 16083-16088.

[105] Worlitzsch D, Tarran R, Ulrich M, Schwab U, Cekici A, Meyer K.C., Birrer P, Bellon G, Berger J, Weiss T, Botzenhart K, Yankaskas J.R., Randell S, Boucher R.C., Doring G. (2002) Effects of reduced mucus oxygen concentration in airway *Pseudomonas* infections of cystic fibrosis patients. *J Clin Invest 109*: 317–325.

[106] Irokawa T, Krouse ME, Soo Joo N, Wu JV, Wine JJ (2004) A "virtual gland" method for quantifying epithelial fluid secretion. *Am. J. Physiol. Lung Cell Mol. Physiol 287*: L784-L793.

[107] Roomans, G.M., Kozlova, I., Nilsson, H., Vanthanouvong, V., Button, B. & Tarran, R. (2004) Measurements of airway surface liquid height and

mucus transport by fluorescence microscopy, and of ion composition by X-ray microanalysis. *J. Cyst. Fibros.* 3 Suppl 2, 135-139.

Annex 1

(A) Images of the initial side-view imaging chamber:

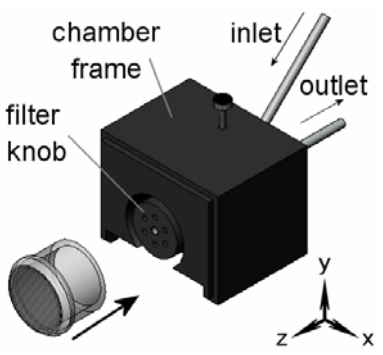

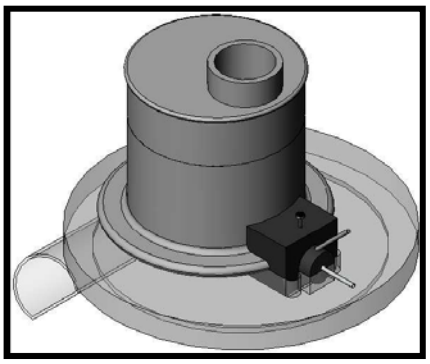

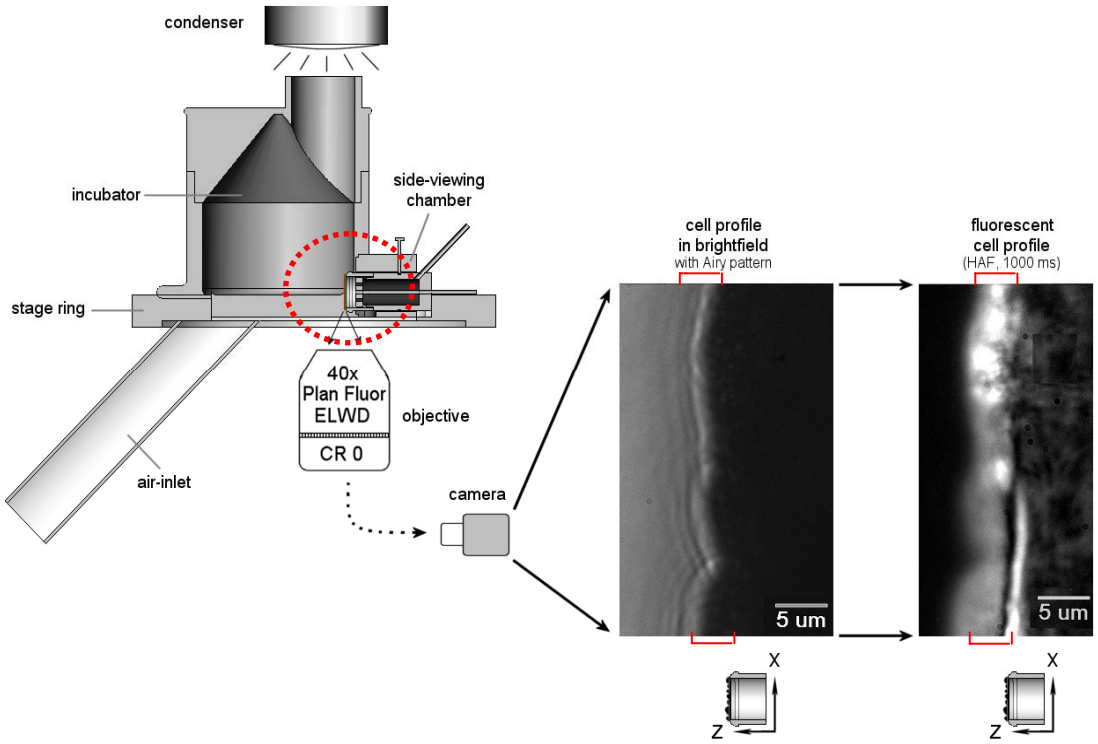

(B) Preliminary images of the optimized side-view imaging chamber:

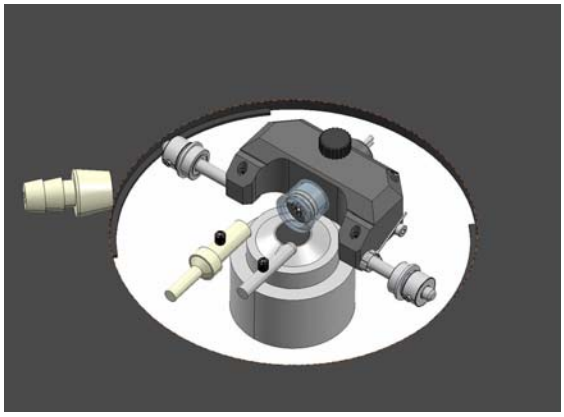

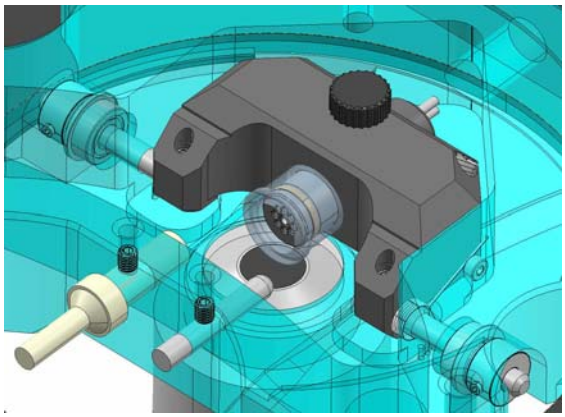

(A) (B)

Images (A) and (B) depict the filter holder, in which we insert the filter. This filter holder allows for perfusion onto the basolateral side of the monolayer, as well as air flow on the apical side of the cell monolayer.

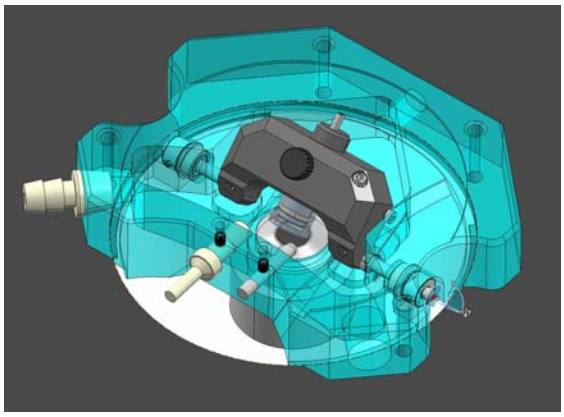

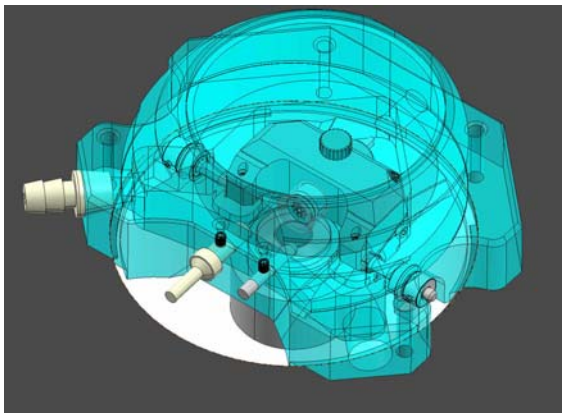

(C) (D)

Images (C) and (D) are depictions the side-view imaging chamber which (C) allows the tilting of the filter to 45º or 90º. Image (D) shows the closed chamber, with a cover on it that ensures temperature and humidity stability during experiments.

(B) Preliminary images of the optimized side-view imaging chamber (continued):

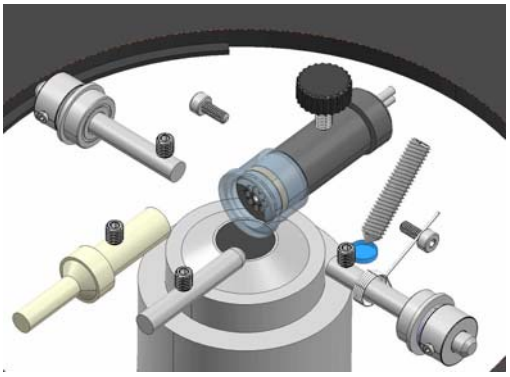

(A)

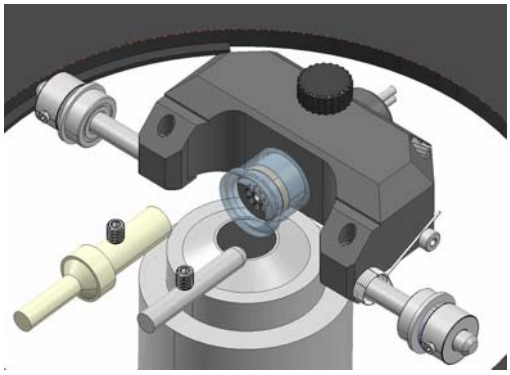

(B)

Images (A) and (B) depict every element in the filter holder, as well as how it comes together to form the final product. With these images, we can see that a slot is kept for both the humidity and temperature probes.

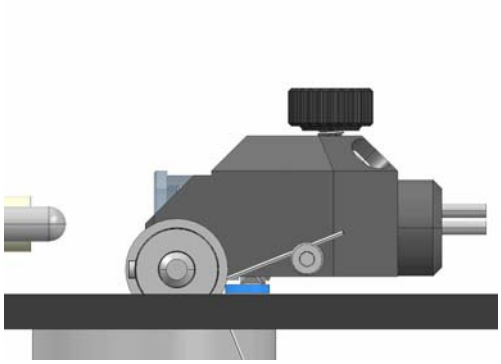

(C)

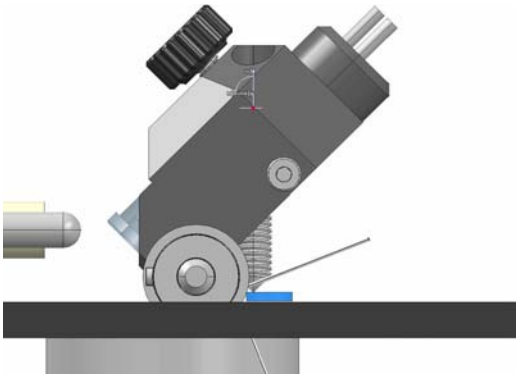

(D)

Images (C) and (D) demonstrate how our side-view chamber allows for the tilting of the filter. The filter holder rotates around a wheel that rests against the microscope stage, keeping our filter above the microscope objective, but allowing for the observation of the filter at different angles.

(C) Images of the finalized, optimized side-view imaging chamber:

(A)

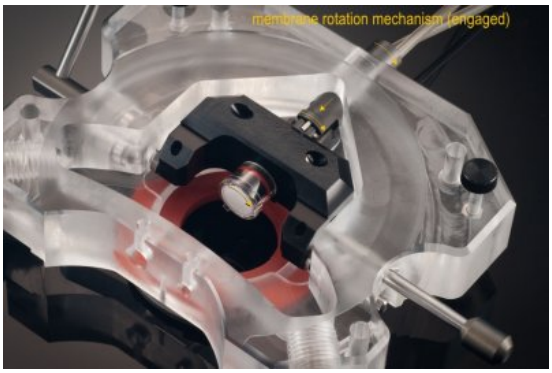

(B)

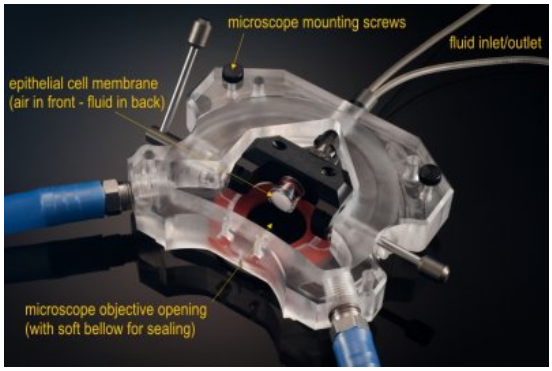

(C)

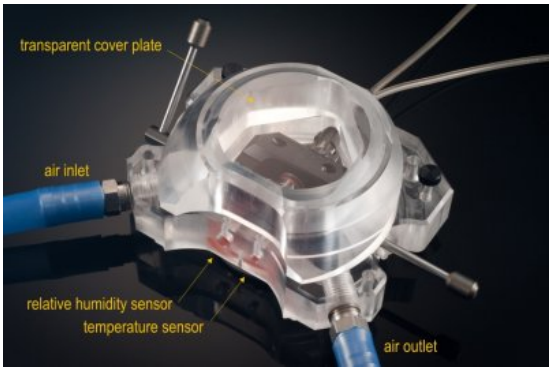

(D)

Images (A) through (D) depict the completed, real side-view imaging chamber, with blue tubes connected to the chamber for air flow, as well as smaller, clear tubing connected for the perfusion of solution onto the basolateral side of our cell monolayer.